

**ULTIMATE LIMIT STATE RESPONSE OF REINFORCED
CONCRETE COLUMNS FOR USE IN PERFORMANCE-BASED
ANALYSIS AND DESIGN**

A Thesis

by

CHRISTOPHER RICHARD URMSON

Submitted to the Office of Graduate Studies of
Texas A&M University
in partial fulfilment of the requirements for the degree of

MASTER OF SCIENCE

August 2010

Major Subject: Civil Engineering

Ultimate Limit State Response of Reinforced Concrete Columns for Use in

Performance-Based Analysis and Design

Copyright 2010 Christopher Richard Urmson

**ULTIMATE LIMIT STATE RESPONSE OF REINFORCED
CONCRETE COLUMNS FOR USE IN PERFORMANCE-BASED
ANALYSIS AND DESIGN**

A Thesis

by

CHRISTOPHER RICHARD URMSON

Submitted to the Office of Graduate Studies of
Texas A&M University
in partial fulfilment of the requirements for the degree of

MASTER OF SCIENCE

Approved by:

Co-Chairs of Committee,	John B. Mander
	Rashid K. Abu Al-Rub
Committee Member,	Anastasia H. Muliana
Head of Department,	John Niedzwecki

August 2010

Major Subject: Civil Engineering

ABSTRACT

Ultimate Limit State Response of Reinforced Concrete Columns for Use in
Performance-Based Analysis and Design. (August 2010)

Christopher Richard Urmson, B.E. (Hons), University of Canterbury,
Christchurch, New Zealand

Co-Chairs of Advisory Committee: Dr. John B. Mander
Dr. Rashid K. Abu Al-Rub

The design of reinforced concrete structures for extreme events requires accurate predictions of the ultimate rotational capacity of critical sections, which is dictated by the failure mechanisms of shear, hoop fracture, low-cycle fatigue and longitudinal bar buckling. The purpose of this research is to develop a model for the full compressive behavior of longitudinal steel including the effects of bar buckling. A computational algorithm is developed whereby experimental data can be rigorously modeled. An analytical model is developed from rational mechanics for modeling the complete compressive stress-strain behavior of steel including local buckling effects. The global buckling phenomenon is then investigated in which trends are established using a rigorous computational analysis, and a limit analysis is used to derive simplified design and analysis equations. The derived buckling models are incorporated into well-established sectional analysis routines to predict full member behavior, and the application of these routines is demonstrated via an incremental dynamic analysis of a ten-storey reinforced concrete building. The buckling models and the sectional analysis routine compare favorably with experimental data. Design recommendations and topics for further research are presented.

To my parents

ACKNOWLEDGEMENTS

The work conducted as part of this thesis would not have been possible without the input of several people. Firstly, I would like to express my deepest gratitude to my advisor, Dr. John Mander. His advice, guidance and generous financial support are greatly appreciated. I would also like to extend my thanks to Dr. Rashid Abu Al-Rub from the Zachry Department of Civil Engineering, and Dr. Anastasia Muliana from the Department of Mechanical Engineering. Their involvement on my advisory committee has been a great help. I would like to thank Mr. Pankaj Deshmukh for his assistance with running analyses, and the support of the staff of the Zachry Department of Civil Engineering is also acknowledged. Also, thank you to Dr. Stefan Hurlebaus for the last-minute use of his laptop computer.

I would like to thank my friends and family in Texas for making this experience both bearable and enjoyable, in particular Mr. Reece Scott, Mr. Thomas Mander, Mr. Warren “Uncle Waz” Urmson and Mr. Jason Zidek. The encouragement of my friends and family in New Zealand and elsewhere is also appreciated.

Finally, a special thank-you to Dominica for her continued patience, love and encouragement.

NOMENCLATURE

ACI	American Concrete Institute
ASTM	American Society for Testing and Materials
CCANZ	Cement and Concrete Association of New Zealand
DBE	design basis earthquake
FEM	finite element method
IDA	incremental dynamic analysis
IM	intensity measure
LVDT	linear variable differential transducer
MCE	maximum considered event
PEER	Pacific Earthquake Engineering Research
PGA	peak ground acceleration
PHZ	plastic hinge zone
RC	reinforced concrete
RHS	right-hand side
SCWB	strong-column weak-beam
SDL	superimposed dead load
SNZ	Standards New Zealand
UDL	uniformly distributed load
A_g	gross cross-sectional area
A_s	area of steel

A_{sp}	cross-sectional area of spiral steel
A_{trib}	tributary area
a	height of equivalent concrete stress block
a_i	normalized area of i^{th} fiber in Gaussian quadrature formulation
b	exponent in axial-lateral strain relationship
b_i	width of i^{th} fiber in Gaussian quadrature formulation
C_h	nodal concrete force
c	depth of neutral axis
D'	diameter of core concrete
d	diameter
d_b	diameter of longitudinal reinforcing bars
d_{bh}	diameter of transverse reinforcing bars
E_{eff}	effective modulus of steel
E_s	elastic modulus of steel
E_{sh}	initial modulus of strain-hardening portion of steel stress-strain curve
E_T	tangent modulus
EI_{eff}	effective flexural rigidity
EI_g	gross flexural rigidity
e	instantaneous eccentricity of buckled bar
e_o	initial eccentricity of reinforcing bar prior to application of axial strain
e_{SF}	eccentricity imposed by shape function
F_h	force in layer of transverse reinforcement

F_i	applied lateral load at i^{th} storey
F_{yh}	yield force of transverse steel
f_c'	compressive strength of plain concrete
f_{cc}'	compressive strength of confined concrete
f_{cb}	critical buckling stress at intersection of “strength controlled” and “stability controlled” curves
f_{cr}	critical buckling stress
f_{cs}	compressive steel stress
f_{gb}	crippling stress from global buckling
f_h	stress in layer of transverse reinforcement
f_o^-	compressive steel stress at onset of strain reversal
f_s	steel stress
f_{su}	ultimate steel stress in tension
f_{su}^-	inferred ultimate steel stress in compression
f_{uh}	ultimate hoop stress
f_y	yield stress of steel
f_{yh}	hoop yield stress
g	acceleration due to gravity
h_i	height of i^{th} storey
I	second moment of area
i,j,k	general indices
k_o	initial stiffness
k_u	unloading stiffness

L	length
L_e	effective buckling length
L_h	length of transverse reinforcement
L_{ph}	length of plastic hinge zone
M	bending moment
M_{cb}	bending moment at intersection of “strength controlled” and “stability controlled” curves
M_h	moment resisted by transverse steel
M_{pp}	peak plastic bending moment
M_{pu}	plastic bending moment at ultimate axial load of steel
M_{py}	plastic bending moment at yield point of steel
M_y	yield moment
M_{SF}	moment imposed by the shape function
N_b	number of longitudinal bars in circular section
N_h	number of layers of transverse reinforcement in buckled length
N_s	number of spaces of transverse reinforcement in buckled length
P	axial force
P_{cb}	axial load at intersection of “strength controlled” and “stability controlled” curves
P_{cr}	critical buckling force
P_e	experimental axial load
P_i	inelastic lateral load
P_{SF}	axial load imposed by the shape function

P_{su}	axial load when entire section is under a stress of f_{su}
P_y	yield force of longitudinal steel
p	steel strain hardening exponent
q	steel reversal branch exponent
q_i	normalized first moment of area of i^{th} fiber in Gaussian quadrature formulation
R	steel reversal branch exponent
R^*	closest distance to fault rupture
r	radius of gyration of cross-section
S_A	spectral acceleration
s	spacing of adjacent layers of transverse reinforcement
$(s / d_b)_{cb}$	reinforcing bar slenderness ratio at intersection of “strength controlled” and “stability controlled” curves
T	period of structure
U_s	strain energy
V	shear force
W_i	seismic weight of i^{th} storey
w_i	weighting factor for i^{th} fiber in Gaussian quadrature formulation
x,y,z	general coordinates
β	exponent in critical moment-curvature relationship
Δx	incremental change in x
δx	infinitesimal change in x
∂x	partial differentiation with respect to x

ε	strain
ε_b	secondary geometric nonlinear buckling strain
ε_{cr}	cripling strain at buckling
ε_{cs}	compressive steel strain
ε_{cu}	axial strain at hoop fracture
ε_f	fracture strain
ε_{fh}	hoop fracture strain
ε_{gb}	cripling strain from global buckling
ε_h	hoop strain
ε_{max}	maximum section strain
ε_o	strain at reference axis of bar cross-section
ε_o^-	compressive steel strain at onset of strain reversal
ε_{oc}	control point reference strain for axial-lateral strain relationship
ε_s	steel strain
ε_{sh}	steel strain at the onset of strain-hardening
ε_{su}	steel strain at ultimate stress
ε_t	transverse strain
ε_{tc}	control point transverse strain for axial-lateral strain relationship
ε_{ult}	governing strain from hoop fracture and global buckling
ε_y	yield strain of steel
ε_{yh}	hoop yield strain

Φ^*	component of earthquake record
ϕ	curvature
ϕ_{pp}	peak plastic curvature
ϕ_{pu}	ultimate curvature
κ	geometric hoop efficiency factor
Λ	lateral displacement of globally buckled reinforcing bar
Λ_{SF}	lateral displacement imposed by the shape function
μ	ductility
μ_θ	rotation ductility
γ	descending branch shape factor
θ	rotation
θ_m	rotation at initial unloading
θ_p	plastic rotation
θ_y	yield rotation
ρ_s	volumetric ratio of confining reinforcing steel
σ	stress
ξ_i	distance multiplier for i^{th} fiber in Gaussian quadrature formulation

TABLE OF CONTENTS

	Page
ABSTRACT	iii
DEDICATION	iv
ACKNOWLEDGEMENTS	v
NOMENCLATURE	vi
TABLE OF CONTENTS	xiii
LIST OF FIGURES	xvii
LIST OF TABLES	xx
 CHAPTER	
I INTRODUCTION	1
1.1 Background	1
1.2 Motivation and Research Objectives	2
1.3 Outline of Thesis	3
1.4 Significance of Current Research	4
II LITERATURE REVIEW	6
2.1 Theoretical Buckling Models	6
2.1.1 Classical Buckling Theories	6
2.1.2 Local Buckling of Longitudinal Steel	7
2.2 Local Buckling Experiments	12
2.2.1 Overview of Experimental Studies	12
2.2.2 Criteria for Selection of Experimental Results for Model Verification	13
2.3 Theoretical and Experimental Studies on Global Buckling	15
2.3.1 Theoretical Studies	15
2.3.2 Experimental Studies	17
2.4 Design Code Requirements	20

CHAPTER	Page	
III	COMPUTATIONAL ALGORITHM FOR BUCKLING ANALYSIS	21
	3.1 Introduction	21
	3.2 Computational Theory	21
	3.2.1 Section Actions for a Given Strain Profile	21
	3.2.2 Moment-Curvature Analysis of Critical Section	22
	3.2.3 Imposing the Shape Function	24
	3.3 Computing Procedures	25
	3.3.1 Data Input and Output	25
	3.3.2 Computational Method for Curvature-Driven Analysis ..	27
	3.3.3 Computational Method for Strain-Driven Analysis	30
	3.4 Extension to Global Buckling Analysis	32
	3.4.1 Contribution of Transverse Steel	33
	3.4.2 Algorithm for Incipient Buckling	34
	3.5 Illustrative Numerical Examples	35
	3.5.1 Local Buckling Analysis	35
	3.5.2 Global Buckling Analysis	37
IV	LOCAL BUCKLING ANALYSIS OF LONGITUDINAL REINFORCING BARS	41
	4.1 Introduction	41
	4.2 Previous Research	44
	4.2.1 Classical Buckling Theories	44
	4.2.2 Theoretical Models for Local Buckling of Longitudinal Reinforcing Steel	44
	4.2.3 Experimental Studies on Local Buckling of Longitudinal Reinforcing Bars	46
	4.3 Coupled Axial and Lateral Deformation Analysis	48
	4.3.1 Material Characterization	48
	4.3.2 Lateral Deformation Analysis	50
	4.3.3 Axial-Lateral Deformation Coupling	52
	4.3.4 Moment-Curvature Analysis at the Critical Section	54
	4.4 Results of Computational Buckling Analysis	56
	4.4.1 Empirical Observations from Computational Results	56
	4.5 Prediction of Ultimate Stress at Crippling	59
	4.5.1 Simplified Analysis of Ultimate Failure Stress	61
	4.5.2 Application to Experimental Results	62
	4.6 Prediction of Strain at Crippling	62
	4.7 Implimentation of Analytical Model	64
	4.7.1 Summary of Analytical Modeling Parameters	66

CHAPTER	Page
4.8 Chapter Closure	70
V GLOBAL BUCKLING ANALYSIS OF LONGITUDINAL REINFORCING BARS	72
5.1 Introduction and Motivational Background	72
5.2 Previous Research	77
5.2.1 Theoretical Models for Global Buckling of Longitudinal Reinforcing Steel	77
5.2.2 Experimental Studies on Global Buckling	79
5.3 Computational Modeling of Global Bar Buckling	80
5.3.1 Lateral Deformation Analysis	81
5.3.2 Resistance by Transverse Steel	82
5.3.3 Full Buckling Analysis	82
5.4 Observations from Computational Analysis	84
5.5 Simplified Limit Analysis	89
5.5.1 Prediction of Crippling Stress due to Global Buckling ..	89
5.5.2 Prediction of Crippling Strain due to Global Buckling ..	90
5.5.3 Tie Effectiveness and Circular Sections	91
5.5.4 Full Compressive Stress-Strain Model	91
5.6 Chapter Closure	93
VI APPLICATION TO PERFORMANCE-BASED ANALYSIS AND DESIGN	95
6.1 Introduction	95
6.2 Moment-Curvature and Force-Deformation Analysis of Critical Reinforced Concrete Members	97
6.3 Structural Analysis Model of Red Book Building	101
6.4 Pushover Analysis	110
6.5 Incremental Dynamic Analysis	114
6.6 IDA Results and Implications	116
6.7 Chapter Closure	116
VII SUMMARY AND CONCLUSIONS	118
7.1 Summary	118
7.2 Design Considerations	119
7.3 Recommendations for Future Research	120
7.3.1 Experimental Investigations	120
7.3.2 Theoretical Investigations	121

	Page
REFERENCES	124
APPENDIX A	132
APPENDIX B	156
VITA	171

LIST OF FIGURES

FIGURE	Page
3.1 Validation of Computational Algorithm for Local Buckling Analysis ...	36
3.2 Column Specimens Used for Model Validation Showing Number of Hoops in Buckled Length	38
3.3 Steel Stress-Strain Curves Compared with Column Strains and Axial Loads	39
4.1 Local Buckling in a Reinforced Concrete Member	43
4.2 Material Characterization of Steel	49
4.3 Computational Bar Buckling Analysis – Method and Results	53
4.4 Empirical Observations from Computational Analysis	58
4.5 Generalized Analytical Buckling Curves with Experimental Values	63
4.6 Comparison between Experimental and Analytically Predicted Stress and Strain Values	65
4.7 Compressive Stress-Strain Curves: Experimental, Computational and Analytical	67
5.1 Global Buckling in a Reinforced Concrete Member	73
5.2 Plastic Hinge Behavior in the Context of Global Buckling	75
5.3 Characterization of Hoop Behavior	83
5.4 Computational Analysis to Find Critical Buckling Length	86
5.5 Computational Analysis to Show Variation in Behavior with Hoop Force	87
5.6 Computational Analysis to Show Variation in Behavior with Hoop Spacing	88

FIGURE	Page
5.7 Multipliers for Different Configurations of Transverse Steel	92
6.1 Geometry of Column Specimens Tested by Park et al. (1982)	99
6.2 Results of Computational Analyses of RC Columns Tested by Park et al. (1982)	100
6.3 Red Book Building (adapted from CCANZ, 1998) – Typical Floor Plan	103
6.4 Red Book Building (adapted from CCANZ, 1998) – Grid F Elevation ..	104
6.5 Schematic Diagram of SAP2000 Model of Red Book Building	107
6.6 Schematic Diagram of Takeda Hysteretic Model	107
6.7 Backbone Curves of Hinges Used in SAP2000 Model	111
6.8 Results of Pushover Analysis for Red Book Building	113
6.9 Acceleration Response Spectra and IDA Results for Red Book Building	117
7.1 Proposed Experimental Set-up for Global Buckling Experimental Investigation	122
B1 Computational Results for Grade 300 D16 Steel Bars from Mander (1983)	158
B2 Comparison of Results from Steels Tested by Mander (1983)	159
B3 Computational Results for Mild Steel Bars from Mander et al. (1994) ..	160
B4 Computational Results for High-Strength Steel Bars from Mander et al. (1994)	161
B5 Comparison of Results for Steels Tested by Mander et al. (1994)	162
B6 Computational Results for #10 Steel Bars from Rodriguez et al. (1999).....	163
B7 Computational Results for M20 Steel Bars from Bayrak and Sheikh (2001)	164

FIGURE	Page
B8 Comparison of Results for Steels Tested by Bayrak and Sheikh (2001) .	165
B9 Computational Results for #8 Steel Bars from Bae et al. (2005)	167
B10 Computational Results for #10 Steel Bars from Bae et al. (2005)	168
B11 Comparison of Results from #8 Steel Bars Tested by Bae et al. (2005) .	169
B12 Comparison of Results from #10 Steel Bars Tested by Bae et al. (2005)	170

LIST OF TABLES

TABLE	Page
3.1	Integration Points and Weighting Factors for 24-Point Gauss Quadrature 23
3.2	Input Parameters Used in the Bar Buckling Analysis Program 26
3.3	Steel Stress-Strain Parameters Used in Model Validation 36
3.4	Column Specimen Details Used in Model Validation 38
4.1	Properties of Steel Bars Tested in Monotonic Compression 64
6.1	Details of RC Specimens Tested by Park et al. (1982) 101
6.2	Tensile Stress-Strain Parameters for Longitudinal Steel Used in Specimens Tested by Park et al. (1982) 101
6.3	Details of Critical Sections in Red Book Building 102
6.4	Beam Distributed Gravity Loads and Cumulative Column Axial Loads for Red Book Building under Ultimate Earthquake Loads 106
6.5	Comparison of Modes of Vibration of Red Book Building 108
6.6	Vertical Distribution of Lateral Forces 112
6.7	Details of 20 Ground Motion Records Used in IDA 115
B1	Steel Stress-Strain Parameters for Steels from Mander (1983) 157
B2	Steel Stress-Strain Parameters for Steels from Mander et al. (1994) 160
B3	Steel Stress-Strain Parameters for Steels from Rodriguez et al. (1999) .. 163
B4	Steel Stress-Strain Parameters for Steels from Bayrak and Sheikh (2001) 164
B5	Steel Stress-Strain Parameters for Steels from Bae et al. (2005) 166

CHAPTER I

INTRODUCTION

1.1 Background

It has long been recognized in the design of reinforced concrete (RC) structures that the demands imposed during a major seismic event cannot be efficiently resisted within the elastic range of the structure's components. Instead, certain levels of damage are acceptable, depending on the magnitude of the earthquake, whereby the energy imposed on the structure is dissipated. For example, under more frequent, smaller magnitude earthquakes, only small amounts of "patch and repair" damage may be acceptable. Under a moderate "Design Basis Event" (DBE), some amount of permanent damage may be acceptable. Under a "Maximum Considered Event" (MCE) with a return period greater than about 2500 years, considerable energy dissipation requirements necessitate high levels of damage. Whatever the case, the ultimate goal is the prevention of structural collapse.

Because of the increased risk associated with incorporating damage as a means of energy dissipation, it is of utmost importance that undesirable modes of failure be prevented. Instead, a ductile collapse mechanism should be engineered, by design. This is normally achieved by the formation of plastic hinges at strategic locations in the structure. This concept is the basis of the capacity design philosophy, championed by Park and Paulay (1975). Under this design philosophy, ductile flexural plastic hinges form in the beams at each level, and in the base of the columns, to produce a "Strong Column Weak Beam" (SCWB) side-sway mechanism. These plastic hinges are then detailed in order to protect against undesirable modes of failure. Dutta and Mander (1998) identified these to be:

This thesis follows the style of *Journal of Structural Engineering*.

- (i) Premature compressive failure of the concrete due to lack of confinement;
- (ii) Compressive buckling of longitudinal reinforcement, in turn causing (i);
- (iii) Fracture of transverse reinforcement, causing (i) and (ii);
- (iv) Low cycle fatigue failure of longitudinal reinforcement.

By providing sufficient levels of transverse confining reinforcement, all of the above failure modes can be deferred until the unavoidable fourth case (fatigue) governs. Although fundamental theories are well-known and established for the prevention of (i), compressive buckling (ii) has not been given the attention it deserves. Consequently many “bird-cage” buckling failures have been observed. This research seeks to demystify this phenomenon.

1.2 Motivation and Research Objectives

As part of the current state-of-the-practice in seismic design of RC structures, a performance-based analysis of a designed structure is carried out to ascertain the damage expected under a DBE and an MCE. Since damage can usually be considered to be proportional to displacement limit states, it is necessary to conduct either a pushover analysis or an incremental dynamic analysis (IDA) to determine what the seismic demands on plastic hinge zones are. Due to the highly nonlinear behavior expected in structural components, the demand (pushover / IDA) analysis should be compared with capacity (moment-curvature or plastic hinge rotation) analyses of critical plastic sections in the structure.

Structural capacity analyses of the critical sections can be done with relative ease using current knowledge. The elastic, plastic, peak and post-peak behavior of RC sections can be described with sufficient accuracy for use in a pushover analysis / IDA. However, identification of the critical case, at which failure is caused by one of the four failure mechanisms described above, is an area that is largely undeveloped.

It is the aim of this thesis to incorporate the four modes of failure, outlined above, into a seismic capacity analysis procedure. A particular emphasis will be directed at modeling the effects of inadequate transverse reinforcement details. This will give a more realistic prediction of ultimate rotation capacities of RC members. When blended with seismic demand analyses (e.g. IDA), a better indicator of likely failure at a particular seismic intensity can be obtained. To achieve this objective, it is desirable to have a simple yet accurate capacity model, for each failure mode, that lends itself to be used in a fiber element based member model. This is the case for concrete confinement failure (Mander et al., 1988a,b), shear failure (Kim and Mander, 2006) and low-cycle fatigue (Dutta and Mander, 2001). However, no satisfactory model has been found for buckling of longitudinal reinforcement. As such, it is a further aim of this thesis to develop such a model.

1.3 Outline of Thesis

This thesis is arranged into six chapters that aim to address the objectives outlined above, as follows:

Chapter II provides a comprehensive investigation of previous studies into global and local buckling. The chapter starts with a description of classical elastic and plastic buckling theories, and follows the progression of buckling models to the present day. Both experimental and theoretical investigations are described, and aspects of each study are critically reviewed.

Chapter III presents a computational algorithm developed for buckling analysis of longitudinal reinforcement. The underlying computational theory is explained and the steps of the algorithm are outlined. Illustrative numerical examples that simulate physical tests are presented as validation of the algorithm.

Chapter IV investigates the local buckling behavior of longitudinal reinforcing steel. A rational mechanics approach is used to examine the full plastic behavior of the steel and

the effects of true stress and strain. A computational fiber element analysis is used to compute the coupled effect of axial compression and lateral buckling. The results of the computational analysis are then used to develop a simple model for the compressive behavior of longitudinal reinforcing steel in engineering stress-strain coordinates.

Chapter V develops a global buckling model that is an extension of the model developed in Chapter IV. This allows for the possibility of a longitudinal bar buckling over several layers of transverse steel. As with the model for local buckling, the aim is to have a model that predicts the compressive stress-strain parameters of longitudinal reinforcing steel. In addition, a design criterion for transverse steel is developed based on global buckling requirements. The model is again verified with available experimental evidence although this will be considerably more difficult than for the local buckling case.

Chapter VI examines the derived buckling models which are incorporated into a moment-curvature analysis routine for a RC section. The analysis also includes the confined concrete model from Mander et al. (1988), the low-cycle fatigue model from Dutta and Mander (2001), and a shear model from Kim and Mander (2006). This routine is then validated against experimental data from RC column tests, and a demonstration is given of how the moment-curvature analysis is coordinated with a pushover analysis / IDA of a ten-storey RC building.

Finally, Chapter VII presents a summary of the work presented in each chapter, the main conclusions of the thesis, recommendations for design and future work.

1.4 Significance of Current Research

The proposed local and global buckling models presented in Chapters IV and V are shown to work well in predicting the overall compressive behavior of longitudinal reinforcing steel. The models are derived from rational mechanics and validated against experimental observations for a wide range of steel types. They can be applied with

minimal effort in design and analysis contexts. Existing models that are accurate involve too much specialized computational (FEM) effort for practical use. Other models that are simpler to use often rely on high degrees of empiricism and as such are only strictly valid over the range of steels for which they were calibrated.

The member capacity analysis presented in Chapter VI is able to give an accurate representation of elastic, plastic, peak, post-peak and ultimate behavior of RC members. This is necessary when comparing seismic demands versus capacities in a probabilistic framework.

CHAPTER II

LITERATURE REVIEW

2.1 Theoretical Buckling Models

2.1.1 Classical Buckling Theories

Elastic buckling was first studied in the classical papers by Euler (1744; 1759), who formulated the following solution for the critical buckling load P_{cr} :

$$P_{cr} = \frac{\pi^2 E_s I}{L_e^2} \quad (2.1)$$

where E_s = Young's modulus; I = the second moment of area of the member's section; and L_e = the effective length of the member about the axis of buckling. Recognizing that, for the case of a reinforcing bar with fixed ends with transverse steel spaced at s , the spacing is expressed as $s = 2L_e$. Hence one can determine the critical buckling stress, f_{cr} :

$$f_{cr} = \frac{P_{cr}}{A_g} = \frac{4\pi^2 E_s r^2}{s^2} \quad (2.2)$$

where r = the radius of gyration of the circular bar. For a circular section, $r = d_b / 4$. However, for a reinforcing bar with rolled deformations, Mander (1983) showed that $r = 0.955 (d_b / 4)$. Hence the critical elastic buckling length of a reinforcing bar can be expressed as

$$\frac{s}{d_b} = 1.5 \sqrt{\frac{E_s}{f_{cr}}} \quad (2.3)$$

According to elastic buckling theory, the Euler buckling curve is capped by the theoretical yield stress, f_y . Other early researchers investigated buckling that occurs at stresses above f_y , at which point buckling becomes an inelastic problem. It is well accepted that (2.3) still holds for inelastic buckling; however the Young's modulus E_s is replaced with

E_{eff} , the effective gradient of the stress-strain curve. For elastic buckling (where $f_{cr} < f_y$), $E_{eff} = E_s$. For cases where $f_{cr} \geq f_y$, E_{eff} takes some other value. Various theories have emerged for inelastic buckling, the first of which was the tangent modulus theory formulated by Engesser (1889). He essentially extended Euler's model to the inelastic range by using the tangent modulus E_T in (2.3), usually taken as E_{sh} , the modulus at the onset of strain-hardening. It was assumed that the entire cross-section would be subjected to this constant value of E_T .

However, experimental evidence consistently showed that real columns were stronger than Engesser predicted. It was pointed out that the reason for this is that, while some fibers of the section increase in compressive stress with a modulus of E_{sh} , other fibers will unload, initially with an elastic modulus E_s . Considère (1891) and Engesser (1891) both independently proposed solutions to this problem, using what eventually became known as the double modulus theory. This theory allows for the fact that some fibers of the section will unload during buckling, however experimental evidence consistently showed that the double modulus theory overestimated the true buckling strength of columns.

Shanley (1947) discussed the *column paradox*. He explained that the double modulus theory assumes that at the instant of buckling, the section of the member will be subjected to the assumed distribution of moduli, which is true for a column that is perfectly straight before buckling. However, since no column is perfectly straight, lateral deflections occur before the peak load is reached, and the distribution of moduli assumed by the double modulus theory becomes an upper bound solution. As such, the true effective modulus lies between the tangent modulus and the double modulus.

2.1.2 Local Buckling of Longitudinal Steel

Bresler and Gilbert (1961) first identified the need to investigate buckling of longitudinal steel in reinforced concrete members. Since then, studies on inelastic buckling of

reinforcing bars have produced various theoretical models. These models occur in two groups – linearized solutions, and more recently, computational solutions. The models that are discussed below were derived for local buckling only, using a rational mechanics approach. Models simply calibrated from experiments and models for global buckling are discussed in following sections.

Mander (1983), in a study of reinforcing steel behavior in compression, compared buckling predictions using the elastic modulus, the tangent modulus and the double modulus. This comparison confirmed that the tangent modulus theory and double modulus theory are lower and upper bound approaches, respectively. An alternative solution based on the double modulus theory was proposed, where the secant modulus is used in the calculation of the “double modulus”, instead of the tangent modulus. This approach allowed for the fact that, at the point where buckling commences, the fibers that increase in compressive stress do not immediately load with the tangent modulus. As such, this approach lies between the upper and lower bound approaches.

Mau and El-Mabsout (1989) carried out a computational study on local buckling of reinforcing bars. They performed a finite element analysis on a quarter-length of buckled reinforcing bar, using Gauss Quadrature to integrate stresses across the section, and Simpson’s rule to integrate along the length of the bar. In most cases, it was found that the results from the finite element analysis agreed with experiments very well for a wide range of steels. For very low spacings of transverse steel, a “straightening” phenomenon was observed, where after an initial lateral deflection the bar straightened again until a much higher buckling load was reached. This phenomenon has not been observed in experiments, and this suggests that other physical effects are occurring at these low spacings of transverse steel which were not captured in the finite element analysis.

Mau (1990) used the results of the previous study to draw a generalized buckling curve for critical load as a function of slenderness ratio. He found that for low slenderness

ratios ($s / d_b \leq 7$), the tangent modulus theory can be used to accurately estimate the critical buckling load.

Dhakal and Maekawa (2002a) performed a similar finite element approach to the local buckling problem. They examined the effects of longitudinal bar slenderness ratio, yield strength and post-yield behavior on the stress-strain curve of a buckled bar. They proposed that the average stress-strain relationship under monotonic compression could be characterized for any grade of steel in terms of a parameter $(L / d_b) \sqrt{f_y}$. This proposed relationship was incorporated into a cyclic stress-strain relationship (Dhakal and Maekawa, 2002b).

Gil-Martín et al. (2006, 2008) also carried out a finite element study on locally buckling reinforcing bars. The results of this analysis were then used to develop simple mathematical expressions for approximating the stress-strain curve in compression using statistically derived parameters. This model was incorporated into a sectional analysis of reinforced concrete members. While the general approach is good in that it starts with a rigorous analysis and develops simple, practical expressions, the analyses were not compared with experiments in any cases, and hence the model was not adequately validated. This led to erroneous conclusions about the effects of initial eccentricity on the capacity of the bar.

Monti and Nuti (1992) considered the effects of inelastic buckling on the cyclic behavior of a reinforcing bar. They developed a hardening rule-based plasticity model, using kinematic, isotropic, memory and saturation hardening rules that were modified for buckling. An empirical relationship was derived for monotonic compression which was used in the modification of the cyclic hardening rules. Experimental results were predicted well for cyclic tests.

Rodriguez et al. (1999) proposed a simpler cyclic model. This model used the cyclic stress-strain model for reinforcing steel from Mander (1993), modified by a parameter that predicts the onset of buckling. This parameter is based on the strain at which buckling occurs in monotonic tests, and this strain is simply applied at the point of reloading in a cyclic test.

Kunnath et al. (2009) developed a comprehensive model for reinforcing bars under cyclic axial load. The model incorporates the effects of true stress, and it uses the buckling model proposed by Dhakal and Maekawa (2002a), the low-cycle fatigue models from Coffin (1954, 1971), Manson (1965) and Mander et al. (1994) and the cyclic stress-strain model from Chang and Mander (1994) but with more memory points. The model was validated by favorable comparison with experimental results.

Gomes and Appleton (1997) considered the buckling problem using an energy minimization approach. The cyclic stress-strain model for steel developed by Menegotto and Pinto (1973) was used as the basis for cyclic behavior. A hyperbolic stress-strain relationship was then found for the buckled stress-strain curve using energy minimization, both with and without considering the interaction between bending moment and axial load in the bar. This approach showed reasonable agreement with experiments on full concrete columns however there is a need to verify the model with experiments on bare steel bars. The model is very simple in that it considers only a bilinear material with modification for the Bauschinger effect on strain reversals. A model that includes strain-hardening would be more rigorous in emulating actual stress-strain behavior of buckled steel bars.

Dutta and Mander (1998) also adopted an energy minimization approach to solve the local buckling problem, but this was done in a far more rigorous manner than in the study by Gomes and Appleton (1997). Firstly, a full moment-curvature analysis of a reinforcing bar section was carried out, where for a given axial load, the curvature was

incrementally increased. The strain and stress profiles of the section were found from constitutive relations and section equilibrium, and the complete stress-strain curve (including strain-hardening) was used. This moment-curvature data was used together with moment-axial load interaction relationships and the virtual work mechanism of a buckled bar to obtain a simplified relationship between s / d_b and f_{cr} / f_y . While the approach is sensible and the resulting relationship is easy to apply for both analysis and design situations, the study itself contained several errors. The moment-curvature analysis neglected the possibility of load reversal on any of the cross-sectional fibers. The moment-curvature analyses also assumed the same material behavior in tension and compression. In a continuum sense this is a valid assumption, however Poisson's effect causes the cross-sectional area of the bar to increase in compression and decrease in tension. From this arises the distinction between engineering stress and true stress.

Dodd and Restrepo-Posada (1995) characterized the relationship between engineering stress and true stress. Whereas the former neglects the change in bar cross-sectional area, the latter incorporates it such that in true stress co-ordinates, the material behavior is identical in tension and compression.

Massone and Moroder (2009) used a fiber-hinge approach to model the response of the reinforcing bar's section to compressive loads where an initial imperfection exists. The purpose of this was to model the experiments by Bayrak and Sheikh (2001) of monotonic tests on reinforcing bars with initial imperfections. The model incorporates true stress effects and allows for load reversals. Unlike other studies, their model did not assume a deflected shape for the buckled reinforcing bar. Rather, plasticity was lumped at four plastic hinges along the member length and elastic and plastic components of rotation are evaluated using sectional analysis and global equilibrium. When the model was compared to the experiments, good agreement was found for higher bar slenderness ratios ($s / d_b \geq 8$), but not for lower slenderness ratios.

Bae et al. (2005) formulated a model to characterize the stress-strain curves from Bayrak and Sheikh (2001) using a parametric approach with better results.

It can be seen that many theoretical models exist for local buckling of steel reinforcing bars. Many of these models involve a highly rigorous approach. However, good agreement with experimental evidence comes at a heavy computational cost. Clearly there is a need to develop an easy-to-use analytic model that is practical enough to use in design situations, yet sufficiently accurate to use in nonlinear sectional analyses of reinforced concrete members.

2.2 Local Buckling Experiments

2.2.1 Overview of Experimental Studies

Several researchers have carried out experimental investigations into local bar buckling by considering a bar under compression with the ends fixed against rotation. Mander (1983) carried out monotonic compression tests on Grade 275 and Grade 380 steels manufactured in New Zealand. The bar diameters of the specimens were 16mm, 20mm, 24mm and 28mm; s / d_b ratios were 5.5, 6.0, 6.5, 10 and 15; and rates of applied strain ranged from 0.00001 /s to 0.013 /s. In a study by Monti and Nuti (1992) a series of monotonic and cyclic tests were performed on FeB44 steel manufactured in Italy. Bar diameters of 16mm, 20mm and 24mm were used, and s / d_b ratios were 5, 8 and 11. As part of a study on low-cycle fatigue behavior in reinforcing steel, Mander et al. (1994) carried out monotonic compressive tests on ASTM A615 Grade 40 deformed reinforcing bars at $s / d_b = 6$, and on ASTM A722 type II hot-rolled proof-tested alloy-steel prestressing thread bar with s / d_b ratios of 6, 8 and 9.

Rodriguez et al. (1999) performed an experimental study consisting of monotonic and cyclic tests specimens machined from ASTM A706 reinforcing steel commercially available in Mexico. Ratios of s / d_b used were 2.5, 4, 6 and 8.

Bayrak and Sheikh (2001) conducted an extensive experimental study on Grade 400 reinforcing bars loaded in monotonic compression. The bars were all 20mm in diameter. Seven s / d_b ratios were used, ranging from 4 to 10. Initial imperfections at mid-height, ranging from 0 to $0.3d_b$, were applied to the specimens. Further tests on No. 8 and No. 10 Grade 60 reinforcing bars from the U.S. were conducted by Bae et al. (2005). The specimens had s / d_b ratios ranging from 4 to 12, and initial eccentricities ranging from 0 to $0.5d_b$.

2.2.2 Criteria for Selection of Experimental Results for Model Verification

When considering the results of experimental studies, several important aspects must be examined. Firstly, machining of specimens from reinforcing bars alters the behavior of the specimen. Most reinforcing bars develop a case-hardened shell as part of the manufacturing process (González et al., 2006). By removing this layer, average stresses in the section will change significantly, and hence it is better experimental practice to use un-machined specimens as is the case with all studies mentioned except Rodriguez et al (1999).

Secondly, the method by which strain is measured is important. In general, LVDTs are preferred over strain gauges for measuring axial strain. Strain gauges attached to the surface of a specimen do not provide meaningful results for two reasons. On one hand, this method requires the removal of some of the bar deformations, which will alter the specimen behavior. On the other hand, a strain gauge will measure the local strain over a gauge length of 5mm or so, which becomes meaningless at the onset of buckling. For sectional analysis, it can be assumed that Bernoulli's hypothesis (that plane sections remain plane) holds at levels of transverse steel during buckling, but not between these levels. Since a gauge length must account for buckling yet still be valid for use in a sectional analysis, strain must be measured over a multiple of the full effective length of the buckled bar. Again, this is the case for all studies measured above with the exception of Mander (1983), Rodriguez et al. (1999) and Bae et al. (2005), which used arbitrary

gauge lengths. Note that all experiments have used LVDTs, however those that have used arbitrary gauge lengths may not capture full buckling effects.

Thirdly, one needs to consider the experimental parameters that are of interest. In considering a reinforcing bar that is buckling, it is important to realize that for low effective lengths the load carrying capacity may increase even after buckling has caused the bar to undergo lateral deflections. For design and analysis purposes, of interest is the maximum load that the bar can carry. As such, experimental studies that report values other than this must be approached with caution. This is the case for all experimental studies mentioned apart from Rodriguez et al. (1999), who arbitrarily define the onset of buckling to occur when the strains on either side of the bar section differed by more than 20 percent. Since the load at this “onset of buckling” is the value of the load that is reported, it is of no use for validation of analytical predictions.

Finally, it will be noted that some experimental studies have been done on the effects of buckling on cyclic behavior of reinforcing steel. Several researchers have then proceeded to develop models to simulate these cyclic experiments. It was noted that for the experiments carried out using a cyclic loading regime, the ultimate compressive capacity of the bars for a given effective length did not differ significantly from that for the monotonic case. However, it was found that the strain at which buckling occurs will be different, and is based on the final plastic strain at zero load prior to the load cycle at which buckling occurs. As such, a monotonic model will be sufficient to capture the required parameters of interest.

Ahead of all of these points, the shortcomings of the local bar buckling approach need to be recognized. The fundamental assumption used in deriving all of the models described above is that transverse reinforcement is sufficiently stiff to limit buckling over more than one hoop spacing. However, many experimental studies and inspections of real buildings damaged by earthquakes have shown that buckling may occur in a global

manner. That is, the effective buckling length may be larger than one hoop spacing. As such, a suitable buckling model should include the effectiveness of transverse steel in resisting global buckling. Existing models and experiments to this end are described below.

2.3 Theoretical and Experimental Studies on Global Buckling

2.3.1 Theoretical Studies

Bresler and Gilbert (1961) were first to investigate global buckling of longitudinal reinforcing steel over two hoop spacings. A deflected shape was assumed and the Ritz method was used to solve for an equivalent lateral tie stiffness in terms of its effective modulus. The distinction was made in this study between ties that behave in flexure and ties that behave in tension to resist buckling of longitudinal steel.

Scribner (1986) also carried out an analytical investigation into global bar buckling using an energy minimization approach similar to Bresler and Gilbert, using elastic tie forces. It was proposed that ties should be at least half the diameter of the longitudinal bar being restrained. An analytical model by Russo (1988) considered the problem of global buckling as a beam-on-elastic-foundation with the tie stiffness depending on geometrical and material characteristics. Papia et al. (1988) made this model more systematic by creating a system matrix and incrementally increasing its size (incrementally increasing the number of hoops in the system) until buckling was identified when the matrix determinant became zero. Essentially, this approach is used to determine E_{eff} in a computational manner. Papia and Russo (1989) used these results to derive a simplified parametric model that determines the stress and strain for a globally buckled bar.

Dhakal and Maekawa (2002c) used an energy minimization approach to determine the required stiffness of lateral ties to prevent global buckling. They then combined this with

their local buckling model (Dhakal and Maekawa, 2002b) and determined the critical buckling load for global buckling, given the stiffness of the lateral reinforcement.

Other analytical studies on global buckling were carried out by Pantazopoulou (1998) and Bayrak and Sheikh (2001). All of these studies assumed some form of elastic or pseudo-elastic tie forces in their formulations. However, it is well recognized that transverse steel invariably yields in situations where global buckling occurs (Sato and Ko, 2007; Dhakal and Maekawa, 2002c), and hence any approach based on stiffness is fundamentally flawed because it is inconsistent with physical reality.

Dutta and Mander (1998) used a virtual work approach to model the global buckling problem. The simplified design equation derived in their study for local buckling was extended to become a function of the hoop geometrical and material parameters. Comparisons with experimental results by other researchers showed good agreement with the predictions of this model. Because this model allows for the fact that transverse steel will yield, it is a fundamentally correct approach to the global buckling problem. Caution is needed, however, to find the correct collapse mechanism since failure to do so will overestimate the buckling capacity of the longitudinal bars.

Falk and Govindjee (2000) developed an analytical model for the global buckling problem. This was represented as an inverted beam-on-elastic foundation problem, where each spring had an associated mass whose inertias needed to be overcome before displacement of the spring (and hence buckling). This associated mass can then be represented as a multiple of the critical load needed to cause buckling in the bar. While the elastic approach is not strictly valid for the reasons outlined above, the model is likely to be a better representation of reality if a very low spring stiffness is used, and some combination of the mass and the spring represent the yield force of the ties.

Bayrak and Sheikh (2001) identified that while Bernoulli's hypothesis is still valid at the stirrup level, it is not valid between stirrups after buckling has occurred, because strains at the section level of longitudinal steel do not match the strains in the concrete at the same level. In order to model the strains between stirrups, the expansive effect of the confined concrete was used to apply a lateral forcing function to the steel bar along its length between stirrups. Elastic and plastic expressions for the maximum deflection of the bar were derived, and this maximum deflection was used to determine which of the 56 experimental stress-strain curves to use in a section analysis. There are several interesting points to note about this study. Firstly, the formulation used to obtain the plastic deflection of the longitudinal bar is based on the assumption of plastic moments at the ends of the bar. This approach may underestimate the actual deflection, since the bar will continue to deflect for a given plastic moment until the onset of strain hardening. Secondly, the assumption used to get the initial imperfection in the bar is questionable. In order to obtain a concrete expansion of the magnitude necessary to deflect a longitudinal bar, significant axial load is required. Such axial load is likely to induce bar buckling. The approach assumes that there is no axial load in the bar at the application of this initial imperfection, which is a highly unlikely situation. As such, it does not seem justifiable for the bar buckling curve to be a function of a significant initial e / d_b (see also Gil-Martín et al., 2006 and 2008). In addition to this, the procedure is cumbersome as it relies on the selection of the appropriate stress-strain curve based on an initial deflection although attempts have been made to characterize these stress-strain relationships (Bae et al., 2005 and Massone and Moroder, 2009).

2.3.2 Experimental Studies

In order to validate global buckling models, experiments have been performed by various researchers. Most of these experiments involve full reinforced concrete members, since it is very difficult to accurately simulate global buckling using bare steel specimens.

Bresler and Gilbert (1961) conducted an experimental study on four reinforced concrete columns. The columns were 8 x 8 x 60 in. reinforced with No.4 Grade 40 steel bars, and subjected to monotonic compression. Two of the columns had 6 longitudinal bars, and two of the columns had 8 bars. Since reinforced concrete columns are usually designed so that the ultimate compressive capacity is much higher than its compressive demand, the tests performed do not reflect current practice. Bar buckling effects are more prominent under combined bending moment and axial load.

Scribner (1986) tested six beam specimens under cyclic lateral load. The beams had different configurations of longitudinal and transverse steel, which consisted of Grade 40 and Grade 60 steel. Two of the specimens tested failed due to pull-out of inadequately anchored longitudinal steel, and two specimens failed in shear due to inadequate shear capacity. In the two specimens where buckling was the cause of failure, buckling occurred in a direction parallel to the face of the column due to the fact that ties were resisting buckling using flexure. This caused the author to prematurely reject his proposal for tie size, as he did not make the distinction between different modes of resistance of transverse steel as Bresler and Gilbert (1961) had done.

Sato and Ko (2007) conducted an experimental investigation into global buckling. They tested four reinforced concrete columns reinforced with 10-19mm diameter bars of Grade 400 steel. Lateral reinforcing varied between specimens, with two of the specimens being jacketed in fiber-reinforced polymer sheets. The columns were fixed at both ends and subjected to a constant axial force of $0.15f'_cA_g$. A cyclic lateral force was then applied to the columns until failure occurred. During the tests, lateral deflections of buckled longitudinal bars were measured as well as stresses and strains in the restraining lateral steel. The ratio of yielded transverse reinforcement region length to buckled-longitudinal bar length was then calculated for each specimen, and it was found that this ratio ranged between 0.45 and 0.76. This is an important finding, since it experimentally

invalidates any global buckling model in which transverse steel is assumed to remain partially elastic.

Moyer and Kowalsky (2003) experimentally examined the effects of tension strain on buckling of longitudinal steel in cyclically loaded reinforced concrete columns. They tested four identical circular columns reinforced with 12-No.6 bars and transverse steel consisting of a No.3 bar at 3 in. pitch. The only variable between specimens was the applied lateral load history. One specimen was subjected to progressively increasing cycles in both directions up to displacement ductility 5. The second specimen was tested similarly up to a displacement ductility of 7 in one direction, but the displacement ductility in the reverse direction was kept at 1 for the whole test. The third and fourth specimens were loaded on one cycle in both directions up to displacement ductility 7 and 9, respectively. By comparing the first two specimens' results, they concluded that the displacement required to induce buckling in the bars subjected to increasing tension was much greater than for bars subjected to equally increasing tension and compression. While these strains can be indirectly related to ultimate curvatures using parametric models, no comment was made in the study about the loads at which buckling occurs.

Other researchers have adopted an empirical approach to constructing models of global buckling in reinforced concrete members. As part of these studies, extensive databases of reinforced concrete member experiments have been built up for a range of loading regimes, geometrical and material parameters, steel configurations and other control parameters. The aim of most of these experiments was not primarily to investigate global buckling however they can still be used for this purpose, particularly where good photographic evidence exists.

Pantazopoulou (1998), for example, constructed a database of over 300 specimens and used these to derive empirical design equations between concrete axial strain, displacement ductility and the required size and spacing of transverse reinforcement. Dhakal and

Maekawa (2002c) collected results from 45 column specimens to validate their model for global buckling. Berry and Eberhard (2005) constructed a database of tests of 62 rectangular-reinforced and 42 spiral-reinforced concrete columns to derive an empirical relationship for the drift ratio at the onset of bar buckling in reinforced concrete columns. Syntzirma et al. (2010), in a similar study, proposed a relationship for the drift ratio at the onset of bar buckling.

2.4 Design Code Requirements

Most concrete codes recognize the need for transverse reinforcement in reinforced concrete columns for confinement of core concrete, resistance of shear forces, and resistance of lateral buckling of longitudinal steel. ACI-318 (2008), for example, stipulates the maximum spacing of transverse steel as the smaller of 16 longitudinal bar diameters, or 48 transverse bar diameters. The first of these limits the unsupported length of longitudinal steel bars, while the second aims to ensure sufficient lateral restraint against global buckling. Within potential plastic hinge regions, the spacing of transverse steel is limited to 6 longitudinal bar diameters. The size of transverse steel in these locations is based more on forces from the dilating core concrete than restricting global buckling (Wight and MacGregor, 2009). Other codes, such as the New Zealand Concrete Code (SNZ, 2006) stipulate that the capacity of transverse reinforcing bars should be at least one-sixteenth the combined capacity of the longitudinal bars being restrained. Although this attempts to size transverse steel to resist global buckling, it is somewhat arbitrary. Both codes also have limits on the configuration of transverse steel, stating that longitudinal bars should be restrained by a corner of a hoop set, and spacing between longitudinal bars being restrained by the same hoop-set should not exceed six inches.

CHAPTER III

COMPUTATIONAL ALGORITHM FOR BUCKLING ANALYSIS

3.1 Introduction

The computational algorithm described in this chapter is designed to carry out a rigorous buckling analysis for a steel reinforcing bar using the routine outlined in Chapter IV. For expediency, the problem was separated into two parts that are solved at each increment of the analysis. The first part involves carrying out a moment-curvature analysis of the critical section of the bar, using a Gauss Quadrature numerical integration scheme. The second part involves satisfying global force equilibrium and displacement compatibility, imposed via an assumed (and later verified) shape function.

The algorithm was coded using the numerical analysis package MATLAB, and consists of a main run function and several subroutines which can be easily modified by the user. The program uses real material and geometric parameters from user inputs, and produces normalized results which allow them to be compared with those from other analyses and experiments.

3.2 Computational Theory

3.2.1 Section Actions for a Given Strain Profile

Invoking Bernoulli's hypothesis for a given curvature ϕ and reference strain ε_o , fiber strains can be found anywhere in the section assuming a linear strain profile:

$$\varepsilon(y) = \varepsilon_o + \phi y \quad (3.1)$$

The corresponding stresses can be found from the steel material model, and Gauss Quadrature is used to numerically integrate the stresses across the section to find the axial load P and bending moment M :

$$P = \int \sigma b(y) dy \quad (3.2)$$

$$M = \int \sigma y b(y) dy \quad (3.3)$$

where σ = material stress and $b(y)$ = section width as a function of y . Equations (3.2) and (3.3) can be solved numerically using Gaussian Quadrature as follows:

$$P = d^2 \{\sigma_s\}^T \{a\} \quad (3.4)$$

$$M = d^3 \{\sigma_s\}^T \{q\} \quad (3.5)$$

in which $\{\sigma_s\}^T = \{\sigma_1, \sigma_2, \dots, \sigma_n\}$ with σ_i being the stress in the i^{th} fiber; $\{a\}^T = \{a_1, a_2, \dots, a_n\}$ with a_i being the normalized fiber area; and $\{q\}^T = \{q_1, q_2, \dots, q_n\}$ with q_i being the normalized first moment of area of each fiber. Using Gauss Quadrature, each fiber is defined by a location factor ξ_i and a weighting factor w_i , obtained from any standard reference such as Hornbeck (1982). Thus for a unit diameter circular section:

$$a_i = \frac{1}{2} w_i \sqrt{1 - \xi_i^2} \quad (3.6)$$

$$q_i = \frac{1}{2} a_i \xi_i \quad (3.7)$$

The parameters for a circular section are given in Table 3.1.

3.2.2 Moment-Curvature Analysis of Critical Section

Obtaining P and M for a given section strain profile does not mean that equilibrium is satisfied at the section level. Instead, it is necessary to iterate on either or both of ϕ and ε_o until both equilibrium and displacement compatibility are obtained. This can be done using the Newton-Raphson algorithm. Considering the first two terms in the Taylor's series expansion of ϕ and ε_o :

$$\begin{Bmatrix} \varepsilon_{o,i+1} \\ \phi_{i+1} \end{Bmatrix} = \begin{Bmatrix} \varepsilon_{o,i} \\ \phi_i \end{Bmatrix} + \begin{Bmatrix} \Delta\varepsilon_{o,i} \\ \Delta\phi_i \end{Bmatrix} \quad (3.8)$$

where the strain and curvature increments are determined from:

$$\begin{Bmatrix} \Delta P_i \\ \Delta M_i \end{Bmatrix} = \begin{bmatrix} \frac{\partial P}{\partial \varepsilon_o} & \frac{\partial P}{\partial \phi} \\ \frac{\partial M}{\partial \varepsilon_o} & \frac{\partial M}{\partial \phi} \end{bmatrix} \begin{Bmatrix} \Delta\varepsilon_{oi} \\ \Delta\phi_i \end{Bmatrix} \quad (3.9)$$

Table 3.1: Integration Points and Weighting Factors for 24-Point Gauss Quadrature

i	Integration Point, ζ_i	Weighting Factor, w_i	Circular Shape Factors	
			a_i	q_i
1, 24	± 0.9951872200	0.0123412298	0.000604670	0.000300880
2, 23	± 0.9747285560	0.0285313886	0.003186850	0.001553157
3, 22	± 0.9382745520	0.0442774388	0.007657593	0.003592462
4, 21	± 0.8864155270	0.0592985849	0.013724373	0.006082748
5, 20	± 0.8200019860	0.0733464814	0.020990321	0.008606052
6, 19	± 0.7401241916	0.0861901615	0.028980158	0.010724458
7, 18	± 0.6480936519	0.0976186521	0.037171262	0.012045229
8, 17	± 0.5454214714	0.1074442701	0.045027848	0.012279578
9, 16	± 0.4337935076	0.1155056681	0.052036015	0.011286443
10, 15	± 0.3150426797	0.1216704729	0.057737354	0.009094865
11, 14	± 0.1911188675	0.1258374563	0.061758941	0.005901649
12, 13	± 0.0640568929	0.1279381953	0.063837721	0.002044623

For a given moment demand that arises from the buckling effect, the incremental reference strain may be found using the first row of (3.9) as follows:

$$\Delta \varepsilon_{oi} = \left(\Delta P_i - \frac{\partial P}{\partial \phi} \Delta \phi_i \right) \bigg/ \frac{\partial P}{\partial \varepsilon_o} \quad (3.10)$$

Alternatively, the incremental curvature may be found using the second row of (3.9):

$$\Delta \phi_i = \left(\Delta M_i - \frac{\partial M}{\partial \varepsilon_o} \Delta \varepsilon_{oi} \right) \bigg/ \frac{\partial M}{\partial \phi} \quad (3.11)$$

The partial derivatives are found from numerical backward differences. Equations (3.10) and (3.11) give rise to two different solution strategies for finding section equilibrium:

- Using (3.10): March forward in constant increments of $\Delta \phi_i$, iterating on $\Delta \varepsilon_{oi}$ to remove an out-of-balance ΔP_i .
- Using (3.11): March forward in constant increments of $\Delta \varepsilon_{oi}$, iterating on $\Delta \phi_i$ to remove an out-of-balance ΔM_i .

Both strategies converge to the same solution.

3.2.3 *Imposing the Shape Function*

To determine what P or M is in each of the above solution strategies, an assumption is usually made. For instance, in a moment-curvature analysis of an RC column, P is usually held constant throughout the analysis. In the case of the buckling analysis, P or M can be determined from the shape function imposed on the bar. The deflected shape at critical load is widely accepted to resemble a sine curve. As such, the eccentricity e and the curvature ϕ are related by the shape function parameters:

$$\phi = 4\pi^2 \frac{e}{s^2} \quad (3.12)$$

Then, from global equilibrium, P and M are related by:

$$M = Pe \quad (3.13)$$

For this analysis, (3.12) is used to impose the shape function on the system and (3.13) is used to check convergence in terms of an out-of-balance e :

$$\Delta e = e_{SF} - M / P \quad (3.14)$$

where e_{SF} is the eccentricity imposed by the shape function. M or P can be adjusted, depending on the solution strategy used, to remove Δe as follows:

$$M_{i+1} = M_i + \frac{\partial M}{\partial e} \Delta e \quad (3.15)$$

$$P_{i+1} = P_i + \frac{\partial P}{\partial e} \Delta e \quad (3.16)$$

The partial derivatives are found using first order numerical backward differences as follows:

$$\frac{\partial y(x)}{\partial x} = \frac{y_i - y_{i-1}}{x_i - x_{i-1}} \quad (3.17)$$

3.3 Computing Procedures

3.3.1 Data Input and Output

Input parameters are written in an input matrix at the start of the run file. This enables a wide range of various steel types at various spacings to be done in one run. The input parameters and their required units are shown in Table 3.2. It is important to note that the program uses the convention that tension is positive. Geometric and material parameters are described more thoroughly in Chapter IV. Material parameters can be determined graphically from a tensile stress-strain plot using a plotting function in Microsoft Excel.

Table 3.2: Input Parameters Used in the Bar Buckling Analysis Program

Input Variable	Description	Units	Range
Material and Geometric Parameters:			
spacing	Vector of normalized spacings of transverse reinforcement, s / d_b	-	> 0
BarDiam	Diameter of reinforcing bar, d_b	mm	> 0
YieldStress	Steel yield stress in tension, f_y	MPa	> 0
YoungsMod	Elastic modulus of steel, E_s	MPa	> 0
ShStrain	Steel strain at which tensile strain hardening commences, ϵ_{sh}	-	> 0
ShMod	Initial slope of tensile strain-hardening portion of steel stress-strain curve, E_{sh}	MPa	> 0
UltStress	Ultimate tensile stress of steel, f_{su}	MPa	> 0
UltStrain	Ultimate tensile strain of steel, ϵ_{su}	-	> 0
InitEccent	Initial eccentricity of quarter-length of steel bar, e_o . User enters the multiplier for this formula, which is based on d_b and s	mm	> 0
Precision and Control Parameters:			
alphaSteel	Defines rate of convergence to yield plateau of steel stress-strain curve	-	> 1 ; even
GradFactor	Multiplier for curvature step in determining $\frac{\partial P}{\partial \phi}$	-	> 0 ; < 1
DeltaRefStrain	Increment of reference strain for moment-curvature analysis, $\Delta \epsilon_o$	-	< 0
CurveIncStep	Increment of reference strain in determining $\frac{\partial P}{\partial \epsilon_o}$	-	> 0
maxits	Maximum number of increments / iterations	-	-
Tolerance	Tolerance for out-of-balance axial load	N	> 0
TolEccent	Tolerance for out-of-balance eccentricity. User enters multiplier for this, which is based on e_o	mm	> 0

As an output, the program writes a text file with tab delimited entries at six point precision, formatted for use in Microsoft Excel for post-processing purposes. The text file displays the following information:

- Input parameters
- Peak axial load, and the corresponding moment, curvature, eccentricity and reference strain
- Stress and strain profiles at various points in the loading history
- A complete history of the axial load, moment, curvature, eccentricity and reference strain

3.3.2 Computational Method for Curvature-Driven Analysis

The buckling analysis can be either strain-driven or curvature-driven. Providing no numerical instability or rounding errors accumulate, both approaches should give essentially the same result. Prior to either approach being used, a small initial eccentricity is applied to ensure that the trivial solution (for $s / d_b = 0$) is not found. In this procedure, the indices i, j and k correspond respectively to an iteration, a point in the section profile, and an increment. A full code listing is given in Appendix A.

STEP 1: The curvature increment $\Delta\phi$ is added to the curvature at the last successful solution to give the new total curvature:

$$\phi_k = \phi_{k-1} + \Delta\phi \quad (3.18)$$

from which the new eccentricity is found via the shape function:

$$e_{SF,k} = \frac{s^2 \phi_k}{4\pi^2} \quad (3.19)$$

STEP 2: From the out-of-balance force remaining from the last iteration, determine the required change in the centroidal strain $\Delta\varepsilon_o$ to find force equilibrium at the new strain profile:

$$\Delta\varepsilon_{oi} = \left(\Delta P_i - \frac{\partial P}{\partial \phi} \Delta \phi_i \right) / \frac{\partial P}{\partial \varepsilon_o} \quad (3.20)$$

where

$$\frac{\partial P}{\partial \varepsilon_o} = \frac{P_{i(+\delta\varepsilon)} - P_i}{\varepsilon_{o,i(+\delta\varepsilon)} - \varepsilon_{o,i}} \quad (3.21)$$

from which the total centroidal strain is found:

$$\varepsilon_{oi} = \varepsilon_{o,i-1} + \Delta\varepsilon_{oi} \quad (3.22)$$

STEP 3: Determine the revised strain profile:

$$\{\varepsilon_j\}_i = \{\varepsilon_o\}_i + \phi_k \{y\} \quad (3.23)$$

STEP 4: Determine the section stresses $\{f_j\}_i$ using the following rules:

- If the strain at a depth y is tensile and has not undergone a strain reversal, then the corresponding tensile stress is found directly from the monotonic stress-strain curve
- If the strain at a depth y is tensile, but has undergone a strain reversal from compression, then the corresponding stress is found from the re-loading stress-strain curve
- If the strain at a depth y is compressive and has not undergone a strain reversal (or has only done so before ε_y), then:
 - 1. The compressive strain is converted to an equivalent tensile strain;

- 2. The corresponding stress is found from the monotonic stress-strain curve in tension;
- 3. The stress is converted back into engineering co-ordinates
- If the strain at a depth y is compressive, but has undergone a strain reversal from a strain greater than ε_y , then:
 - 1. The compressive strain is converted to an equivalent tensile strain;
 - 2. The corresponding stress is found from the reloading stress-strain curve;
 - 3. The stress is converted back into engineering co-ordinates
 - 4. If this is the first increment at which the strain reverses, then the reversal point is stored for future increments of the analysis. The reversal point is only stored at the successful iteration for a given increment.

Integrate to obtain P_i and M_i for the section:

$$P_i = \{f_j\}_i^T \{a_j\} \quad (3.24)$$

$$M_i = \{f_j\}_i^T \{q_j\} \quad (3.25)$$

Hence calculate the out-of-balance force:

$$\Delta P_i = P_{SF} - P_i \quad (3.26)$$

where P_{SF} is the axial load calculated using the shape function.

STEP 5: If $|\Delta P_i| \leq \text{Tolerance}$, then proceed to STEP 6. Otherwise, set $\Delta\phi = 0$, and return to STEP 2.

STEP 6: Calculate out-of-balance eccentricity:

$$\Delta e_i = e_{SF,k} - M_i / P_i \quad (3.27)$$

If $|\Delta e_i| \leq \text{Tolerance}$, then proceed to STEP 7. Otherwise, modify the applied axial load:

$$P_{i+1} = P_i + \frac{\partial P}{\partial e} \Delta e_i \quad (3.28)$$

where

$$\frac{\partial P}{\partial e} = \frac{P_{i(+\delta e)} - P_i}{e_{k(+\delta e)} - e_k} \quad (3.29)$$

Set $\Delta \phi = 0$, and return to STEP 2.

STEP 7: Store strain reversal points (if applicable) for use in future iterations. Store results for the correct step. Calculate the slope of the strain diagram for use in the next iteration:

$$\frac{\partial P}{\partial \phi} = \frac{P_{k(+\delta \phi)} - P_k}{\phi_{k(+\delta \phi)} - \phi_k} \quad (3.30)$$

3.3.3 Computational Method for Strain-Driven Analysis

As with the curvature-driven approach, a small initial eccentricity is applied to ensure that the trivial solution (for $s / d_b = 0$) is not found.

STEP 1: The curvature increment $\Delta \varepsilon_o$ is added to the reference strain at the last successful solution to give the new total curvature:

$$\varepsilon_{ok} = \varepsilon_{ok-1} + \Delta \varepsilon_o \quad (3.31)$$

and the new eccentricity is found via the shape function using the current estimate of the curvature:

$$e_{SF,i} = \frac{s^2 \phi_i}{4\pi^2} \quad (3.32)$$

STEP 2: From the out-of-balance force remaining from the last iteration, determine the required change in the curvature $\Delta\phi$ to find force equilibrium at the new strain profile:

$$\Delta\phi_i = \left(\Delta M_i - \frac{\partial M}{\partial \varepsilon_o} \Delta \varepsilon_{oi} \right) / \frac{\partial M}{\partial \phi} \quad (3.33)$$

where

$$\frac{\partial M}{\partial \phi} = \frac{M_{i(+\delta\phi)} - M_i}{\phi_{i(+\delta\phi)} - \phi_i} \quad (3.34)$$

from which the new estimate of the curvature is made:

$$\phi_i = \phi_{i-1} + \Delta\phi_i \quad (3.35)$$

STEP 3: Determine the revised strain profile:

$$\{\varepsilon_j\}_i = \{\varepsilon_o\}_k + \phi_i \{y\} \quad (3.36)$$

STEP 4: Determine the section stresses $\{f_j\}_i$ using the same rules as for the previous method. Integrate to obtain P_i and M_i for the section:

$$P_i = \{f_j\}_i^T \{a_j\} \quad (3.37)$$

$$M_i = \{f_j\}_i^T \{q_j\} \quad (3.38)$$

Hence calculate the out-of-balance moment:

$$\Delta M_i = M_{SF} - M_i \quad (3.39)$$

where M_{SF} is the axial load calculated using the shape function.

STEP 5: If $|\Delta M_i| \leq \text{Tolerance}$, then proceed to STEP 6. Otherwise, set $\Delta \varepsilon_o = 0$, and return to STEP 2.

STEP 6: Calculate out-of-balance eccentricity:

$$\Delta e_i = e_{SF,i} - M_i / P_i \quad (3.40)$$

If $|\Delta e_i| \leq \text{Tolerance}$, then proceed to STEP 7. Otherwise, modify the applied axial load:

$$M_{i+1} = M_i + \frac{\partial M}{\partial e} \Delta e_i \quad (3.41)$$

where

$$\frac{\partial M}{\partial e} = \frac{M_{i(+\delta e)} - M_i}{e_{k(+\delta e)} - e_k} \quad (3.42)$$

Set $\Delta \varepsilon_o = 0$, and return to STEP 2.

STEP 7: Store strain reversal points (if applicable) for use in future iterations. Store results for the correct step. Calculate the slope of the strain diagram for use in the next iteration:

$$\frac{\partial M}{\partial \varepsilon_o} = \frac{M_{k(+\delta \varepsilon)} - M_k}{\varepsilon_{o,k(+\delta \varepsilon)} - \varepsilon_{o,k}} \quad (3.43)$$

3.4 Extension to Global Buckling Analysis

The algorithm described above can be easily extended to the global buckling case by including an allowance for two key factors. Firstly, the contribution of hoops within the buckled length to the resisting moment must be accounted for, and this can be done with minor modifications to the main algorithm. Secondly, interaction with the concrete

becomes very important, as this is what leads to incipient buckling. This is dealt with by including an additional step prior to the main algorithm. It should be noted that under global buckling the deformed shape will extend over a number of hoops N_h or a number of spaces N_s where $N_s = N_h + 1$. The case for N_h (or N_s) as a minimum is critical. Note $N_s = 1$ or $N_h = 0$ is the local buckling solution.

3.4.1 Contribution of Transverse Steel

From equilibrium of a buckled reinforcing bar, the driving and resisting moments can be written as:

$$P_{cr}\Lambda = M_{pp} + \frac{N_s s}{8} \sum_{j=1}^{N_h} (F_{hj} - C_{hj}) - \frac{s}{2} \sum_{j=1}^{N_h} \langle 0.5N_s - j \rangle (F_{hj} - C_{hj}) \quad (3.44)$$

with

$$F_{hj} = \frac{\pi d_{bh}^2}{4} f_{hj} \quad (3.45)$$

$$f_{hj} = f(y_j / L_h) \quad (3.46)$$

$$y_j = \Lambda - \Lambda \cos\left(\frac{2\pi j}{N_s}\right) + \frac{6\varepsilon_t L_h (N_s - j)s}{L_{ph}} \left(1 - \frac{N_s s}{L_{ph}}\right) \quad (3.47)$$

where Λ = deflection of the buckled bar at the quarter points; N_s = number of hoopsets or spiral spaces in the buckled length; F_{hj} = individual tie forces; f_{hj} = individual tie stresses; and d_{bh} = diameter of the ties. The final term on the RHS allows for displacement due to bulging of the PHZ. The value of ε_t used is the maximum in the loading history. For global buckling, the contribution from the hoops is considered when determining the out-of-balance eccentricity:

$$\Delta\Lambda = \Lambda_{SF} - (M + M_h) / P \quad (3.48)$$

where M_h = the moment resisted by the ties.

3.4.2 Algorithm for Incipient Buckling

Prior to starting the main buckling algorithm (described previously), the following algorithm is run to determine when incipient buckling occurs. No iteration is required, since a solution satisfying equilibrium and displacement compatibility can be found at each step. The theory behind this algorithm is presented in Chapter V, and a full code listing can be found in Appendix A.

STEP 1: Apply an increment of reference strain to the last solution:

$$\varepsilon_{ok} = \varepsilon_{ok-1} + \Delta\varepsilon_o \quad (3.49)$$

from which the transverse strain, eccentricity and curvature can be found directly:

$$\varepsilon_{tk} = \varepsilon_f \left| \frac{\varepsilon_{ok}}{\varepsilon_u} \right|^b \quad (3.50)$$

where $b = \ln(\varepsilon_{ic} / \varepsilon_f) / \ln(\varepsilon_{oc} / \varepsilon_u)$ with $(\varepsilon_{ic}, \varepsilon_{oc})$ being a control point for the relationship between axial and lateral strains;

$$\Lambda_k = \frac{3\varepsilon_{tk} L_h N_s^2 S^2}{4L_{ph}^2} \quad (3.51)$$

$$\phi_k = \frac{4\pi^2 \Lambda}{N_s^2 S^2} \quad (3.52)$$

STEP 2: Determine the revised strain profile:

$$\{\varepsilon_j\}_k = \{\varepsilon_o\}_k + \phi_k \{y\} \quad (3.53)$$

STEP 3: Determine the section stresses $\{f_j\}_k$ using the same rules as for the previous method. Integrate to obtain P_k and M_k for the section:

$$P_k = \{f_j\}_k^T \{a_j\} \quad (3.54)$$

$$M_k = \{f_j\}_k^T \{q_j\} \quad (3.55)$$

STEP 4: Determine the tie force at each level, and hence the contribution of the ties to the resisting moment:

$$M_{hk} = \frac{N_s s}{8} \sum_{j=1}^{N_h} F_{hj} - \frac{s}{2} \sum_{j=1}^{N_h} \langle 0.5N_s - j \rangle F_{hj} \quad (3.56)$$

where F_{hj} is defined in (3.45).

STEP 5: Determine the average concrete nodal force, C_{hk} :

$$C_{hk} = \frac{16(M_k + M_{hk} - P_k \Lambda)}{[N_h^2 + 2N_h + \sin^2(N_h \pi / 2)]s} \quad (3.57)$$

If $C_{hk} \geq 0$, return to STEP 1; otherwise continue to the main buckling algorithm.

3.5 Illustrative Numerical Examples

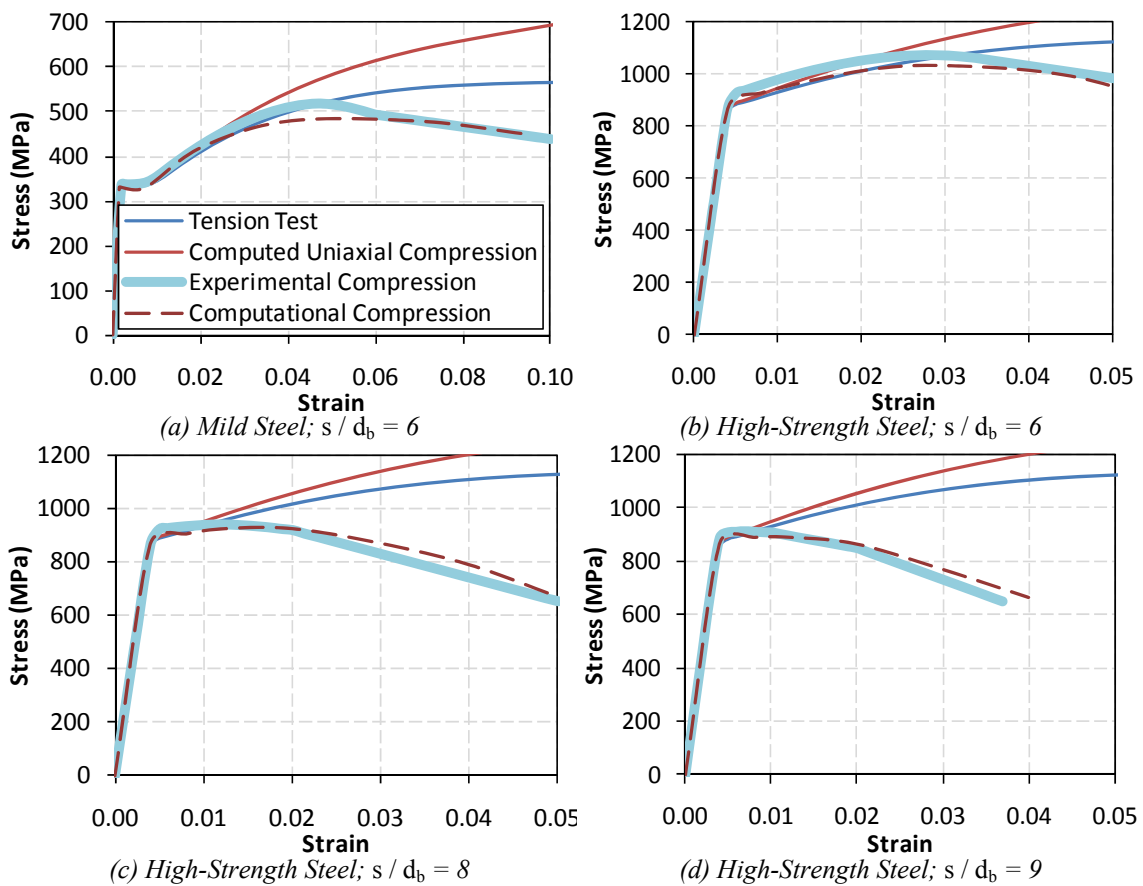
3.5.1 Local Buckling Analysis

As a numerical example, the ASTM A615 deformed reinforcing bar at $s / d_b = 6$ and ASTM A722 type II hot-rolled proof-tested alloy-steel prestressing thread bar with $s / d_b = 6, 8$ and 9 , tested by Mander et al. (1994) were modeled using the computational algorithm described above. The details of the steels are shown in Table 3.3, and the results of this analysis are shown in Fig. 3.1 where they are compared with the tensile, fully restrained compressive, and experimental compressive stress-strain curves. The computational model compares favorably with experiments for the steels analyzed for this comparison, and the model was deemed satisfactory for use in further analyses.

Table 3.3: Steel Stress-Strain Parameters Used in Model Validation

Result*	Bar	s / d_b	f_y (MPa)	f_{su} (MPa)	E_s (GPa)	E_{sh} (MPa)	ϵ_{sh}	ϵ_{su}
T	R	-	331	565	215	8274	0.0091	0.144
CE		6	-338	-531	215	8300	-0.0080	-0.045
T	P	-	869	1130	221	11030	0.0039	0.063
CE		6	-917	-1076	221	12130	-0.0041	-0.028
CE		8	-915	-936	219	4380	-0.0042	-0.012
CE		9	-908	-914	234	1170	-0.0039	-0.007

* T = Tension; CE = Compression, Experimental

**Fig. 3.1:** Validation of Computational Algorithm for Local Buckling Analysis

3.5.2 Global Buckling Analysis

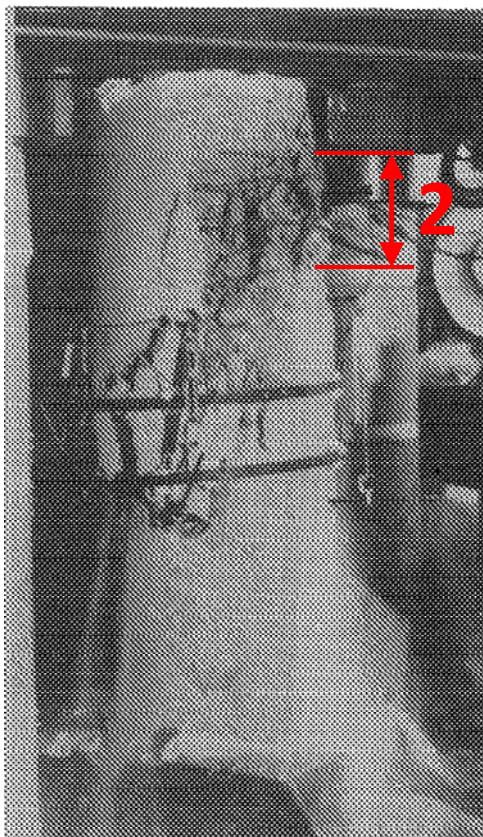
As part of a study on the confinement effects of transverse steel on the core concrete, Mander (1983) tested circular columns under monotonic axial compression. Two of these columns were selected to validate the global buckling model. Photographic evidence (Fig. 3.2) indicates the plausible region over which buckling is possible – that is, where the longitudinal steel is visible. The actual buckling length in terms of N_h can be observed in these photographs. The axial-transverse strain relationship was determined from strain gauges on the hoops. Allowances were made for the geometry of the column, as described in Chapter V. The parameters for each column are shown in Table 3.4. Steel stress-strain parameters were inferred from steels with similar yield strengths.

The predicted stress-strain curves for the steel bars are shown in Fig. 3.3, as are the experimental results from Mander (1983). Since it is virtually impossible to measure the stress-strain history of the compression bars in the column, a buckling stress-strain comparison between experimental and computational results is not feasible. Instead, an analysis was run for each number of hoops over the possible buckling length, and the N_h corresponding to the lowest axial stress was deemed critical case. In both cases, this corresponded to the number of hoops in the possible buckling length. In addition, the strains at incipient buckling for the critical cases are in good agreement with the strains at ultimate column load. As expected, global buckling brings about a rapid deterioration in the axial capacity of the column. Hoop fracture is also predicted to within an acceptable error, given the difficulty in predicting steel fracture strain. These rudimentary checks may not be conclusive validation of the computational algorithm, but they should be enough to provide sufficient confidence that it can predict global buckling behavior with adequate accuracy.

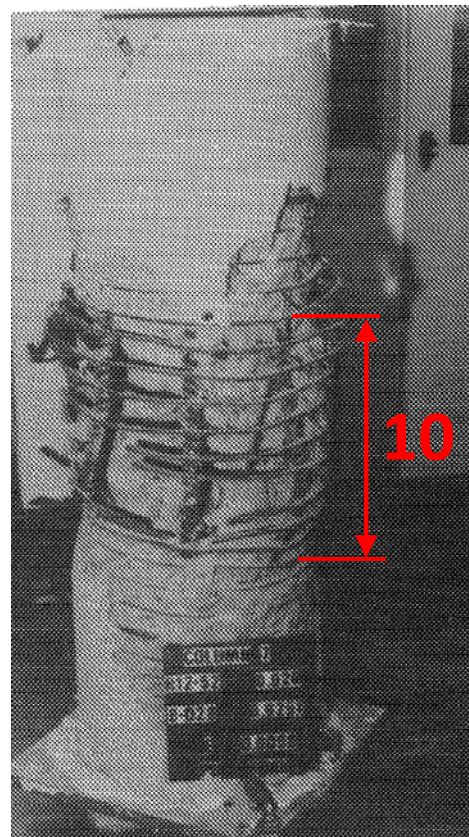
Table 3.4: Column Specimen Details Used in Model Validation

Column*	b	ϵ_u	ϵ_f	f_y (MPa)	f_{yh} (MPa)	N_h Expt	N_h Comp	Reinforcing Details
4	1.90	0.035	0.2	310	320	2	2	12-D16; R10@119
7	1.69	0.06	0.2	300	340	10	10	8-D28; R12@52

* As defined by Mander (1983)

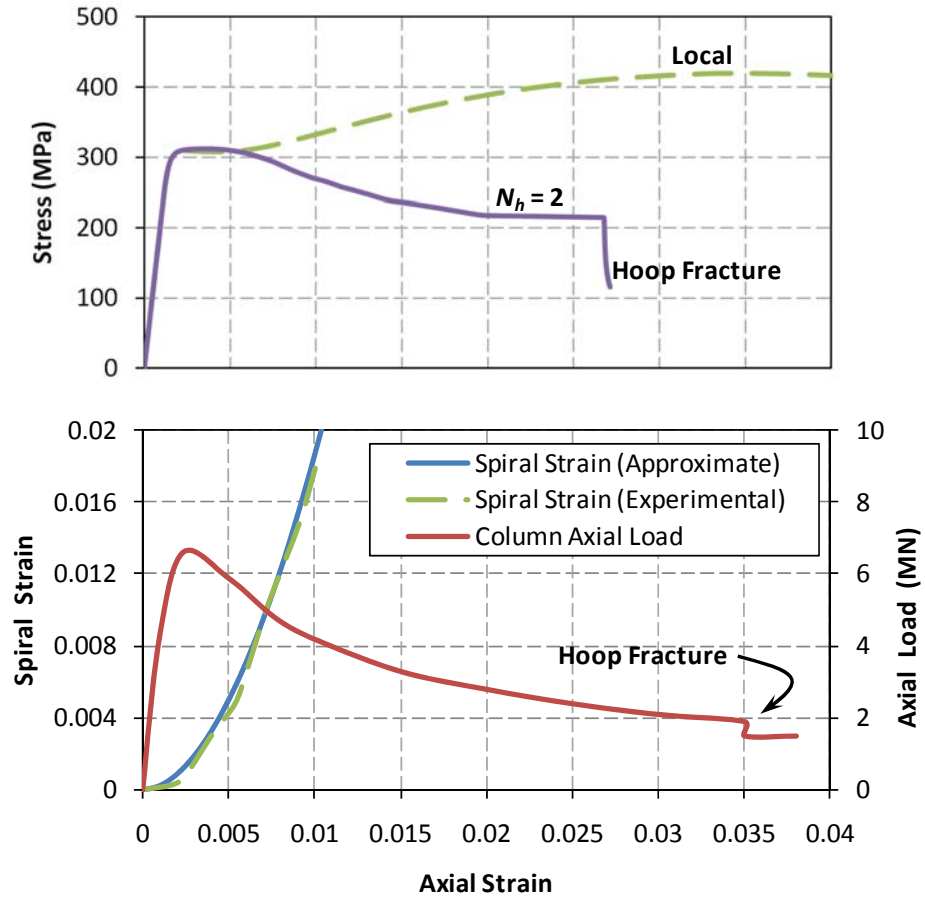


(a) Column Specimen 4



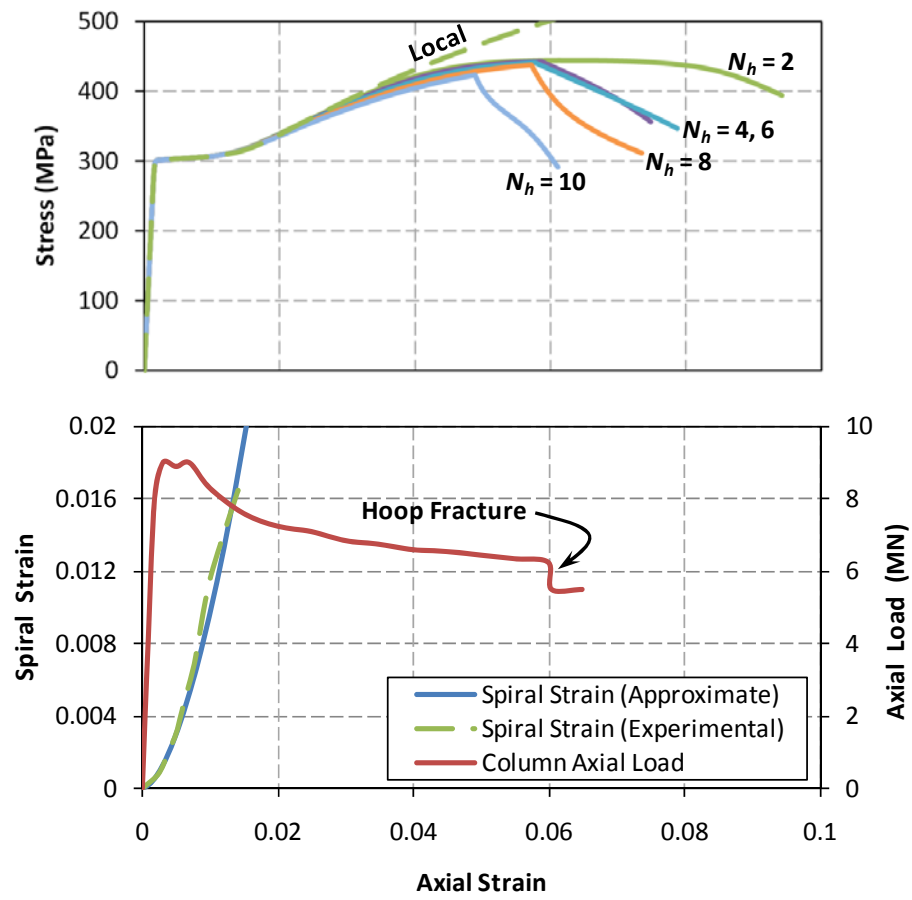
(b) Column Specimen 7

Fig. 3.2: Column Specimens Used for Model Validation Showing Number of Hoops in Buckled Length



(a) Column Specimen 4

Fig. 3.3: Steel Stress-Strain Curves Compared with Column Strains and Axial Loads



(b) Column Specimen 7

Fig. 3.3: Continued

CHAPTER IV

LOCAL BUCKLING ANALYSIS OF LONGITUDINAL REINFORCING BARS

The local buckling behavior of longitudinal reinforcing steel is examined using rational mechanics, taking into account the full plastic behavior of the steel and the effects of true stress and strain. A computational fiber element analysis is used to compute the coupled effect of axial compression and lateral buckling. The results of the computational analysis are then used to develop a simple model for the compressive behavior of longitudinal reinforcing steel in engineering stress-strain coordinates. Although several models exist which are capable of predicting compressive behavior with a moderate degree of precision, these models are generally computationally intensive and therefore of little practical use to structural designers. Other existing simple models either have a high degree of built-in empiricism or are based on overly simplified assumptions about the plastic behavior of the steel. The model developed in this study is compared with available experimental results. A statistical study shows favorable correlation between the proposed analytical model and experimental results.

4.1 Introduction

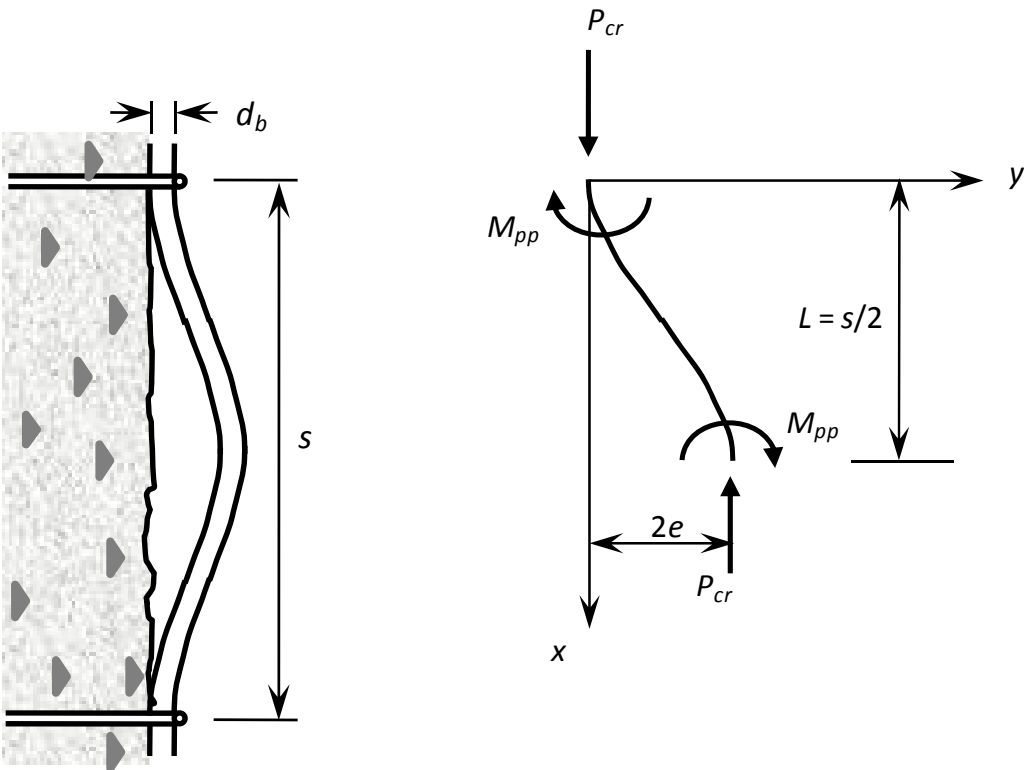
Buckling of longitudinal reinforcing bars is a commonly reported mode of failure in reinforced concrete columns, particularly when exposed to a moderate to high seismic hazard. Insufficient closely spaced transverse (hoop) steel may mean that the longitudinal bars under high compressive strains are inadequately restrained against lateral inelastic buckling when the cover concrete spalls at compressive axial strains of 0.005 or greater. Once buckling commences, these reinforcing bars become less effective in resisting axial deformations; this in turn places a greater demand on the now inadequately confined core concrete. Consequently, lateral buckling of the longitudinal

reinforcement in concrete columns often marks the start of rapid deterioration in moment capacity, particularly under cyclic loading excursions.

If the transverse steel restraining the longitudinal bars is sufficiently strong and the spacing between successive layers is also moderate, then the buckled length will be restricted to two adjacent layers of transverse steel. Such behavior is referred to herein as local buckling and is illustrated in Fig. 4.1. Current design practice to inhibit local buckling (e.g. ACI318-08 and NZS 3101:2006) requires the spacing of the transverse steel in plastic hinge regions not to exceed $6d_b$, where d_b is the diameter of the longitudinal reinforcing bars. This requirement has now existed for many years and is largely based on experimental verification, but has also been validated by analytical studies described below. Existing computational models of local buckling are generally complex, especially for use in design situations. Simplified analytical models that exist often have a high degree of empiricism.

Ideally, it is desirable to have an analytical model that is sufficiently simple to be used for design purposes, yet is also sufficiently accurate for use in computational analyses of structural concrete sections. Such a model should be derived, where possible, from rational mechanics principles and validated against experimental evidence. In particular, the model should be of sufficient accuracy to be used in fiber element analyses of structural concrete members. Although many current models predict experimental data with adequate precision, this may come at a heavy computational cost.

This chapter presents and discusses a selection of previous research on local buckling of reinforcing steel. Several experimental results are then modeled computationally in true stress and strain using a rigorous fiber element analysis with the aim of investigating characteristic aspects of mechanical behavior. Empirical observations of key results are made and these are parameterized to enable the critical inelastic buckling stress and



(a) Physical Problem

(b) One-half Buckled Bar

Fig. 4.1: Local Buckling in a Reinforced Concrete Member

strain to be predicted. These results are then applied in a single analytic equation to enable the entire monotonic compression behavior in engineering stress and strain to be predicted. Comparisons are then made between experimental observations, the computational simulation developed herein and the proposed analytic equation. A statistical assessment is then used to confirm the accuracy of the model.

4.2 Previous Research

4.2.1 Classical Buckling Theories

The problem of elastic buckling of columns was first reported by Euler (1759). Several early theories were posed to explain inelastic buckling, the first of which was the *tangent modulus* theory formulated by Engesser (1889), where the whole cross-section was assumed to buckle with a modulus that is a tangent to the post-elastic stress-strain curve for steel. However, experimental evidence consistently showed that the *tangent modulus* under-predicts column strength, and so Engesser (1891) proposed the reduced modulus theory which allows for the fact while some fibers of the cross-section continue to load with a tangent modulus, other fibers unload with the elastic modulus.

Although the reduced modulus theory may be more accurate, Shanley (1947) posed the *column paradox*. This explained that the reduced modulus theory is only valid for a column that is perfectly straight prior to the onset of buckling. However, since no column is initially perfectly straight, lateral deflections occur before the peak buckling (crippling) load is reached; the reduced modulus theory thus becomes an upper bound solution. As such, the true effective modulus lies between the tangent modulus and the reduced modulus.

4.2.2 Theoretical Models for Local Buckling of Longitudinal Reinforcing Steel

Research into the buckling of longitudinal reinforcing steel commenced with a study by Bresler and Gilbert (1961). Since then, the issue of local buckling in particular has received much attention from researchers. In addition to experimental investigations,

there have been many attempts at formulating suitable models to describe the behavior of reinforcing bars under compressive strains. Early models, for example the one formulated by Mander (1983), involved a linearized solution based on plastic buckling theories developed by Engesser (1891) and Shanley (1947). Other models have been derived using an energy minimization approach, for example by Gomes and Appleton (1997) and Dutta and Mander (1998). While these models are simple and easy to apply, they have invariably been derived using overly simplified assumptions about the plastic behavior of the steel.

Many computational models have also been developed. Studies that utilized a full finite element analysis approach have been carried out by Mau and El-Mabsout (1989), Mau (1990), Dhakal and Maekawa (2002a and b) and Gil-Martín et al. (2006). Other studies, which used a slightly simpler fiber element approach, have been carried out by Dutta and Mander (1998) and Massone and Moroder (2009). Both finite element and fiber element analyses have advantages and disadvantages. The finite element approach can capture the deformed shape and distribution of plasticity quite accurately, but due to constitutive model simplifications may not always be precise at the section level. Conversely, the fiber element approach has the advantage of being quite precise at the critical section because “exact” cyclic constitutive relations can be implemented, however the assumed shape functions for deformations may be slightly imprecise. It is contended however, that both solution approaches are too complex for practical design use. Ideally an analytic function is needed that captures all inelastic behavioral attributes of a buckled reinforcing bar.

Some researchers have examined longitudinal buckling in the context of cyclic loading. Monti and Nuti (1992), for example, developed a rule-based plasticity hardening model, modified for buckling. Rodriguez et al. (1999) developed a simpler model for buckling under cyclic loading conditions based on a modified version of the Euler buckling equation. Kunnath et al. (2009) recently developed a comprehensive cyclic model for

reinforcing steel that included the effects of buckling (using the model from Dhakal and Maekawa, 2002a) and low-cycle fatigue. Again, these models tend to be either computationally expensive or too difficult for direct implementation in design applications.

4.2.3 Experimental Studies on Local Buckling of Longitudinal Reinforcing Bars

Several researchers have carried out experimental investigations on local bar buckling by considering a bar under either concentric or eccentric compression with the ends fixed against rotation. These physical models, described below, are used as the basis for validating the computational model. When considering the results of experimental studies, several important aspects must be examined. Firstly, machining of specimens from reinforcing bars removes the case-hardened shell developed as part of the manufacturing process (González et al., 2006). Secondly, displacement transducers are preferred over strain gauges for measuring axial strain. Strain gauges require the removal of some of the bar deformations, altering the specimen behavior. In addition, strain gauges only measure local strain over a distance of 5mm or so, whereas to capture the full buckling behavior, strains should be measured over some multiple of the effective buckled length. The use of displacement transducers may overcome both of these problems. Thirdly, it is important to realize that plastic stresses and strains increase in reinforcing bars, even after the onset of lateral deflections. As such, experimental studies that report values other than the peak axial stresses and strains may not be useful for comparison with theoretical models. Due to these factors, the experiments by Mander (1983), Mander et al. (1994), Bayrak and Sheikh (2001) and Bae et al. (2005) have been selected for use in this study. Table 4.1 displays the geometric and material properties for these tests. Some details of these experimental investigations follow.

Mander (1983) carried out monotonic compression tests on Grade 275 and Grade 380 steels manufactured in New Zealand. The bar diameters of the specimens were 16mm, 20mm, 24mm and 28mm; s / d_b ratios were 5.5, 6.0, 6.5, 10 and 15; and rates of applied strain ranged from 0.00001 /s to 0.013 /s.

Monti and Nuti (1992) describe a series of monotonic and cyclic tests were performed on FeB44 steel manufactured in Italy. Bar diameters of 16mm, 20mm and 24mm were used, and the s / d_b ratios were 5, 8 and 11.

Mander et al. (1994), as part of a study on low-cycle fatigue behavior in reinforcing steel, carried out cyclic and monotonic compressive tests on ASTM A615 deformed reinforcing bars at $s / d_b = 6$, and on ASTM A722 type II hot-rolled proof-tested alloy-steel prestressing thread bar with s / d_b ratios of 6, 8 and 9.

Rodriguez et al. (1999) conducted an experimental study using monotonic and cyclic test specimens machined from ASTM A706 reinforcing steel commercially available in Mexico. Ratios of s / d_b used were 2.5, 4, 6 and 8. Although the steel from this study was investigated in the computational analyses presented in this paper, the experimental results were not used for verification. This is because machined specimens were used, the ends of the specimen were not adequately restrained against rotation, and compressive stress-strain curves were not presented which could be used for comparison.

Bayrak and Sheikh (2001) conducted an extensive experimental study was conducted by on Grade 400 reinforcing bars loaded in monotonic compression. The bars were all 20mm in diameter. Seven s / d_b ratios were used, which ranged from 4 to 10. Initial “imperfections” (eccentricities) at mid-height, ranging from 0 to $0.3d_b$, were applied to the specimens. Further to the study by Bayrak and Sheikh (2001), tests on No. 8 and No. 10 Grade 60 reinforcing bars from the U.S. were conducted by Bae et al. (2005). The specimens had s / d_b ratios ranging from 4 to 12, and initial eccentricities ranging from 0 to $0.5d_b$.

4.3 Coupled Axial and Lateral Deformation Analysis

As the reinforcing bar buckles under axial compression, lateral deformation and an eccentricity e of the axial load result at the locations of maximum curvature. Therefore, it is necessary to computationally analyze the coupled axial-bending behavior. Thus a computational algorithm is first developed to model the cantilever column shown in Fig. 4.1(b). Section equilibrium is then checked using a force-deformation analysis for each level of e . For computational efficiency the force-deformation analysis was performed using a Gauss-Quadrature technique across the section. Because the buckling problem involves a singularity at the point of buckling, a very small initial eccentricity e_o was applied to the section before application of axial load. This avoids the possibility of finding the trivial solution where $s / d_b = 0$.

4.3.1 Material Characterization

A schematic diagram of the tensile stress-strain curve for reinforcing steel is shown in Fig. 4.2(a). This can be modeled in the form of a single equation as follows:

$$f_s = \frac{E_s \varepsilon_s}{\left\{1 + |\varepsilon_s / \varepsilon_y|^{20}\right\}^{0.05} + |\varepsilon_s / \varepsilon_f|^{20}} + \frac{(f_{su} - f_y)}{1 + |\varepsilon_s / \varepsilon_f|^{20}} \left[1 - \frac{|\varepsilon_{su} - \varepsilon_s|^p}{\left\{|\varepsilon_{su} - \varepsilon_{sh}|^{20p} + |\varepsilon_{su} - \varepsilon_s|^{20p}\right\}^{0.05}} \right] \quad (4.1)$$

in which there are seven control parameters that can be experimentally determined: f_y = yield stress; E_s = Young's modulus; E_{sh} = modulus at the onset of strain hardening; ε_{sh} = strain at the onset of strain hardening; f_{su} = ultimate tensile stress; ε_{su} = strain at ultimate tensile stress; and ε_f = tensile fracture strain. Also, $\varepsilon_y = f_y / E_s$ = yield strain; and the exponent p is calculated from the control parameters, where $p = E_{sh} (\varepsilon_{su} - \varepsilon_{sh}) / (f_{su} - f_y)$. Note that the first and second main parts of (4.1) represent the pre- and post-strain-hardening portions of the stress-strain curve, while the $|\varepsilon_s / \varepsilon_f|$ term in the denominator simulates tensile fracture.

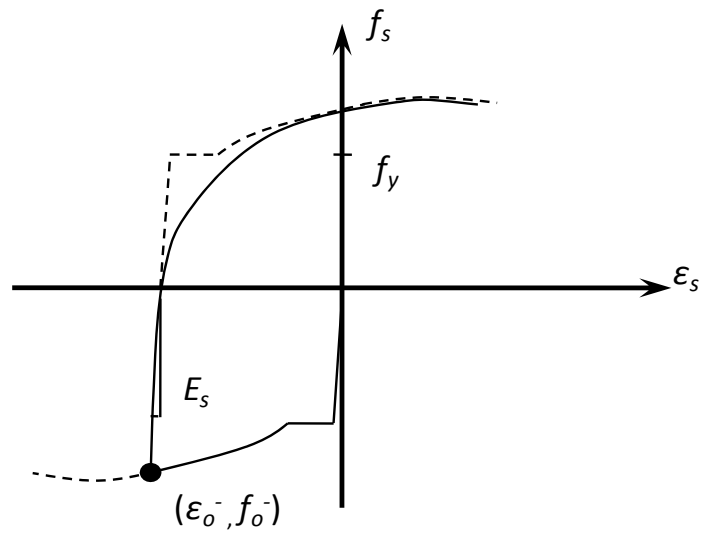
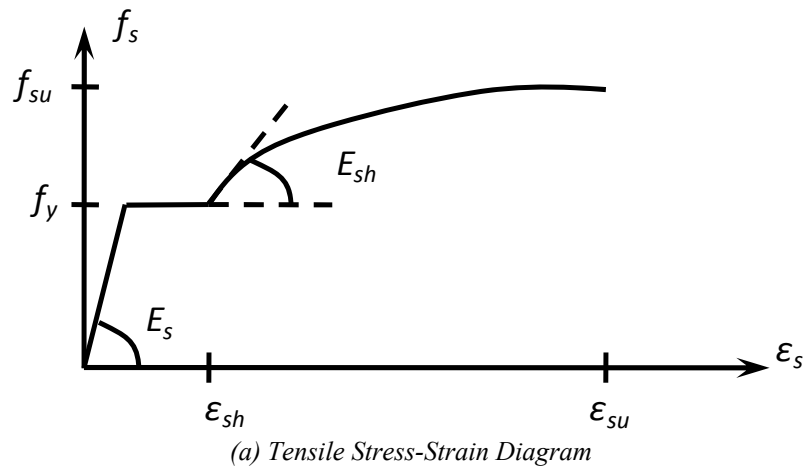


Fig. 4.2: Material Characterization of Steel

The definition of engineering stress uses the initial cross-sectional area of the element. With this definition, experiments show different stress-strain results in tension and compression. However, Dodd and Restrepo (1995) have shown that in terms of natural stress and strain, the behavior in tension and compression is similar. Transformation from tensile engineering stress and strain (f_s, ε_s) to natural stress and strain in compression (f_{cs}, ε_{cs}) can be carried out through the relationships:

$$f_{cs} = -f_s (1 + \varepsilon_s)^2 \quad (4.2)$$

$$\varepsilon_{cs} = -\varepsilon_s / (1 + \varepsilon_s) \quad (4.3)$$

In a buckling analysis it is also necessary to accommodate some cyclic loading effects as some fibers in the bar cross-section will continue to load monotonically, while other fibers may unload from a reversal strain and stress (ε_o^-, f_o^-). Due to the influence of the strain history, the unloading and reloading branches of the stress-strain curve are softer than the monotonic curve. This Bauschinger effect, shown in Fig. 4.2(b), can be modeled by:

$$f_s = f_o^- + E_s (\varepsilon_s - \varepsilon_o^-) \left\{ 1 + \left| \frac{E_s (\varepsilon_s - \varepsilon_o^-)}{f_y - f_o^-} \right|^{qR} \right\}^{-1/R} \quad (4.4)$$

where $R = 2 - 0.4 \varepsilon_o^- \leq 1$; and q = a constant controlling the gradient of the curve. For reinforcing steel with a yield stress of 450 MPa, it was found that $q = 0.935$. This equation is a simplified version of a formulation by Chang and Mander (1994), which in turn is based on the Menegotto-Pinto Equation (1973).

4.3.2 Lateral Deformation Analysis

Consider the case of a reinforcing bar buckled between two successive layers of transverse reinforcing steel spaced at a distance s as shown in Fig. 4.1(a). Assuming the buckled shape function conforms to a cosine curve as in elastic buckling (Euler, 1759),

the deflection, slope and curvature of the bar segment shown in Fig. 4.1(b) may be found as follows:

$$y = e - e \cos\left(\frac{2\pi x}{s}\right) \quad (4.5)$$

where e = the maximum eccentricity at the tip of the cantilever. Differentiating twice gives the curvature:

$$\frac{d^2 y}{dx^2} = 4\pi^2 \frac{e}{s^2} \cos\left(\frac{2\pi x}{s}\right) \quad (4.6)$$

The maximum curvature can thus be written:

$$\phi = 4\pi^2 \frac{e}{s^2} \quad (4.7)$$

from which an exact solution for the buckling curve can be presented in dimensionless form:

$$\frac{s}{d_b} = 2\pi \sqrt{\frac{(e/d_b)}{(\phi d_b)}} \quad (4.8a)$$

It should be noted that a slight difference is expected between the theoretical models and the experimental results. This is because the computational and analytical models were both derived for a circular section, whereas a reinforcing bar has deformations. This affects the results via the radius of gyration, r . By measuring the cross-sectional properties of the reinforcing bar and comparing them with those for a true circle, Mander (1983) found that r for the reinforcing bar is about 0.955 times that for a circle. Thus (4.8a) becomes:

$$\frac{s}{d_b} = 1.5 \sqrt{\frac{(e/d_b)}{(\phi d_b)}} \quad (4.8b)$$

Note that the assumed cosine curve shape function implied in the above formulation will need to be verified later for inelastic buckling.

4.3.3 Axial-Lateral Deformation Coupling

The total buckling strain of the bar is measured between the restrained ends of the buckled bar. At crippling, defined as the maximum buckling load, this strain is:

$$\varepsilon_{cr} = \varepsilon_o + \varepsilon_b \quad (4.9)$$

in which ε_b = secondary (geometric) nonlinear buckling strain; and ε_o = central axial strain which from strain compatibility requirements can be defined in terms of the curvature (see also Fig. 4.3(b)):

$$\varepsilon_o = (\phi d_b)(0.5 - c/d_b) \quad (4.10)$$

Secondary strains ε_b , resulting from the shortening effect of the buckled shape, are dealt with in a similar fashion to that proposed by Dhakal and Maekawa (2002c). Noting that the arc length of the buckled bar spaced between two adjacent stirrups is s , this can be formulated in terms of the deformed shape given by (4.5):

$$s = \int_0^{s(1-\varepsilon_b)} \sqrt{1 + \left(\frac{dy}{dx}\right)^2} dx = 2 \int_0^{s(1-\varepsilon_b)/2} \sqrt{1 + \left(\frac{e\pi}{2s(1-\varepsilon_b)} \sin\left(\frac{2\pi x}{s(1-\varepsilon_b)}\right)\right)^2} dx \quad (4.11)$$

where $s(1 - \varepsilon_b)$ is the net distance between adjacent layers of transverse steel under bending of the reinforced concrete member. Simplifying using a Taylor's series expansion and carrying out the integration leads to the following solution for the secondary strain:

$$\varepsilon_b = \left(\pi \frac{e}{s}\right)^2 \quad (4.12)$$

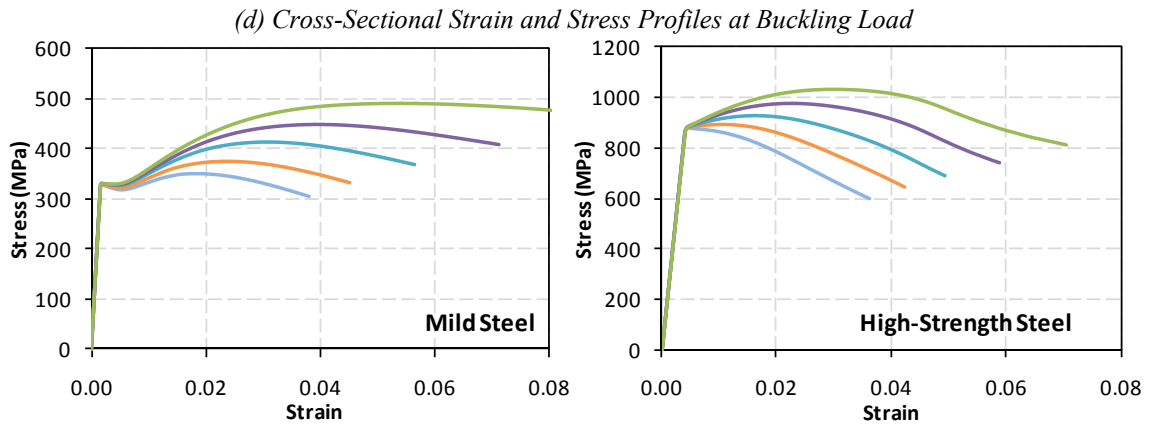
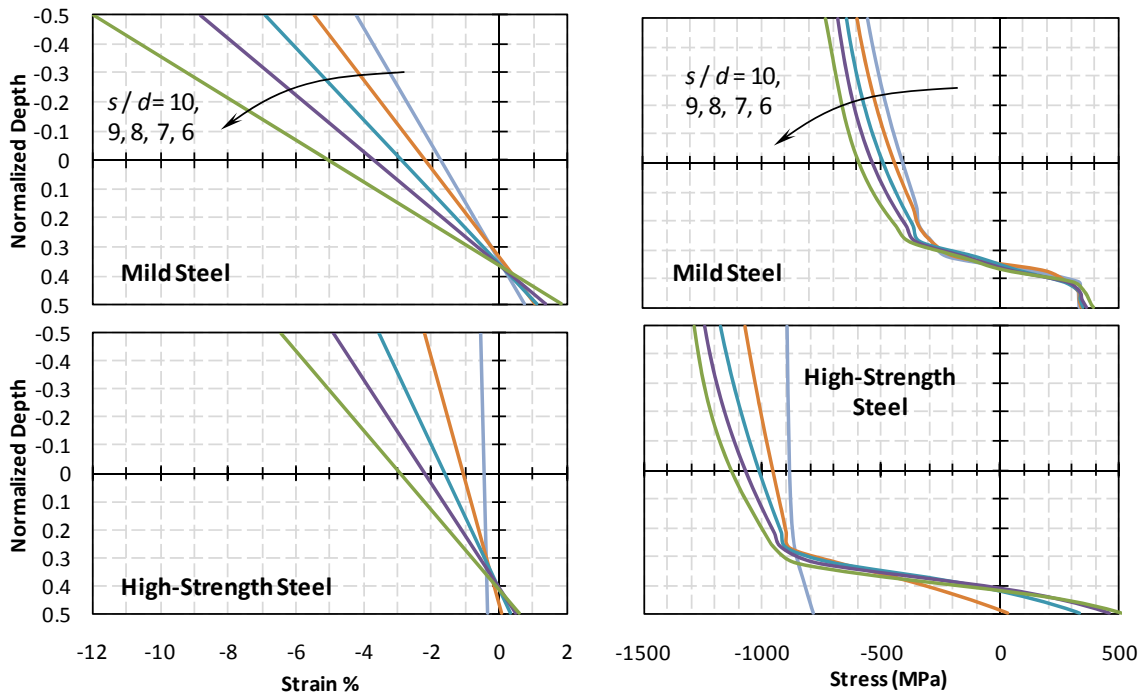
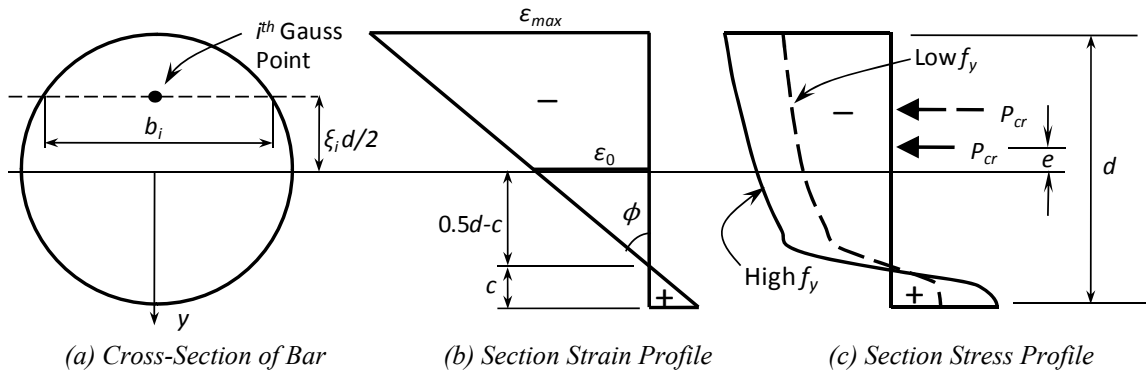


Fig. 4.3: Computational Bar Buckling Analysis – Method and Results

4.3.4 Moment-Curvature Analysis at the Critical Section

A simplified analytical procedure was used to evaluate the behavior of a reinforcing bar during buckling. This involved using a monotonic nonlinear force-deformation analysis procedure to capture the full sectional behavior and relate it to the global behavior. Since there is no active lateral force applied to the reinforcing bar during the buckling process, it is implicitly assumed that shear stresses do not contribute significantly to the deformation behavior, thus uniaxial relationships are assumed for the entire section. Bernoulli's hypothesis is also assumed to apply, thus plane sections remain plane during bending. Hence, if the curvature ϕ and the strain at the centroidal (reference) axis ε_o are known, the strain at any depth $\varepsilon(y)$ can be determined using:

$$\varepsilon(y) = \varepsilon_o + \phi y \quad (4.13)$$

Consider the circular cross-section of a reinforcing bar of diameter d_b shown in Fig. 4.3(a). The strain profile given by (4.13) is shown in Fig. 4.3(b), and Fig. 4.3(c) shows the resulting stress distribution, which can be obtained by applying (4.1) through (4.4). In order to obtain the total axial load P and bending moment M acting on the section, the stresses given by the constitutive relations must be integrated over the section. This can be done using a Gaussian Quadrature formulation, where the section is discretized into n Gauss-points with an associated width b_i and located at a distance $d\xi_i / 2$ from the reference axis, where the subscript i refers to the i^{th} Gauss-point. Each point is assigned an area weighting factor, w_i . The total axial load and bending moment are given in (4.14) and (4.15) respectively.

$$P = \int \sigma b(y) dy = \frac{d}{2} \sum_{i=1}^n w_i \sigma_i b_i = d^2 \{\sigma\}^T \{a\} \quad (4.14)$$

$$M = \int \sigma y b(y) dy = \frac{d^2}{4} \sum_{i=1}^n w_i \xi_i \sigma_i b_i = d^3 \{\sigma\}^T \{q\} \quad (4.15)$$

in which $a_i = 0.5w_i\sqrt{1-\xi_i^2}$ and $q_i = 0.5a_i\xi_i$, where σ_i , w_i and ξ_i are the respective stress, weighting and position factors for the i^{th} Gauss-point.

In the nonlinear buckling analysis, the known variables are the applied curvature, and via an assumed shape function, the eccentricity, e . The analysis proceeds in strain increments, and some iteration is required to ensure strain compatibility and force equilibrium for each step. The coupling of the section axial load P and moment M with respect to the axial strain and curvature at the critical section are found from the following incremental relationship.

$$\begin{Bmatrix} \Delta P_i \\ \Delta M_i \end{Bmatrix} = \begin{bmatrix} \frac{\partial P}{\partial \varepsilon_o} & \frac{\partial P}{\partial \phi} \\ \frac{\partial M}{\partial \varepsilon_o} & \frac{\partial M}{\partial \phi} \end{bmatrix} \begin{Bmatrix} \Delta \varepsilon_{oi} \\ \Delta \phi_i \end{Bmatrix} \quad (4.16)$$

For a given moment demand that arises from the buckling effect, the incremental curvature may be found using the first row of (4.16) as follows:

$$\Delta \phi_i = \left(\Delta M_i - \frac{\partial M}{\partial \varepsilon_o} \Delta \varepsilon_{oi} \right) / \frac{\partial M}{\partial \phi} \quad (4.17)$$

The partial derivatives are found from numerical backward differences. Once the reference strain is found to satisfy section equilibrium, the bending moment must be adjusted to satisfy global equilibrium, and the sectional analysis repeated. Once section and member equilibrium and displacement compatibility are satisfied for a given axial strain, the solution is found for the next increment of strain.

Note that the incremental strain may just as easily be found using the second row of (4.16), with curvature as the known variable at each step. Both methods can be shown to converge to the same solution. Full details of the computational algorithm were explained in Chapter III.

4.4 Results of Computational Buckling Analysis

Rigorous computational analyses of buckling reinforcing bars were carried out on various grades of steel at different hoop spacing to bar diameter ratios (s / d_b). Section stress and strain profiles at crippling were plotted for each type of steel analyzed, as shown in Fig. 4.3(d). Stress-strain curves in compression were also produced for each type of steel (Fig. 4.3(e)). From both sets of plots, it can be seen that the axial strain, average axial stress and section curvature at crippling all increase with decreasing s / d_b ratios. This trend is in agreement with all experimental studies mentioned above. A complete set of computational results is available in Appendix B.

Upon further interrogation of the computational results, the moment-axial stress histories and peaks were plotted for each type of steel, as well as the moment-curvature histories and peaks. These are shown in Figs. 4.4(a) and 4.4(b) respectively. These plots are consistent with the section stress and strain profiles, in that the axial stress and section curvature at crippling increase with decreasing slenderness ratio.

4.4.1 Empirical Observations from Computational Results

From the results of the above analyses, several important observations may be made. First, the neutral axis ratio c / d_b is consistently observed to be about 0.15 for mild steels analyzed, as shown in Fig. 4.3(d). Second, when the peak moment M_{pp} is plotted against the peak buckling stress f_{cr} for each grade of steel, as shown in Fig. 4.4(a), it may be observed that the moment-axial stress interaction diagram for the buckled bar is bounded by three lines as follows:

Line 1: Separates elastic and inelastic performance:

$$\frac{f_{cr}}{f_{su}^-} = \frac{f_y}{f_{su}^-} \quad (4.18)$$

Line 2: Describes the bending moment-axial load failure (strength) surface:

$$\left| \frac{M_{pp}}{M_{pu}^-} \right| + \left(\frac{P_{cr}}{P_{su}^-} \right)^2 = 1 \quad (4.19)$$

where $M_{pu}^- = f_{su}^- d_b^3 / 6$ and $f_{su}^- = f_{su}^+ (1 + \varepsilon_{su})^2$. As the computational results in Fig. 4.4(a) show, for low spacing of lateral steel, the solution approaches Line 2. Although (4.19) represents the exact plastic strength interaction surface if the section is rectangular, Dutta and Mander (1998) showed that for a circular section, (4.19) also gives a sufficiently accurate representation of the failure surface, particularly for high axial loads.

Line 3: At higher slenderness ratios (typically when $s > 4d_b$), the eccentricity of the load begins to affect the interaction between critical stress and peak moment:

$$\frac{M_{pp}}{M_{pu}} = \frac{3\pi}{2} \left(\frac{f_{cr}}{f_{su}^-} \right) \left(\frac{e}{d_b} \right) \quad (4.20)$$

If the stress-strain curve of the steel were elastic-perfectly plastic, then e would be constant for all slenderness ratios. However, due to the presence of strain hardening, e changes as more of the strain hardening curve is engaged during bending. Nevertheless, it may be observed in Fig. 4.4(a) that e is approximately constant for each type of steel. Qualitatively, it can be observed from Fig. 4.3(c) that e will increase as ε_y decreases, since e is most influenced by the post-yield slope. Results for the eccentricity e plotted against the material yield stress ε_y are presented in Fig. 4.4(c). A best fit empirical relationship may be taken as:

$$\frac{e}{d_b} = \frac{0.0011}{\varepsilon_y^{0.75}} \quad (4.21)$$

Another important observation that may be made is that the post-elastic moment-curvature response prior to buckling is essentially linear as is evident from Fig. 4.4(b).

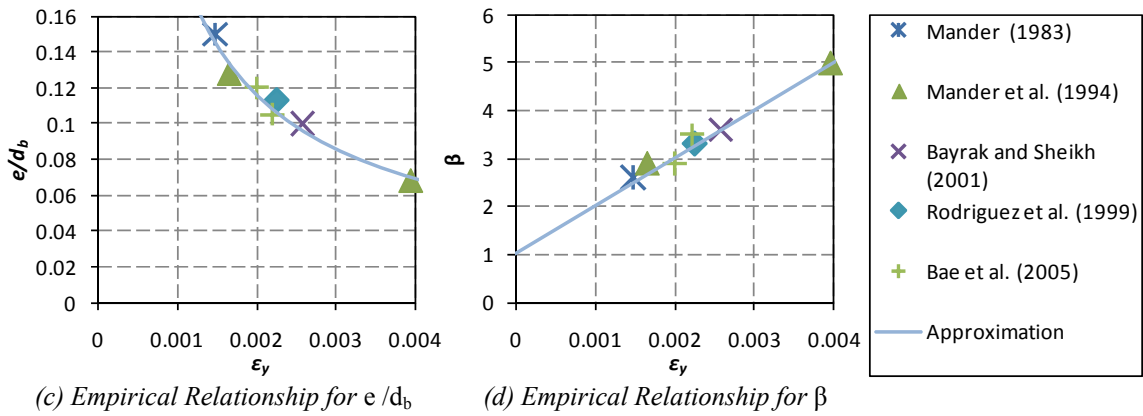
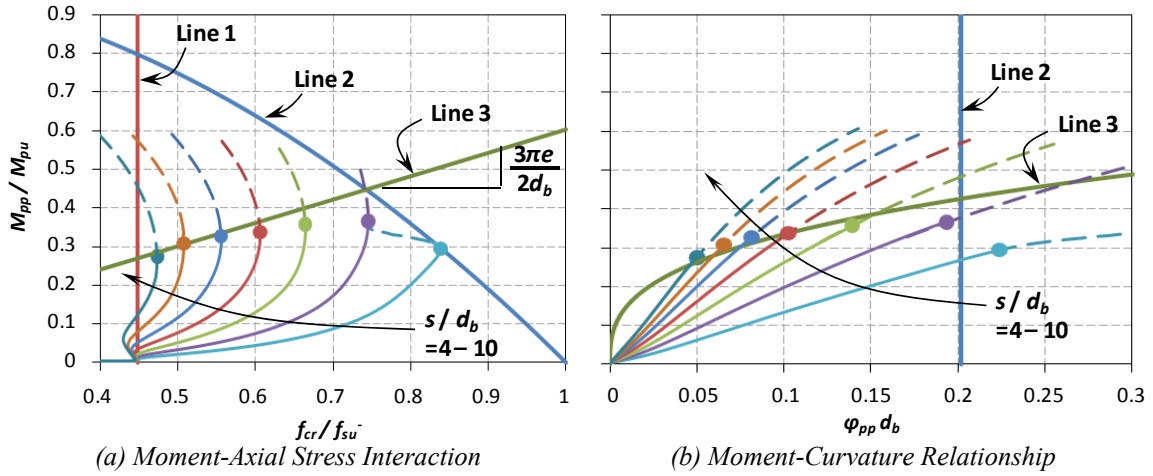


Fig. 4.4: Empirical Observations from Computational Analysis

This justifies the shape function assumption implicitly in (4.8). Also, when the peak curvature ϕ_{pp} is plotted against the peak bending moment M_{pp} , as shown in Fig. 4.4(b), it may be observed that the moment-curvature relationship is bounded by three lines corresponding to Lines 1, 2 and 3 described above:

Line 1: Separates elastic and inelastic performance.

Line 2: Describes the ultimate curvature obtainable at the section level:

$$\phi_{pu}d_b = 1.4\varepsilon_{su} \quad (4.22)$$

Line 3: Can be described by a power curve relationship between bending moment and curvature:

$$\frac{\phi_{pu}}{\phi_{pp}} = \left(\frac{M_{cb}}{P_{cb}e} \right)^\beta \quad (4.23)$$

where P_{cb} = the axial load on the bar at the transition between Lines 2 and 3, and M_{cb} is the corresponding bending moment. The parameter β is an empirically determined constant. From Fig. 4.4(d), it may be observed that β increases linearly with ε_y . A line of best fit is found to be:

$$\beta = 1 + 1000\varepsilon_y \quad (4.24)$$

4.5 Prediction of Ultimate Stress at Crippling

Using the buckling curve expression given by (4.8) and incorporating the empirical observations outlined above, the ultimate stress at crippling can be predicted for the case where Line 2 in Fig. 4.4(a) describes the interaction between bending moment and axial force. From equilibrium, the moment at the fixed end of the buckled shape shall be defined as $M_{pp} = P_{cr}e$, where e = end eccentricity and $P_{cr} = f_{cr}(\pi/4)d_b^2$ = maximum axial force at buckling, therefore:

$$\frac{e}{d_b} = \left(\frac{M_{pp}}{M_{pu}} \right) \frac{M_{pu}}{P_{cr} d_b} = \frac{3}{2\pi} \left(\frac{f_{su}^-}{f_{cr}} - \frac{f_{cr}}{f_{su}^-} \right) \quad (4.25)$$

Substituting (4.22) and (4.25) into (4.8b) gives the required spacing for failure on Line 2 as:

$$\frac{s}{d_b} = \frac{2.34}{\sqrt{\varepsilon_{su}}} \sqrt{\frac{f_{su}^-}{f_{cr}} - \frac{f_{cr}}{f_{su}^-}} \quad (4.26)$$

Thus solving for the buckling stress with respect to the tension coordinates $(\varepsilon_{su}, f_{su}^+)$ and given hoop spacing:

$$f_{cr} = f_{su}^+ (1 + \varepsilon_{su})^2 \left[\sqrt{1 + \frac{(s/d_b)^4}{121} \varepsilon_{su}^2} - \frac{(s/d_b)^2}{11} \varepsilon_{su} \right] \quad (4.27)$$

It is noted that (4.27) is valid for the case where Line 2 in Fig. 4.4(a) describes the interaction between bending moment and axial stress (see Fig 4.4(d)).

To find the coordinates of the transition from strength-based behavior to stability-based behavior, (4.19) and (4.20) are equated:

$$\frac{3\pi}{2} \frac{e}{d_b} = \frac{f_{su}^-}{f_{cb}} - \frac{f_{cb}}{f_{su}^-} \quad (4.28)$$

Substituting the empirical observation from (4.21) into (4.28) and solving the resulting quadratic results in f_{cb} / f_{su}^- , the axial stress ratio at the intersection of Lines 2 and 3:

$$\frac{f_{cb}}{f_{su}^-} = \sqrt{1 + \frac{\pi^2}{1.47 \times 10^6 \varepsilon_y^{1.5}}} - \frac{\pi}{1200 \varepsilon_y^{0.75}} \quad (4.29)$$

and the corresponding s / d_b ratio can be obtained applying the result from (4.29) in (4.26):

$$\left(\frac{s}{d_b}\right)_{cb} = \frac{2.34}{\sqrt{\varepsilon_{su}}} \sqrt{\frac{f_{su}^- - f_{cb}}{f_{cb} f_{su}^-}} \quad (4.30)$$

Hence the spacing of transverse steel for stability-based behavior may be formed as:

$$\left(\frac{s}{d_b}\right)^2 = \left(\frac{s}{d_b}\right)_{cb}^2 \left(\frac{f_{cb}}{f_{su}^-}\right)^\beta \left(\frac{f_{su}^-}{f_{cr}}\right)^\beta \quad (4.31a)$$

$$\left(\frac{s}{d_b}\right)^2 = \left(\frac{s}{d_b}\right)_{cb}^2 \left(\frac{f_{cb}}{f_{su}^-}\right)^\beta \left(\frac{f_{su}^+}{f_{cr}}\right)^\beta (1 + \varepsilon_{su})^{2\beta} \quad (4.31b)$$

For the case where $(s/d_b) \geq (s/d_b)_{cb}$ the expression for f_{su}^- is found by rearranging (4.31b):

$$f_{cr} = f_{su}^+ (1 + \varepsilon_{su})^2 \left(\frac{f_{cb}}{f_{su}^-}\right) \left(\frac{(s/d_b)_{cb}}{s/d_b}\right)^{\frac{0.5}{\beta}} \quad (4.32)$$

where $|f_{cr}| \geq f_y$.

4.5.1 Simplified Analysis of Ultimate Failure Stress

Alternatively to (4.27) and (4.32), an approximate expression for f_{cr} can be written using a linearized moment-axial load interaction surface. The simplified interaction surface is:

$$\frac{M_{pp}}{M_{pu}} = 2 \left(1 - \frac{f_{cr}}{f_{su}^-}\right) \quad (4.33)$$

Substituting (4.22), (4.25) and (4.33) into (4.8b) gives the simplified hoop spacing at failure:

$$\frac{s}{d_b} = \frac{3.3}{\sqrt{\varepsilon_{su}}} \sqrt{\frac{f_{su} (1 + \varepsilon_{su})^2}{f_{cr}} - 1} \quad (4.34)$$

From (4.34), the simplified critical buckling stress is found to be:

$$f_{cr} = \frac{f_{su}^+ (1 + \varepsilon_{su})^2}{1 + (s/d_b)^2 \varepsilon_{su} / 11} \quad (4.35)$$

4.5.2 Application to Experimental Results

The curves given by (4.27), (4.32) and (4.35) are displayed in Fig. 4.5, along with experimental and computationally predicted values for the six of the steel types analyzed. As this figure shows, the computational and experimental values are well-predicted by the full analytical model. In addition, the approximate curve given by (4.35) compares favorably well for all values of f_{cr} above yield. It can also be observed from Fig. 4.5 that the code-specified limit on the spacing of transverse steel to $s / d_b = 6$ is sufficient to ensure failure above f_y .

4.6 Prediction of Strain at Crippling

Using (4.8b) again, but with different empirical observations, an expression for the strain at crippling can be derived. Combining (4.8b), (4.9), (4.10) and (4.12) leads to the solution for the buckled shape in terms of geometry and strain:

$$\frac{s}{d_b} = 1.5 \sqrt{\frac{(e/d_b)[0.5 - c/d_b + 0.25(e/d_b)]}{\varepsilon_{cr}}} \quad (4.36)$$

The total buckling strain at crippling ε_{cr} can be predicted using (4.36), incorporating the simplifying assumptions derived above. Substituting $c / d_b = 0.15$ and (4.21) into (4.36) and applying the shape correction factor, one obtains the results for the compressive buckling strain ε_{cr} as follows. For the case where the ultimate strength surface limits the buckling capacity (Line 2):

$$\varepsilon_{cr} = \frac{0.014 \varepsilon_y^{0.75} + 11 \times 10^{-6}}{(s/d_b)^2 \varepsilon_y^{1.5}} \quad (4.37)$$

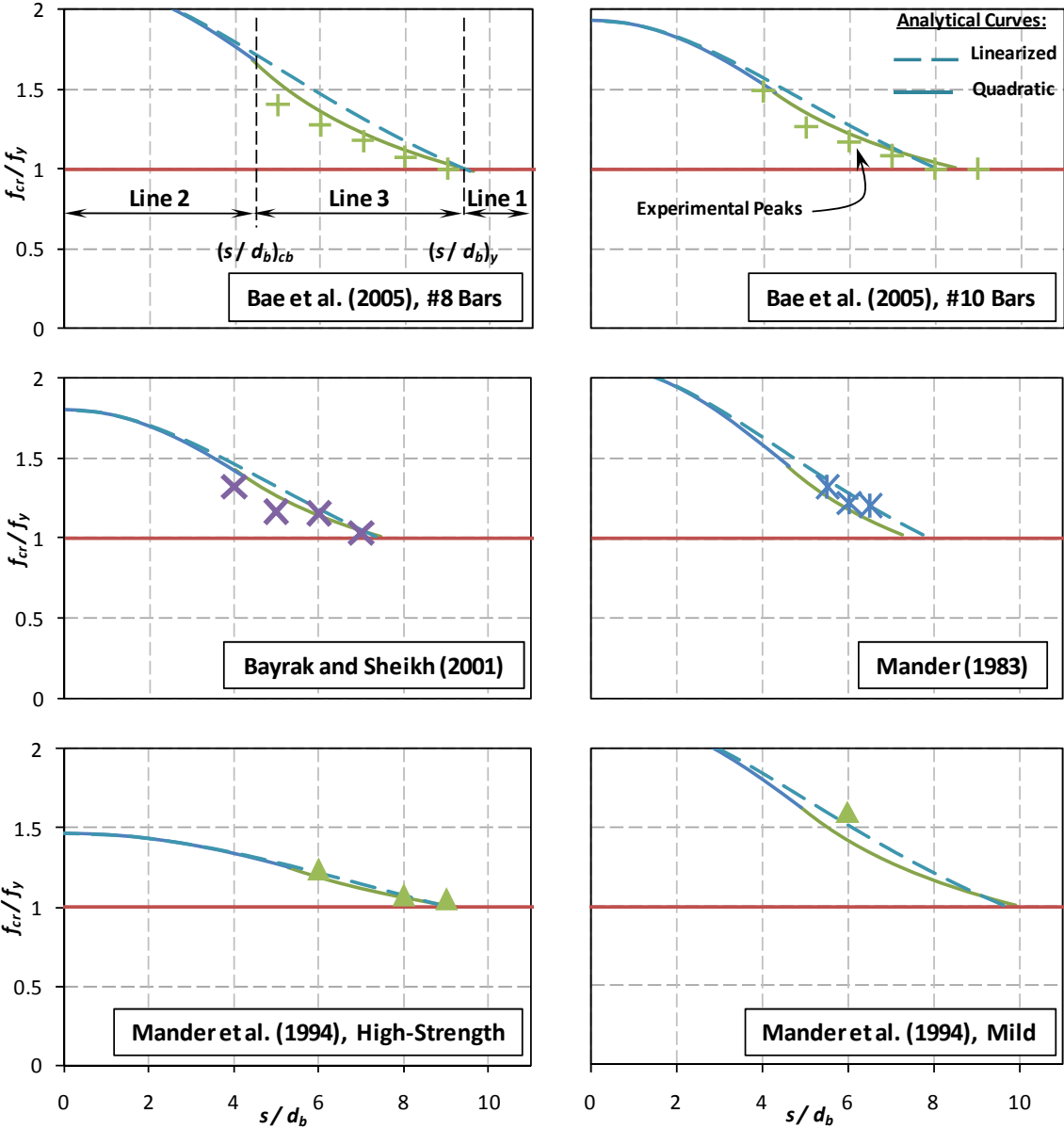


Fig. 4.5: Generalized Analytical Buckling Curves with Experimental Values

For the case where stability limits the buckled capacity (Line 3):

$$\varepsilon_{cr} = \frac{0.405}{(s/d_b)^2} \left(\frac{f_{su} (1 + \varepsilon_{su})^2}{f_{cr}} + 1.52 \right) \left(\frac{f_{su} (1 + \varepsilon_{su})^2}{f_{cr}} - 2.82 \right) \quad (4.38)$$

where $|\varepsilon_{cr}| \geq \varepsilon_y = f_y / E_s$.

4.7 Implementation of Analytical Model

First, prior to applying the results to an overall stress-strain analytical model it is necessary to check whether the predicted crippling stress and strain agree well with experimental observations. This is shown in Fig. 4.6. Although the agreement is evidently not perfect, it will be subsequently shown to be satisfactory. The results of 24 monotonic compression tests on steel bars were selected for model validation and a computational study was carried out for each experimental result. The tensile steel parameters for each type of steel are given in Table 4.1.

Table 4.1: Properties of Steel Bars Tested in Monotonic Compression

		f_y (MPa)	f_{su} (MPa)	E_s (GPa)	E_{sh} (MPa)	ε_{sh}	ε_{su}	$(s / d_b)_{cb}$	f_{cb} (MPa)
1	H16	360	567	200	6000	0.016	0.15	5.17	558
	D16	295	433	200	3500	0.025	0.19	4.95	435
	D20	286	446	200	4000	0.023	0.18	5.14	438
	D24	260	429	195	4500	0.018	0.18	5.33	410
	D28	296	484	203	4700	0.015	0.17	5.22	471
2	H.S.	869	1130	221	11030	0.0039	0.063	5.73	1094
	Mild	331	565	215	8274	0.0091	0.144	5.44	540
3		449	730	200	9000	0.0089	0.12	5.32	712
4		515	690	200	5500	0.012	0.16	4.37	739
5	#8	437	728	199	9000	0.0092	0.147	4.85	741
	#10	444	638	202	7000	0.0091	0.158	4.65	666

¹Mander (1983); ²Mander et al. (1994); ³Rodriguez et al. (1999); ⁴Bayrak and Sheikh (2001); ⁵Bae et al. (2005)

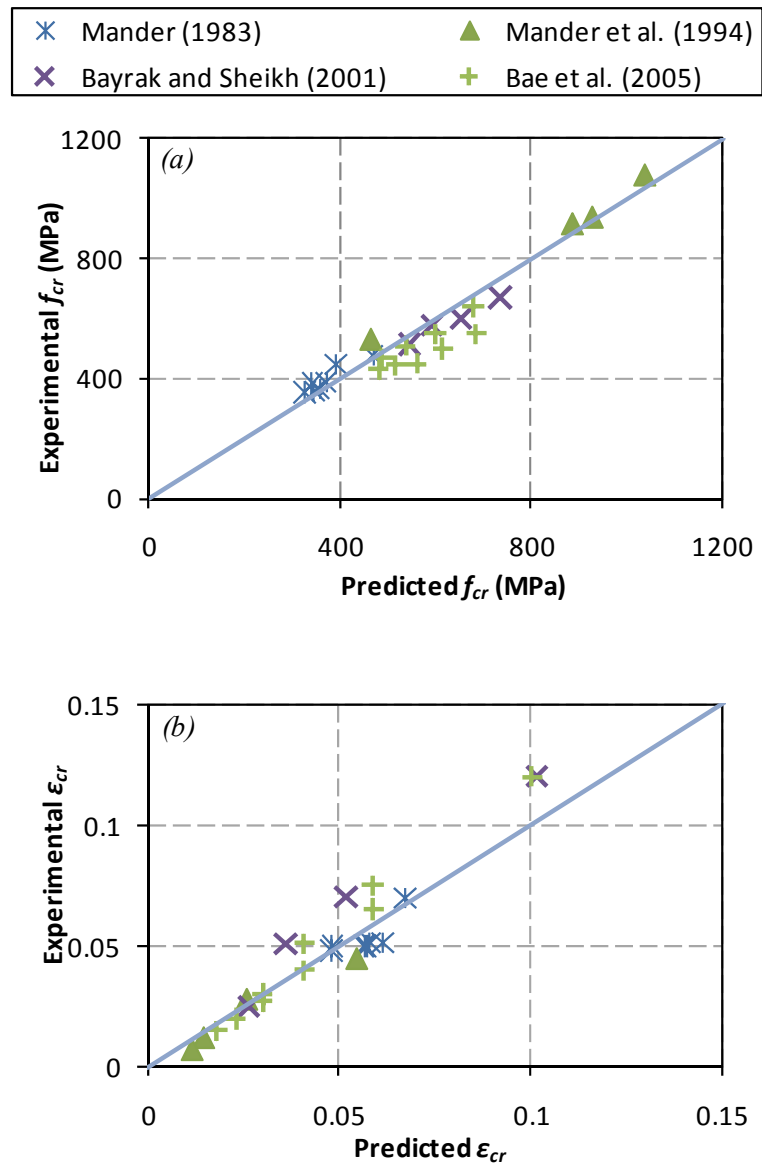


Fig. 4.6: Comparison between Experimental and Analytically Predicted Stress and Strain Values

4.7.1 Summary of Analytical Modeling Parameters

The model derived above for s / d_b may be used in design applications. However, it is desirable to characterize the full compressive stress-strain curve for use in predictive analysis. This can be done using a version of (4.1), modified for compression:

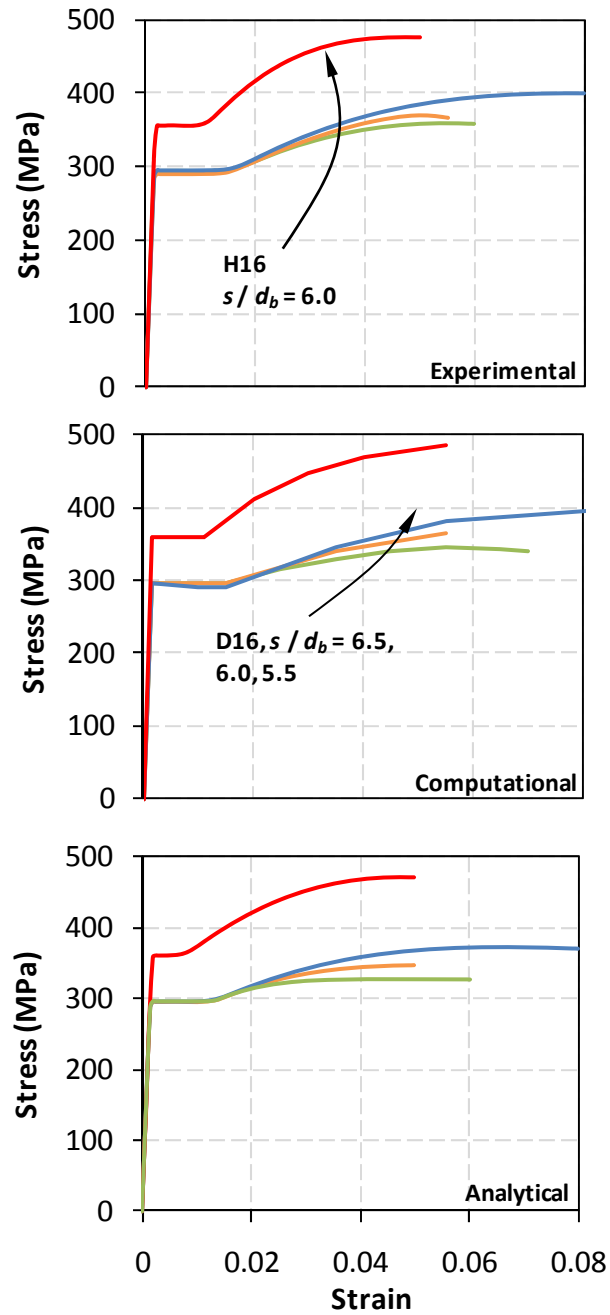
$$f_s = \frac{E_s \varepsilon_s}{\left\{1 + |\varepsilon_s / \varepsilon_y|^{20}\right\}^{0.05} + \gamma \left\{1 + |\varepsilon_s / 2\varepsilon_{cr}|^{40}\right\}^{0.05} - \gamma} + (f_{cr} - f_y) \left[1 - \frac{|\varepsilon_{cr} - \varepsilon_s|^p}{\left\{|\varepsilon_{cr} - \varepsilon_{sh}|^{20p} + |\varepsilon_{cr} - \varepsilon_s|^{20p}\right\}^{0.05}} \right] \quad (4.39)$$

in which the control parameters are defined as for (4.1), with the addition that f_{cr} = ultimate compressive (crippling) stress and correspondingly ε_{cr} = crippling strain. The exponent p is calculated from the control parameters, where $p = E_{sh} (\varepsilon_{cr} - \varepsilon_{sh}) / (f_{cr} - f_y)$. The parameter $\gamma = 4$ for mild steel and $\gamma = 2$ for high-strength steel. This parameter is used to model the shape of the descending branch of the post-peak curve. The strain at the onset of strain-hardening in compression ε_{sh}^- is calculated as:

$$\varepsilon_{sh}^- = 0.5 (\varepsilon_{sh}^+ + \varepsilon_y) \quad (4.40)$$

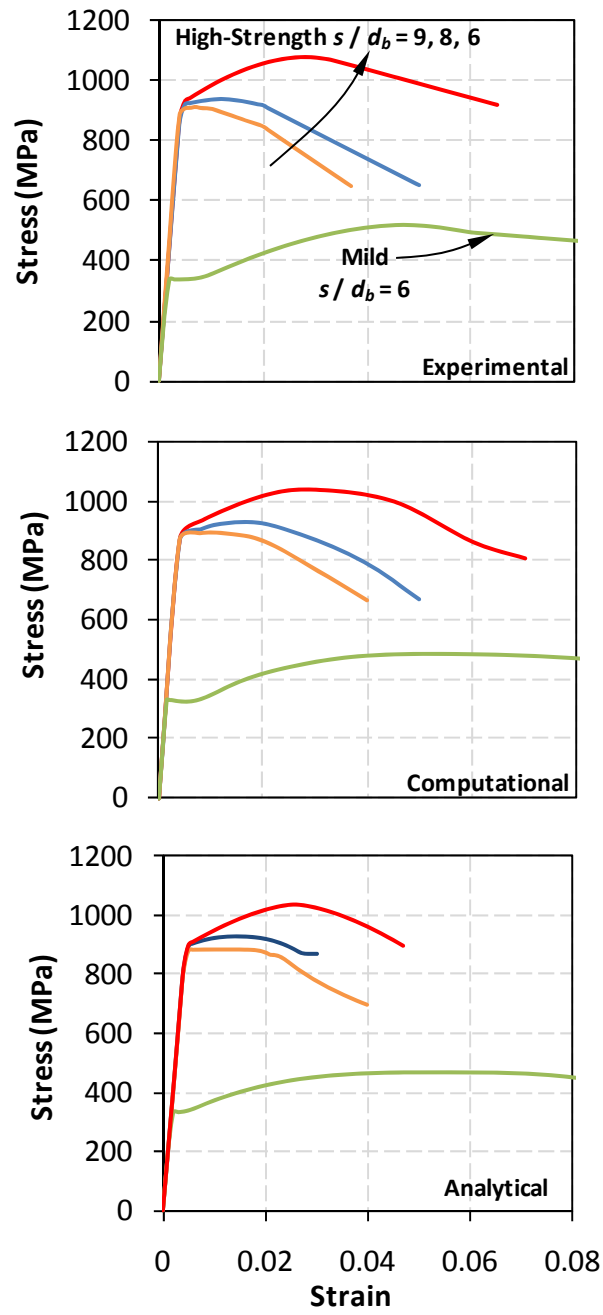
This expression is validated by experimental tests, and has physical significance. At the onset of strain hardening in compression, the curvature induced by buckling means that only the extreme compression fiber will experience strain hardening at this point. Most of the rest of the section will be at yield stress, with the extreme tension fiber dropping down to zero. As such, the average strain on the section at the onset of strain hardening will be the average of ε_{sh} and zero, and (4.40) holds true.

The computational and analytical models were used to predict the full stress-strain curves for the steels described in Table 4.1. A selection of these is shown in Fig. 4.7. Since the computational analysis was carried out without consideration of the shape of



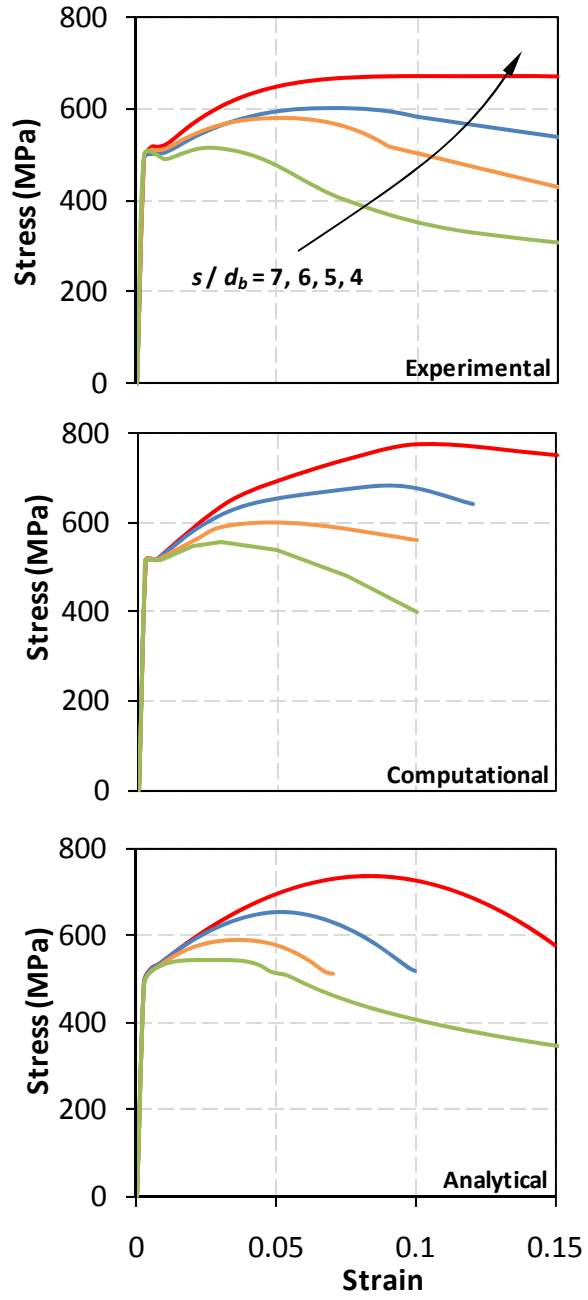
(a) Mander (1983)

Fig. 4.7: Compressive Stress-Strain Curves: Experimental, Computational and Analytical



(b) Mander et al. (1994)

Fig. 4.7: Continued



(c) Bayrak and Sheikh (2001)

Fig. 4.7: Continued

the bar, it is expected that this will overestimate the experimental results slightly. The analytical predictions have been corrected for the expected bias. Overall, there is good agreement between the three plots in terms of peak values and overall shape, especially considering the low computational effort used to obtain these plots.

4.8 Chapter Closure

This chapter has presented a direct computational model to predict the compressive axial force-deformation behavior of reinforcing bars including the effects of local buckling that occurs between hoop-sets. Empirical observations from this computational analysis were then used to derive expressions for the critical buckling stress and strain at crippling (f_{cr} , ε_{cr}). In turn, this coordinate is used along with a single equation to give the complete stress-strain behavior in compression.

The following conclusions can be drawn from this study:

1. An analytical model is provided to define the compressive crippling strain and stress coordinate (ε_{cr} , f_{cr}), a necessary ingredient to predict the overall stress-strain behavior of reinforcing bars in compression restrained by closely spaced hoops such that $s / d_b < 10$.
2. Plastic buckling behavior can be characterized by the s / d_b ratio. At s / d_b ratios above $(s/d_b)_{cb}$, the transverse steel is spaced sufficiently close such that the compressive capacity of longitudinal bars is governed by strength. For s / d_b ratios below $(s/d_b)_{cb}$, compressive capacity is limited by buckling, but enhanced by strain hardening in the bar.
3. The analytical model developed in this study for local buckling of longitudinal reinforcing bars compared favorably to experimental and computational results, after adjusting for the fact that the cross-section of the bar is not perfectly circular.

4. Although dependent on the grade of steel, current code requirements limiting the s / d_b ratio to 6 appears to be satisfactory in ensuring sufficient capacity from compressive steel under local buckling conditions.

CHAPTER V

GLOBAL BUCKLING ANALYSIS OF LONGITUDINAL REINFORCING BARS

In this chapter, the global buckling behavior of longitudinal reinforcing steel is examined using rational mechanics, taking into account the full plastic behavior of the steel and the effects of true stress and strain. In addition the inextricable coupling between global buckling and other aspects of column behavior, such as confinement and dilation of the core concrete, shear and low-cycle fatigue is explored. A computational fiber element analysis is used to compute the coupled effect of axial compression and lateral buckling. General trends are observed, and simplified design and analysis equations are derived. Although several computational and analytical models exist for global buckling, they often assume elastic or quasi-elastic tie forces. Also, no experiments are known to have been performed on the global buckling phenomenon in isolation from other column behavior, so models of this nature may be regarded as somewhat speculative.

5.1 Introduction and Motivational Background

Buckling of longitudinal steel in reinforced concrete (RC) columns often leads to a rapid deterioration in moment capacity, particularly under cyclic loads. In situations where substantially sized (strong) transverse reinforcement exists, the buckled length will be restricted to the spacing between two hoopsets or the spiral pitch. This is referred to as local buckling, and was the subject of Chapter IV. In many instances, the strength of the transverse steel is inadequate to restrict the buckled length of the bar to two hoopsets, and thus global buckling may occur as shown in Fig. 5.1(a). This chapter demonstrates that this mode is less desirable as the deterioration in moment capacity is more rapid.

Currently, design codes such as ACI 318-08 impose transverse steel ratios based on confinement requirements with the aim of preserving axial load capacity, with the

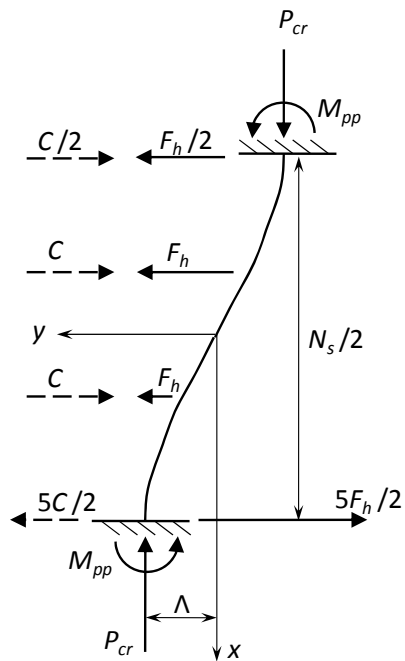
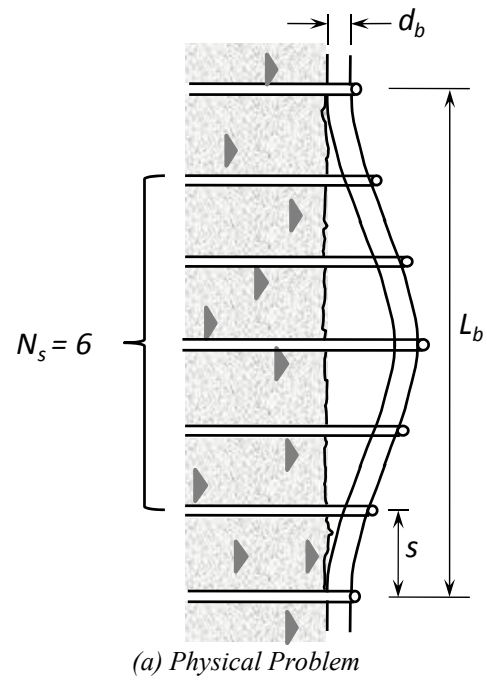


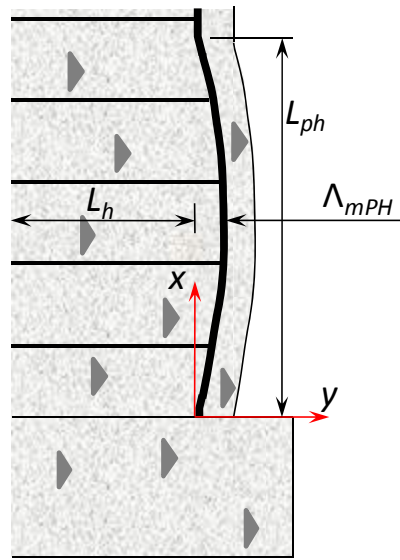
Fig. 5.1: Global Buckling in a Reinforced Concrete Member

spacing of hoopsets restricted to $s = 6d_b$ for local buckling requirements. This leads to a dilemma for structural designers about whether to specify large diameter bars in hoops or spirals at the maximum spacing ($6d_b$), or to use more closely spaced, smaller diameter bars for the hoopsets or spirals. In circular columns, the latter is common and will almost certainly lead to global buckling. Some codes (e.g. NZS 3101:2006) stipulate that the strength of the transverse steel must be at least one-sixteenth the combined strength of the longitudinal bars being restrained. While this requirement attempts to size the steel to inhibit global buckling, it appears somewhat arbitrary and has not been investigated in great detail.

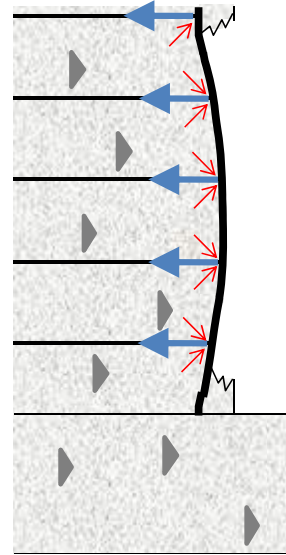
Clearly, there is a need to be able to predict the required strength of transverse steel to prevent global buckling, and conversely, to predict the capacity of a longitudinal bar for a given size and configuration of transverse steel. Where possible, these predictions should be based upon rational mechanics constructs and validated against available experimental observations. Unlike the case for local buckling, this is an area of research that is still largely unexplored, despite being the critical mode of failure in many RC columns.

In developing a model for global buckling of longitudinal reinforcing steel, it is important to pinpoint its cause as this will have a substantial impact on the compressive stress-strain history of the steel. As such, a qualitative analysis of the behavior in the plastic hinge zone (PHZ) is warranted.

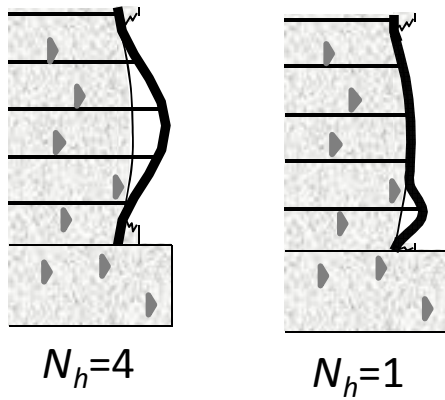
Consider a RC column under general compressive axial load and bending moment. As the axial strain on the compressive side of the plastic hinge (Fig. 5.2(a)) increases, this region of the column will bulge outward. Initially this is due to Poisson's effect, and then by core concrete dilation after spalling of the cover concrete. Eventually, a displacement incompatibility between the steel cage and the cover concrete will cause the cover to spall off, as shown in Fig. 5.2(b). Once this happens, the lateral confinement of the core



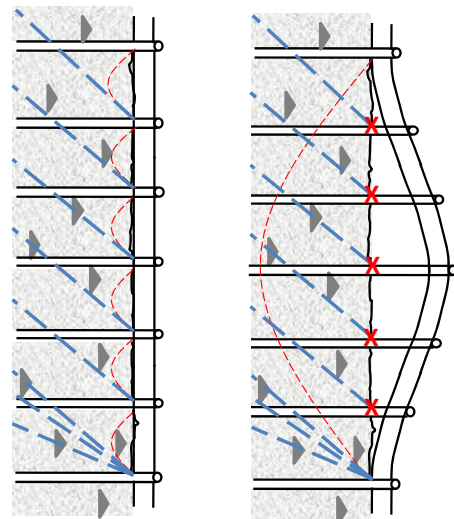
(a) Initial Expansion



(b) After Spalling



(c) Buckling



(d) Interaction with Shear and Confinement

Fig. 5.2: Plastic Hinge Behavior in the Context of Global Buckling

concrete, as well as the lateral buckling restraint of longitudinal bars, must be provided by the transverse steel alone. Each layer of transverse steel will transmit this resistance by means of a nodal force on the longitudinal steel and on the concrete (Mander et al., 1988a). As the axial strain increases, the transverse (radial / circumferential) strain increases dramatically, often at a greater rate than the axial strains, as demonstrated in the historic full scale confinement experiments of Mander et al. (1988b). The longitudinal bars will also begin to buckle outward, and the demand on the ties may become excessive to the point that a bifurcation occurs between the longitudinal steel and the core concrete. This point, characterized by there being no nodal force remaining to act on the core concrete, is defined as incipient buckling and results in plastic flow of the steel.

Global buckling is likely to lead to a truly catastrophic failure of an RC column, since it also affects other modes of failure. When the transverse steel is in contact with the core concrete, as shown in Fig. 5.2(d), it is able to resist concrete nodal forces via the longitudinal steel, as described above. These nodal forces contribute to two mechanisms: the shear truss mechanism, as indicated by the straight dashed lines in Fig. 5.2(d), and the arching mechanism causing confinement of the core concrete, shown by the curved dashed lines in the same figure. As Fig. 5.2(d) shows, once incipient buckling has occurred and these nodal forces are no longer provided, the shear truss mechanism disappears, potentially causing shear failure. Also, the arching must take place over a much longer length meaning that the sectional area of confined concrete now constitutes a considerably smaller percentage of the total area, leading to rapid deterioration in concrete resistance.

Coupled with the shear and confinement issues which are exacerbated by global buckling is the issue of low cycle fatigue. Buckling causes a very large plastic rotation to occur in the longitudinal bar. Upon load reversal after buckling, the compressive stress on the inner side of the bar will go into tension. The combined plastic strain amplitude

will often be sufficient to cause fatigue cracking in the steel. Because of the interplay of global buckling with other modes of failure, global buckling involving multiple hoops is far less desirable than local buckling, as there are no mechanisms to provide any form of residual strength or ductility.

This chapter first summarizes previous research on global buckling of reinforcing steel. A computational model is then developed in true stress and strain using a rigorous fiber element analysis with the aim of investigating characteristic aspects of mechanical behavior. From these analyses, empirical observations of key results are made and these are parameterized to enable the critical inelastic buckling stress and strain to be predicted. A simplified limit state equation is derived for use in analysis and design.

5.2 Previous Research

5.2.1 Theoretical Models for Global Buckling of Longitudinal Reinforcing Steel

Global buckling of longitudinal reinforcing steel was first investigated by Bresler and Gilbert (1961) for buckling over two hoop spacings. A deflected shape was assumed and the Ritz method was used to solve for an equivalent lateral tie stiffness in terms of its effective modulus. Scribner (1986) also carried out an analytical investigation into global bar buckling using an energy minimization approach similar to Bresler and Gilbert (1961), using elastic tie forces. It was proposed that ties should be at least half the diameter of the longitudinal bar being restrained.

Russo (1988) considered the problem of global buckling as a beam-on-elastic-foundation with the tie stiffness depending on geometrical and material characteristics. Papia et al. (1988) made this model more systematic by creating a system matrix in which buckling was identified when the matrix determinant became zero. Papia and Russo (1989) used these results to derive a simplified parametric model that determines the stress and strain for a globally buckled bar.

Dhakal and Maekawa (2002c) used an energy minimization approach to determine the required stiffness of lateral ties to prevent global buckling. They then combined this with their local buckling model (Dhakal and Maekawa, 2002b) and determined the critical global buckling load for a given lateral reinforcement stiffness.

Pantazopoulou (1998) developed a relationship between tie effectiveness, core deformability and bar buckling. A simplified stress-strain model was used for the longitudinal reinforcing bar, while the ties were modeled quasi-elastically.

Falk and Govindjee (2000) used an energy minimization approach to determine how many layers of transverse reinforcement a bar would buckle over. Bayrak and Sheikh (2001) introduced the concept that the expansion of the core concrete leads to incipient buckling, although their model was only applied to local buckling.

Each of these studies assumed some form of elastic or quasi-elastic tie forces in their formulations. However, it is well recognized that transverse steel invariably yields in situations where global buckling occurs (Mander et al., 1988b; Dhakal and Maekawa, 2002c; Sato and Ko, 2007), and hence any approach based on stiffness is fundamentally flawed and inconsistent with physical reality.

Dutta and Mander (1998) eschewed this elasticity approach in favor of a plasticity formulation to model the global buckling problem. The simplified design equation derived in their studies on local buckling was extended to become a function of the hoop geometry and material properties. Comparisons with experimental results by other researchers showed reasonable agreement with the predictions of this model. Because this model assumes that transverse steel yields at modest compressive axial strains (typically 0.005), it is considered to be a fundamentally correct approach to the global buckling problem. Caution is needed, however, to find the correct collapse mechanism from the outset since failure to do so will overestimate the buckling capacity of the

longitudinal bars. This is because it would rely on the erroneous premise that the buckled shape of the bar can change at any time, to incorporate more or less hoops, until the critical buckling load is reached.

Buckling may conceivably occur over any number of hoopsets (N_h) or spiral turns of transverse reinforcement in the PHZ where the cover concrete has spalled off (Fig. 5.2(c)). Several methods have been proposed to determine N_h . One method, used in studies such as those by Dhakal and Maekawa (2002c), and Papia et al. (1988) essentially involves determining the required total tie stiffness to resist buckling for each mode, and comparing this with the provided tie stiffness. As stated previously, allowance needs to be made for the fact that ties will yield well prior to incipient buckling.

Another method, used by Scribner (1986) and Pantazopoulou (1998) predicts that buckling will occur over the entire PHZ (assuming spalling occurs throughout this region). A third method, adopted in studies such as Falk and Govindjee (2000) and Dutta and Mander (1998) uses energy minimization to predict the mode of buckling, which corresponds to the mode with the lowest critical buckling force. In this study, a combination of the second and third methods is used, as explained in subsequent sections.

5.2.2 Experimental Studies on Global Buckling

Several experimental studies considering buckling of longitudinal steel have been carried out (e.g. Bresler and Gilbert, 1961; Scribner, 1986; Dhakal and Maekawa, 2002c). The investigators aimed to validate global buckling models derived in those studies. Other experiments were also used as the basis for empirical relationships between buckling of longitudinal reinforcement and other aspects of column behavior.

Pantazopoulou (1998), for example, constructed a database of over 300 specimens and used that data to derive empirical design equations between concrete axial strain, displacement ductility and the required size and spacing of transverse reinforcement.

Moyer and Kowalsky (2003) examined the effects of tension strain on buckling of longitudinal steel in cyclically loaded reinforced concrete columns. Berry and Eberhard (2005) constructed a database of tests of 62 rectangular-reinforced and 42 spiral-reinforced concrete columns to derive an empirical relationship for the drift ratio at the onset of bar buckling in reinforced concrete columns. In a similar study, Syntzirma et al. (2010) proposed a relationship for the drift ratio at the onset of bar buckling. Sato and Ko (2007) conducted an experimental investigation into lateral shear reinforcement accompanied by global buckling.

It is important to note that in none of these experimental studies have the compression stress-strain behavior of longitudinal steel been reported. It is extremely difficult to measure bar stresses, strains and lateral deflections in a column, and this problem is exacerbated by the fact that it cannot be accurately pre-determined which bar will buckle, or over how many hoopsets or spirals of transverse reinforcing global buckling will take place. Both of these are critical in making accurate measurements. Also, there have been many experiments done on local buckling of longitudinal steel (see Chapter IV) where this was considered in isolation from other aspects of column behavior. However, no studies have been reported for the analogous global buckling experiments. As such, all global buckling models that have been formulated from a mechanical basis may be regarded as somewhat speculative. Moreover, models derived from a database of experimental results tend to lack generality; strictly, they are only valid for the types of column in the database.

5.3 Computational Modeling of Global Bar Buckling

In order to gain a thorough understanding of the global buckling phenomenon, a rigorous computational analysis was carried out for a range of steel types and column geometry. This computational analysis involved two stages: (i) from yield through to the bifurcation point; and (ii) after the bifurcation point.

5.3.1 Lateral Deformation Analysis

From the above description of the behavior in the PHZ, it can be stated that deflections in the longitudinal steel bar are caused initially by Poisson's expansion, followed by core concrete dilation until the point of bifurcation, and by the buckling phenomenon itself beyond bifurcation. Each of these is dealt with separately.

Consider the case of a reinforcing bar buckled over N_s successive spaces of transverse reinforcing steel spaced at a distance s as shown in Fig. 5.1(a). This corresponds to $(N_h + 1)$ hoopsets. Assuming the buckled shape function conforms to a cosine curve as in elastic buckling (Euler, 1759), the deflection, slope and curvature of the bar segment shown in Fig. 5.1(b) may be found as follows:

$$y = \Lambda - \Lambda \cos\left(\frac{2\pi x}{N_s s}\right) \quad (5.1)$$

where Λ = the maximum eccentricity at the quarter-point of the buckled length; and N_s = the number of hoop spaces s in the buckled length. Differentiating (5.1) twice gives the curvature:

$$\frac{d^2 y}{dx^2} = \frac{4\pi^2 \Lambda}{N_s^2 s^2} \cos\left(\frac{2\pi x}{N_s s}\right) \quad (5.2)$$

Thus, the maximum curvature can be written as follows:

$$\phi = \frac{4\pi^2 \Lambda}{N_s^2 s^2} \quad (5.3)$$

From equilibrium requirements in Fig. 5.1(b), the moments can be related as follows:

$$2P\Lambda - 2M = s \sum_{i=1}^{N_h/2} i(F_{hi} - C_i) \quad (5.4)$$

in which F_{hi} = hoop force applied by the hoop (which will normally be in a state of yield); and C_i = net nodal confinement force. Note that instability occurs when $C_i \rightarrow 0$.

5.3.2 Resistance by Transverse Steel

Cold working of the steel to form hoops in circular sections and hooks in rectangular sections will cause the steel to exhibit the same behavior as with the reloading branch in cyclic behavior, with clear evidence of the Bauschinger Effect (Priestley et al., 1981; Mander, 1983). As such, the following stress-strain relationship was adopted for the transverse steel:

$$f_h = \frac{E_s \varepsilon_h}{\sqrt{1 + |\varepsilon_h / \varepsilon_{yh}|^2 + |\varepsilon_h / \varepsilon_{fh}|^{20}}} + \frac{(f_{uh} - f_{yh})}{1 + |\varepsilon_h / \varepsilon_{fh}|^{20}} \left[\frac{2(\varepsilon_h - \varepsilon_{yh})(\varepsilon_{fh} - \varepsilon_{yh}) - (\varepsilon_h - \varepsilon_{yh})^2}{(\varepsilon_{fh} - \varepsilon_{yh})^2} \right] \quad (5.5)$$

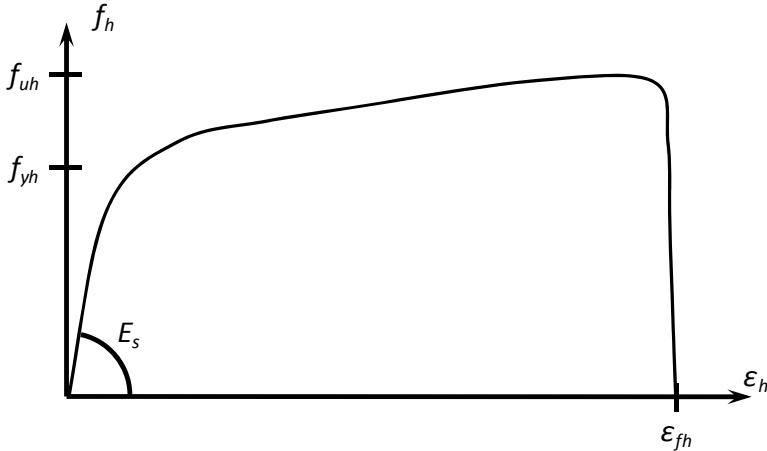
where ε_h = hoop strain; ε_{yh} = hoop yield strain; ε_{fh} = hoop fracture strain; f_{yh} = hoop yield stress; and f_{uh} = hoop ultimate stress. A diagram of the hoop stress-strain curve is given in Fig. 5.3(a). Mander et al. (1988a) found the hoop fracture strain from strain energy considerations by approximating the area under the curve given by (5.5) as follows:

$$U_s = \int_0^{\varepsilon_{fh}} f_h d\varepsilon_h = f_{yh} \varepsilon_{fh} \left(\frac{1}{3} + \frac{2}{3} \frac{f_{uh}}{f_{yh}} \right) = 110 \text{MPa} \quad (5.6)$$

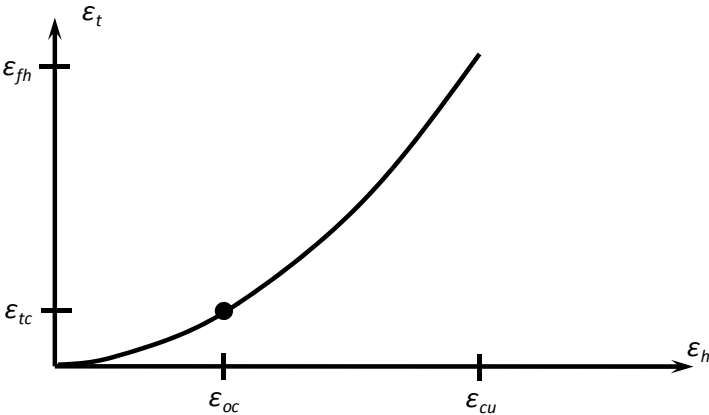
Given f_{uh} / f_{yh} is typically in the range 1.5 to 1.6 (Mander, 1983), the strain can be simplified as $\varepsilon_{fh} \approx 80 / f_{yh}$.

5.3.3 Full Buckling Analysis

Mander (1983) and Mander et al. (1988b) describe axial load experiments on full scale specimens where the hoop strains were measured. These are used here to model the



(a) Hoop Stress-Strain Diagram



(b) Axial-Lateral Strain Relationship

Fig. 5.3: Characterization of Hoop Behavior

dilation of the section under axial load. Axial strain is applied incrementally, from which the transverse strain is found using the following relationship, shown in Fig. 5.3(b):

$$\frac{\varepsilon_t}{\varepsilon_{fh}} = \left| \frac{\varepsilon_s}{\varepsilon_{cu}} \right|^b \quad (5.7)$$

where ε_s = axial strain compression strain in the rebar; ε_{cu} = axial compression strain at first hoop fracture, as defined in Mander et al. (1988a); ε_{sf} = fracture strain of the hoops as defined above; and $b = \ln(\varepsilon_{tc} / \varepsilon_f) / \ln(\varepsilon_{oc} / \varepsilon_u)$ with $(\varepsilon_{tc}, \varepsilon_{oc})$ being a control point for the relationship between axial and lateral strains. Based on analyzing a selection of data from Mander (1983), b varies from 1.5 to 2.5. For typical levels of practical transverse steel details, and in lieu of a more precise analysis, $b = 1.75$ should suffice. The analysis proceeds using the equilibrium equation of the deformed (buckled) shape given by (5.4) until the nodal confinement forces C_i vanish and instability ensues.

Once the point of instability has been identified, the behavior switches to a plastic flow problem as in the case for local buckling. As such, the same computational method used for analyzing local buckling described in Chapter IV is used, modified for the resistance given by the transverse steel using (5.4). Successive increments of reference strain ε_o are applied to the section, with the axial load and curvature being adjusted until force equilibrium and displacement compatibility requirements had been satisfied. Secondary buckling strains are also considered in the same manner as for local buckling. A full description of the computational algorithm was given in Chapter III.

5.4 Observations from Computational Analysis

In order to gain a general understanding of global buckling behavior, several computational analyses were run that were considered representative of current practice and design code requirements. The type of steel was kept constant for the hoops and the longitudinal bars throughout all analyses, with the tensile properties for mild steel taken

from Mander et al. (1994). This steel is considered representative of steels used in construction, representing a “median-value” steel. For example, the yield strength of common mild steels typically varies from about 250MPa to 500MPa, and the yield strength of the steel used is 331MPa, close to the median value of 375MPa. The other value held constant throughout all analyses was the value of ε_{cu} , which was set at 0.05. This is close to the most widely observed value of ε_{cu} in experiments by Mander (1983), and given typical reinforcement and material parameters, is the value estimated from the model given in Mander et al. (1988a).

Firstly, to establish the value of N_s considered to be critical, three analyses were run for $N_s = 3, 5$ and 7 . The s / d_b ratio was kept constant at 6 , the minimum value specified by most design codes. The hoop force ratio, P_y / F_{yh} was kept constant at 4 , a commonly used value in practice. The results of this analysis are shown in Fig. 5.4. Clearly $N_s = 3$ gives the lowest global crippling stress. While this is not necessarily the pre-ordained buckling case, as would be suggested by energy minimization approaches, it is the most critical case that could conceivably occur. As a result, $N_s = 3$ was used for all subsequent analyses. Next, two sets of analyses were run – one set keeping s / d_b constant at the code-specified value of 6 and varying P_y / F_{yh} ; the other set keeping P_y / F_{yh} constant at 16 , as specified by NZS3101:2006 while s / d_b was varied. These sets of results are shown in Figs. 5.5 and 5.6 respectively. As these figures show, for all cases plotted, the global buckling curve follows the local curve until the crippling point is reached, at which point a sharp decrease in capacity is observed.

A further important observation from Figs. 5.5 and 5.6 is the increasing disparity between local and global buckling solutions as s / d_b decreases, regardless of how big the hoops are. While decreasing s / d_b may be good for confinement, clearly it is steering the system towards an unavoidable global buckling failure. In reality, the increased hoop sizes would marginally increase the crippling stress via ε_{cu} , but this is too variable a parameter to be reliable.

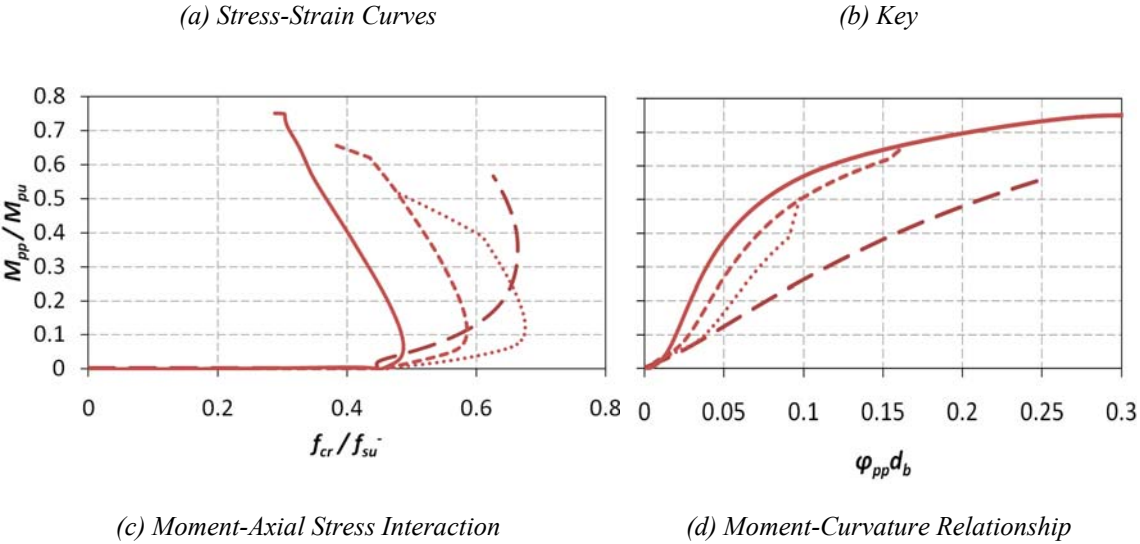
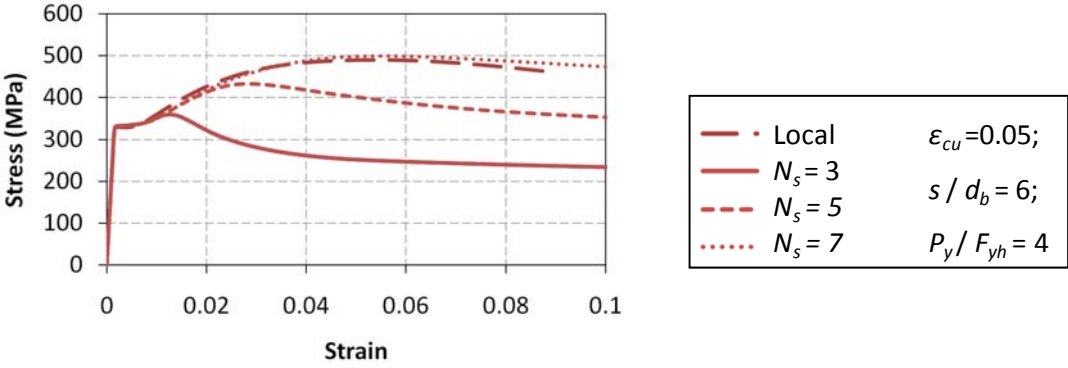
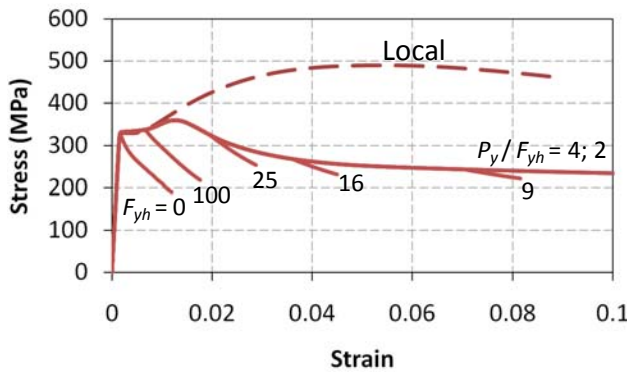


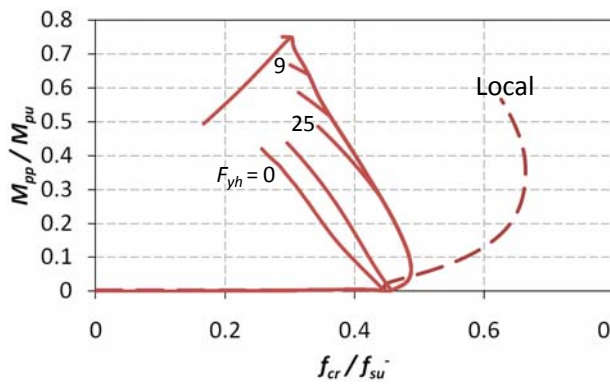
Fig. 5.4: Computational Analysis to Find Critical Buckling Length



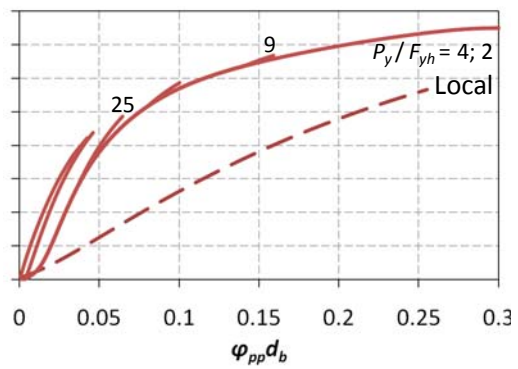
$P_y / F_{yh} = 2; 4; 9;$	$\epsilon_{cu} = 0.05;$
$16; 25; 100;$	$s / d_b = 6;$
$F_{yh} = 0$	$N_s = 3$

(a) Stress-Strain Curves

(b) Key

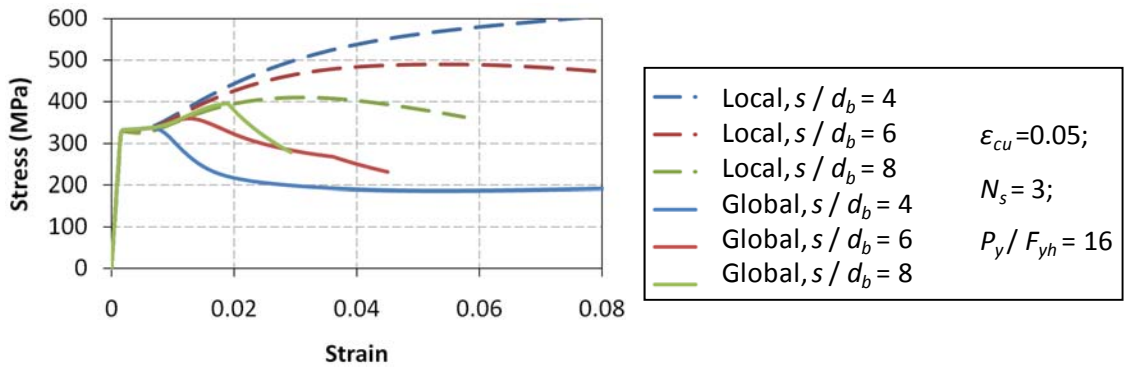


(c) Moment-Axial Stress Interaction



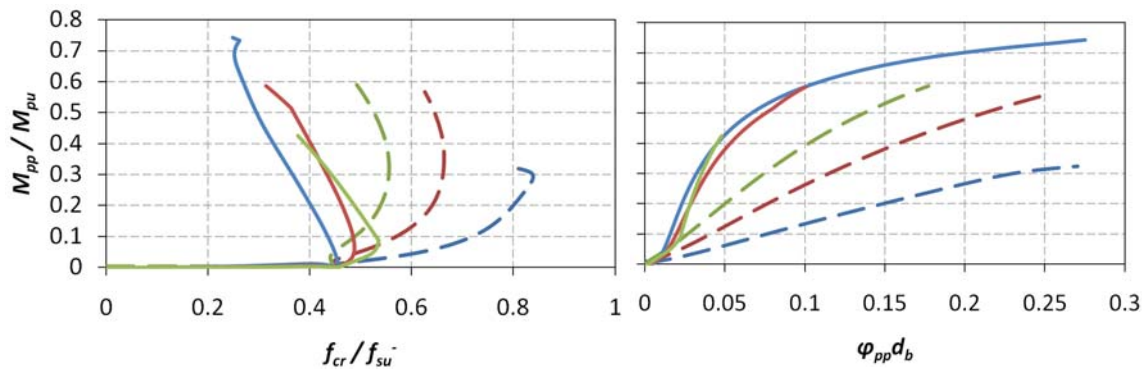
(d) Moment-Curvature Relationship

Fig. 5.5: Computational Analysis to Show Variation in Behavior with Hoop Force



(a) Stress-Strain Curves

(b) Key



(c) Moment-Axial Stress Interaction

(d) Moment-Curvature Relationship

Fig. 5.6: Computational Analysis to Show Variation in Behavior with Hoop Spacing

5.5 Simplified Limit Analysis

Whereas the model described in the preceding sections is well suited for a full computational buckling analysis, it is somewhat cumbersome for use in analysis and design situations. Instead, a simplified limit analysis will suffice for relating the required hoop force to the axial capacity of the longitudinal steel. This limit analysis is based on the rigorous computational analysis, but incorporates several simplifying assumptions as outlined below. Because there is a lot of variability in steel material properties, column geometry and dilation of the core concrete, coupled with the reality of highly nonlinear and somewhat irregular behavior observed in column specimens, it would not be realistic to derive a truly comprehensive analytical model. Thus, the complexity of the problem necessitates the simplicity of the solution.

5.5.1 Prediction of Crippling Stress due to Global Buckling

Firstly, the curvature can be used to relate e and Λ , the eccentricities due to local and global buckling respectively. From (5.3) and the analogous local buckling shape function, e can be written as:

$$e = \Lambda / N_s^2 \quad (5.8)$$

In the limit, it may be assumed that C_i in (5.4) has vanished, thus the equilibrium equation becomes:

$$2P\Lambda - 2M = s \sum_{i=1}^{N_h/2} iF_i \quad (5.9)$$

Normalizing (5.9) with respect to P_y , the yield force of the longitudinal steel and combining with (5.3) and (5.8), the following simplified force ratio equation is obtained for limit analysis and design:

$$\frac{P}{P_y} = \frac{f_{gb}}{f_y} = \frac{s/d_b}{2(\Lambda/d_b)(1-1/N_s^2)} \frac{F_h}{P_y} \sum_{i=1}^{N_h/2} i \quad (5.10)$$

where f_{gb} = crippling stress from global buckling. Now making the simplifying assumptions that the maximum hoop strain ε_h occurs mid-way along the buckled length, the hoop deflection is:

$$\Lambda_h = \varepsilon_h L_h = \Lambda (1 + \cos \pi / N_s) \quad (5.11)$$

Also, it can be reasonably assumed that $F_h \approx 1.4F_y$ near failure and $\varepsilon_h = \varepsilon_{fh} = 80 / f_{yh}$ as shown previously. This is consistent with computational and experimental observations of hoop fracture over part of the buckled length. Substituting these into (5.10) gives:

$$\frac{f_{gb}}{f_y} = \frac{s/d_b}{L_h/d_b} \frac{f_{yh}}{115} \frac{F_{yh}}{P_y} \frac{(1 + \cos \pi / N_s)}{(1 - 1/N_s^2)} \sum_{i=1}^{N_h/2} i \quad (5.12)$$

Using the simplifying assumption that $N_s = 3$, which gives a minimum f_{cr} in (5.12), and is also validated in Fig. 5.4, this can be further simplified as:

$$\frac{f_{gb}}{f_y} = \frac{s/d_b}{L_h/d_b} \frac{f_{yh}}{70} \frac{F_{yh}}{P_y} \geq 1 \quad (5.13)$$

Equation (5.13) can be used in an analysis context, where f_{gb} / f_y will naturally be limited to values below those given by the local buckling solution derived in Chapter IV. For design purposes, (5.13) can be rewritten to give the required hoop force, thus to inhibit global buckling,

$$\frac{F_{yh}}{P_y} \geq \frac{70}{f_{yh}} \left(\frac{f_{cr}}{f_y} \right) \frac{(L_h/d_b)}{(s/d_b)} \quad (5.14)$$

where f_{cr} is given by the local buckling solution.

5.5.2 Prediction of Crippling Strain due to Global Buckling

Using the computational observation that the global buckling curve roughly follows the local buckling curve until the crippling stress f_{gb} is reached, the corresponding strain ε_{gb}

can be estimated using an inverse form of the steel stress-strain curve for local buckling. Using the relationship for the strain-hardening portion of the stress-strain curve from Mander (1983):

$$\varepsilon_{gb} = \varepsilon_{cr} - \left| \varepsilon_{cr} - \varepsilon_{sh} \right| \left| \frac{f_{cr}/f_y - f_{gb}/f_y}{f_{cr}/f_y - 1} \right|^{1/p} \quad (5.15)$$

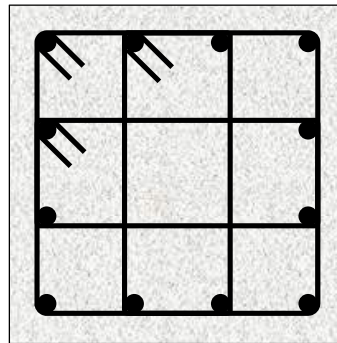
where $(\varepsilon_{cr}, f_{cr})$ is the crippling point from local buckling; and $p = E_{sh} (\varepsilon_{cr} - \varepsilon_{sh}) / (f_{cr} - f_y)$ is the strain-hardening parameter. Also, E_{sh} = strain hardening modulus and ε_{sh} = compressive strain at the onset of strain-hardening. Clearly, (5.15) is valid for the case where $f_{gb} \leq f_{cr}$. For the case where $f_{gb} = f_y$, the corresponding strain could lie anywhere on the yield plateau, so a reasonable assumption of $\varepsilon_{gb} = \varepsilon_{sh}$ is adopted.

5.5.3 Tie Effectiveness and Circular Sections

Allowance must be made for the fact that transverse steel may not necessarily be aligned orthogonal to the longitudinal steel. This will be the case for rectangular and square columns with the transverse steel layout shown in Fig. 5.7(a), and hence the full force in the tie resists lateral deflection of the longitudinal steel. Where tie sets resist more than one longitudinal bar, this may be taken into account in the manner described by Paulay and Priestley (1992). In the case of spiral reinforced or octagonally reinforced columns, a geometric factor κ is applied to the hoop force, as shown in Fig. 5.7(b) and 5.7(c).

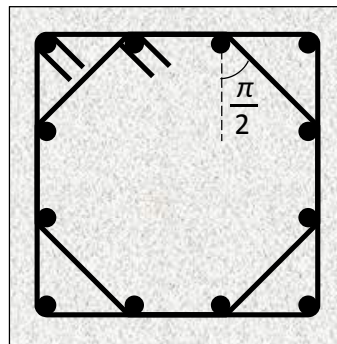
5.5.4 Full Compressive Stress-Strain Model

The crippling point $(\varepsilon_{gb}, f_{gb})$ given by (5.13) and (5.15) is applicable for the case when failure occurs by global buckling of the longitudinal steel. Allowance must also be made for cases when failure occurs due to local buckling of the longitudinal steel, or due to hoop fracture. The ultimate compressive strain at hoop fracture can be conservatively estimated using the following formulation given in Priestley and Calvi (1996):



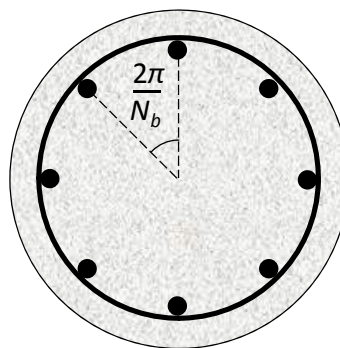
$$\kappa = 1.0$$

(a) *Orthogonal*



$$\kappa = 0.71$$

(b) *Octagonal*



$$\kappa = 2\pi / N_b$$

(c) *Circular*

Fig. 5.7: Multipliers for Different Configurations of Transverse Steel

$$\varepsilon_{cu} = 0.004 + \frac{1.4\rho_s f_{yh} \varepsilon_{su}}{f'_{cc}} \quad (5.16)$$

where ε_{su} = steel strain at maximum tensile stress; f'_{cc} = confined concrete strength, given by the well-known formulation by Mander et al. (1988a); and $\rho_s = 4A_{sp} / D'$ is the volumetric ratio of confining reinforcing steel. Also, A_{sp} = cross-sectional area of spiral steel, and $D' =$ diameter of the core concrete. The stress corresponding to (5.16) can be obtained from the compressive stress-strain curve derived in Chapter IV.

Using the local buckling equations derived in Chapter IV, together with (5.13) and (5.16), the compressive stress-strain curve for steel presented in Chapter IV can be modified to include global buckling and hoop fracture effects:

$$f_s = \frac{E_s \varepsilon_s}{\left\{1 + |\varepsilon_s / \varepsilon_y|^{20}\right\}^{0.05} + \gamma \left\{1 + |\varepsilon_s / 2\varepsilon_{cr}|^{40}\right\}^{0.05} - \gamma + |\varepsilon_s / \varepsilon_{ult}|^{0.05}} + \frac{(f_{cr} - f_y)}{\left(1 + |\varepsilon_s / \varepsilon_{ult}|^{40}\right)^{0.05}} \left[1 - \frac{|\varepsilon_{cr} - \varepsilon_s|^p}{\left\{|\varepsilon_{cr} - \varepsilon_{sh}|^{20p} + |\varepsilon_{cr} - \varepsilon_s|^{20p}\right\}^{0.05}} \right] \quad (5.17)$$

where f_y = yield stress; E_s = Young's modulus; E_{sh} = modulus at the onset of strain hardening; ε_{sh} = strain at the onset of strain hardening; f_{cr} = ultimate compressive (crippling) stress from Chapter IV; ε_{cr} = crippling strain. Also, $\varepsilon_y = f_y / E_s$ = yield strain; and the exponent p is calculated from the control parameters, where $p = E_{sh} (\varepsilon_{su} - \varepsilon_{sh}) / (f_{su} - f_y)$. The parameter $\gamma = 4$ for mild steel and $\gamma = 2$ for high-strength steel. Finally, $\varepsilon_{ult} = \min(\varepsilon_{gb}, \varepsilon_{cu})$.

5.6 Chapter Closure

This chapter has presented a thorough qualitative analysis of the global buckling phenomenon, and described the interplay between global buckling and the confinement

and dilation of the core concrete. A rigorous computational analysis was carried out to establish trends with respect to spacing of hoopsets, size of hoopsets, number of hoopsets in the buckled length, and ultimate strain of concrete. Recognizing the wide variability inherent in the global buckling problem, a simplified equation was derived for analysis and design.

The following conclusions can be drawn from this study:

1. A simplified relationship between hoopset size and spacing, and critical buckling stress is provided for analysis and design applications. This is incorporated into a full compressive stress-strain model which includes the effects of hoop fracture and local and global buckling of longitudinal steel.
2. A rigorous computational method is described for conducting case studies of global buckling scenarios.
3. Due to the subsequent rapid decay in moment capacity involving other modes of failures, global buckling is highly undesirable and should be avoided in favor of local buckling. This can be achieved by using larger diameter hoopsets, spaced further apart.
4. The global buckling behavior of the longitudinal steel is inextricably linked to the confinement and dilation of the core concrete, as it is this interaction which precipitates global buckling.

CHAPTER VI

APPLICATION TO PERFORMANCE-BASED ANALYSIS AND DESIGN

In this chapter, the buckling models derived in Chapters IV and V are incorporated into a full moment-curvature analysis regime for a RC member. The objective of this regime is to predict the full loading history of the member, including elastic, plastic, peak, post-peak and ultimate behavior. The effects of concrete confinement, shear and low-cycle fatigue are also incorporated using well-established models. The analysis regime is validated against experimental tests of RC specimens. The column model is then used in an analysis of a ten storey RC structure to demonstrate how the drifts at the ultimate limit state are determined.

6.1 Introduction

Current state-of-the-practice in performance-based seismic design of reinforced concrete (RC) buildings consists of two phases – seismic design and performance analysis. The design phase involves selecting member sizes, determining design loads, choosing flexural reinforcement and detailing the structure in accordance with the selected design philosophy. In the second phase, a performance-based analysis of the design is carried out to ascertain the damage expected under a design basis event (DBE) and a maximum considered event (MCE). Since damage can usually be considered to be proportional to displacement limit states, it is necessary to conduct a pushover analysis of the designed structure to determine what these limit states are. However the structure's behavior is expected to be highly nonlinear and dependent on various failure mechanisms. As such, the pushover analysis should be coordinated with moment-curvature analyses of critical sections in the structure.

The moment-curvature analyses of these sections can be done with relative ease using current knowledge. The elastic, plastic, peak and post-peak behavior of RC sections can usually be described with sufficient accuracy for use in a pushover analysis. However, identification of the critical member rotation (at which failure is said to occur) is an area that is still largely unrefined. Four critical failure mechanisms have been defined for RC members (Dutta and Mander, 1998):

- (i) Fracture of longitudinal reinforcing bars due to low-cycle fatigue
- (ii) Fracture of transverse steel
- (iii) Failure across a critical section in shear
- (iv) Local or global buckling of longitudinal steel

While the first of these, in the limit, is unavoidable due to it being a metallurgical property of the rebar, the latter three modes are avoidable by proper placement of sufficient transverse reinforcement. However, while modes (ii) and (iii) can easily be negated with more hoops or spirals, it is the nature of how these are placed that will govern whether (iv) can be averted.

It is the aim of this chapter to incorporate these four modes of failure into a moment-curvature analysis, and validate this with experimental results. This will give a more realistic prediction of ultimate rotation capacities of RC members, and hence, a better indicator of when failure is likely to occur under seismic events. The four modes of failure occur at significant levels of plastic rotation (assuming a well-detailed section). Although concrete may split due to tensile stress, cover concrete may spall off and steel may undergo significant plastic behavior, none of these constitutes failure as it has been well-proven that the section can sustain high axial loads and bending moments.

The development of a two dimensional model of a RC frame building, known as the “Red Book building,” (CCANZ, 1998) is then described. This model incorporates the

use of the moment-curvature sectional analysis in critical sections throughout the model. A modal analysis is used to carry out model validation (via comparisons with other studies using the Red Book building). Using the model of the Red Book building, the drift at ultimate capacity is determined using two methods. Firstly, a monotonic pushover analysis of the Red Book building displays how the ultimate drift may be found using an equivalent static analysis according to NZS 1170.5:2004. Secondly, an Incremental Dynamic Analysis (IDA) is carried out. This is a far more rigorous method which incorporates full dynamic and non-linear effects. The IDA results are compared with those from the monotonic pushover analysis.

6.2 Moment-Curvature and Force-Deformation Analysis of Critical Reinforced Concrete Members

The material behavior used in the moment-curvature analysis can be characterized entirely from parameters obtained from experimental testing of steel in tension and the concrete in compression. For a column under relatively low axial load and monotonically increasing lateral load, significant strain reversals are not expected to occur in the steel. As such, monotonic stress-strain relationships can be used for tensile and compressive behavior, using the appropriate models presented in Chapters IV and V. These models take into account the full plastic behavior of the steel including strain hardening, which will certainly be engaged under high levels of curvature.

The behavior of the concrete under monotonically increasing loads can be modeled using the stress-strain model by Popovics (1973). Parameters for unconfined compression are taken directly from a compressive cylinder test. Parameters for confined compression are found using the well known model by Mander et al. (1988a). Tensile parameters can be found using the appropriate formulae in ACI318-08, for example.

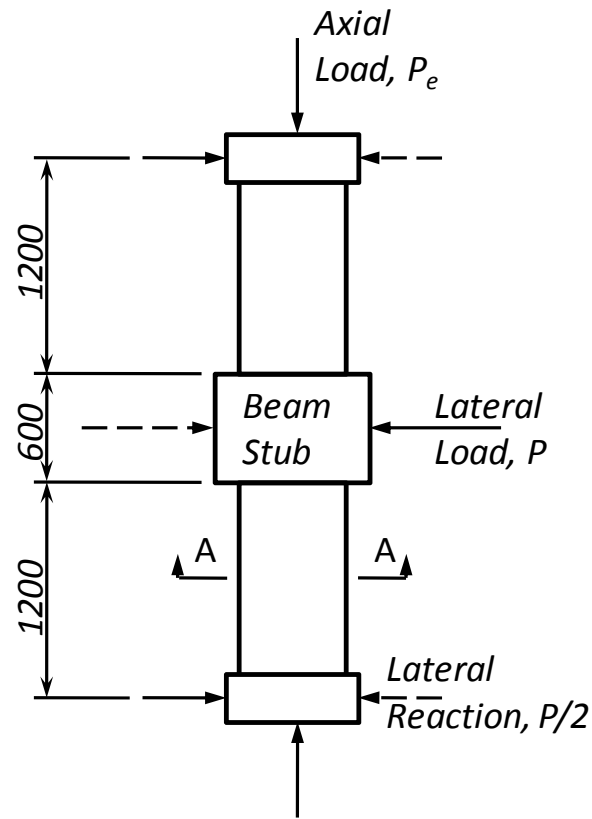
The technique used to analyze an RC member under constant axial load is essentially a simplified version of the algorithm described in Chapter III. First, the section is discre-

tized into fibers over its depth, and the appropriate material models for steel, confined core concrete or unconfined cover concrete are applied. Over successive increments of curvature are applied to the section, the centroidal strain is found to give the correct axial load and the corresponding moments are calculated.

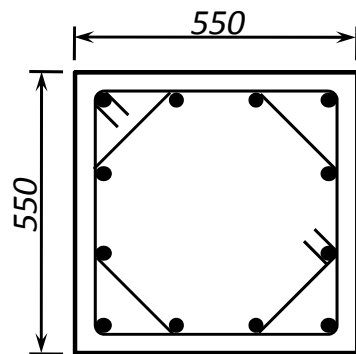
From the full moment-curvature relationship of the section, the lateral force-deflection relationship is determined. Flexural deflections are found from the first moment of area of the curvature distribution. Shear deflections are found using a continuum truss model based on one proposed by Kim and Mander (2006). Other deflections such as those from P-delta effects and support rotations are also included. The critical curvature from low-cycle fatigue is obtained using the model proposed by Dutta and Mander (2001). The moment-curvature and force-deflection procedures are described thoroughly in Mander (1983).

In order to validate the complete column analysis procedure, experiments from a study by Park et al. (1982) were modeled. In their study, four RC specimens were constructed, as shown in Fig. 6.1. Each specimen consisted of two identical 1200mm cantilever columns with a 550mm square section, connected by a heavily-reinforced 600mm beam stub. Each column was reinforced with 12-24mm diameter longitudinal reinforcing bars, and different configurations of transverse hoopsets. Tables 6.1 and 6.2 show the properties of the materials used. The columns were subjected to constant axial loads, also shown in Table 6.1, and lateral loads consisting of full cycles to increasing levels of ductility.

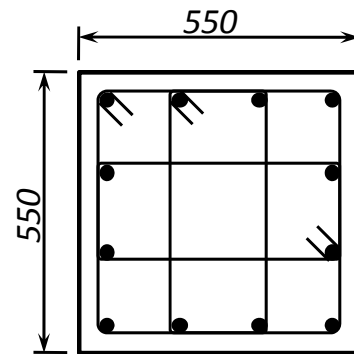
The results of the monotonic column analyses are compared with the backbone curves of the cyclic experiments in Fig. 6.2. Clearly, the comparison is favorable to the end of the experimental tests. To ascertain what would happen at failure, the analyses were continued until a significant change in the lateral load-carrying capacity was observed. For each result, the point considered to be the ultimate drift capacity of the column is



(a) Elevation



(b) Section A-A, Specimens 1 and 2



(c) Section A-A, Specimens 3 and 4

Fig. 6.1: Geometry of Column Specimens Tested by Park et al. (1982)

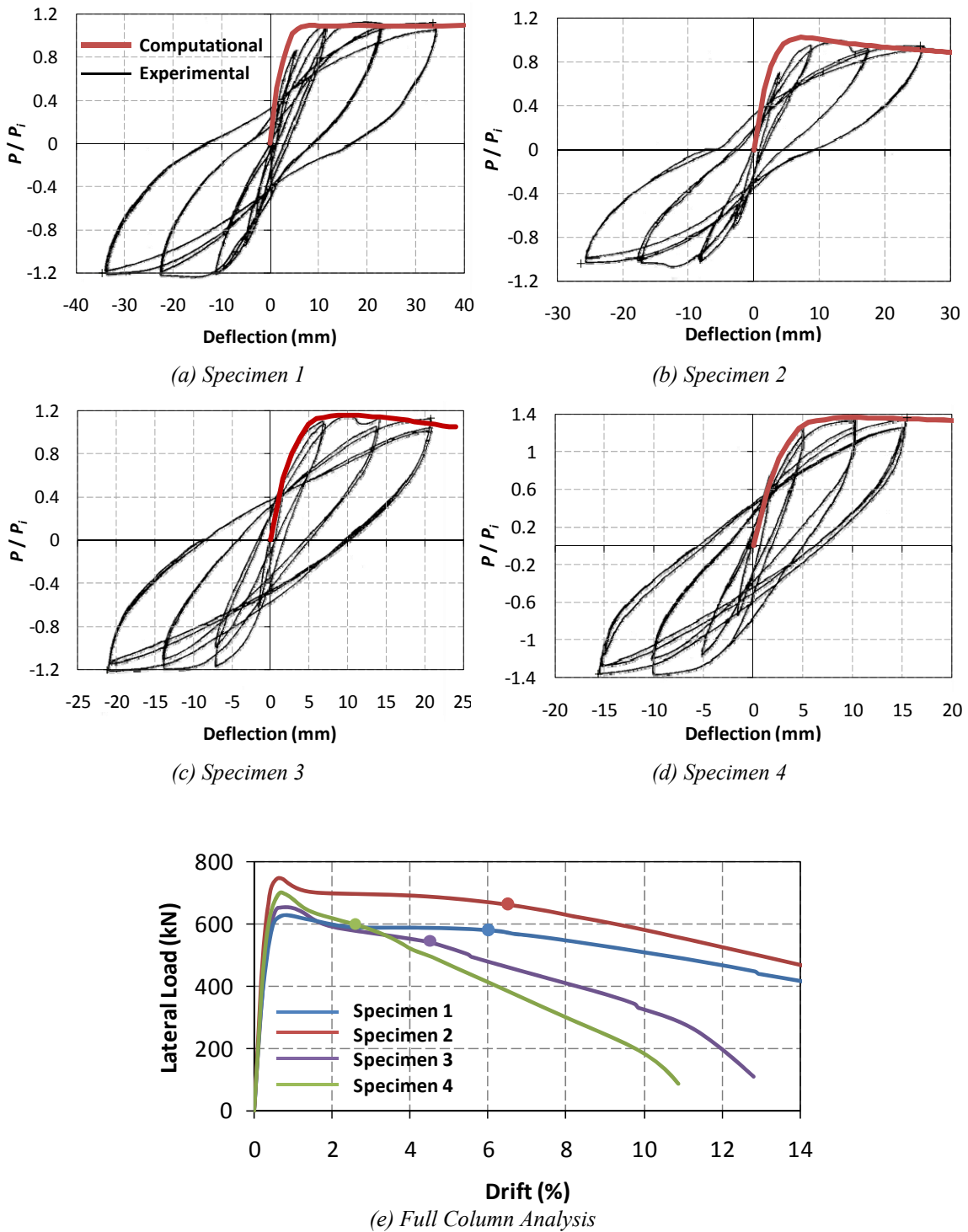


Fig. 6.2: Results of Computational Analyses of RC Columns Tested by Park et al. (1982)

Table 6.1: Details of RC Specimens Tested by Park et al. (1982)

Specimen	f'_c (MPa)	d_{bh} (mm)	s (mm)	f_{yh} (MPa)	P_e (kN)	P_i (kN)
1	23.1	10	80	297	1815	1128
2	41.4	12	75	316	2680	1473
3	21.4	10	75	297	2719	1113
4	23.5	12	72	294	4265	1017

Table 6.2: Tensile Stress-Strain Parameters for Longitudinal Steel Used in Specimens Tested by Park et al. (1982)

f_y (MPa)	f_{su} (MPa)	ϵ_{sh}	ϵ_{su}	E_s (GPa)	E_{sh} (MPa)
375	636	0.0086	0.12	200	8000

marked. Although this does not appear to correspond with a significant drop in load, the global buckling failure identified here is likely to lead to catastrophic failure of the column for the reasons outlined in Chapter V. Since the s / d_b ratios are so small, the failure mechanism appears to be global buckling in each case.

6.3 Structural Analysis Model of Red Book Building

A three-bay ten storey reinforced concrete frame building, whose design is described in CCANZ (1998), popularly known as the “Red Book”, was selected for analysis. It was selected as an example of the current state-of-the-practice in New Zealand building design, as described in the New Zealand Loadings Standard (NZS 1170.5:2004) and the New Zealand Concrete Code (NZS 3101:2006). The seismic design approach adopted in these standards is known as capacity design, which ensures the formation of a ductile strong-column / weak-beam mechanism able to sustain as-large-as-practicable post-yield deformation.

The Red Book building is a square office building with a floor area of approximately 900 m². Lateral loads are resisted by four perimeter moment-resisting frames. As these frames have no corner columns, they are designed to act in one direction only. The building includes internal gravity frames which are not part of the lateral load-resisting system but are detailed to undergo the deformation imposed by the perimeter frames. The floor system used is a unidirectional precast hollow-core system with in-situ topping. The concrete strength throughout the building is specified as 30 MPa, while the reinforcing has a yield strength of 430 MPa. A plan and elevation of the building are shown in Figs. 6.3 and 6.4, while details of critical sections are given in Table 6.3.

The design given in CCANZ (1998) focuses on the beams at level two, which are considered to be the worst case. Beam reinforcements are considered to be the same throughout the structure. Likewise, the column details are assumed to be the same throughout the structure, and are based on the worst case below level two. The analysis of the structure is carried out using the widely available structural analysis software, SAP2000. Half of the Red Book building, consisting of one gravity frame and one

Table 6.3: Details of Critical Sections in Red Book Building

Element	Size	Longitudinal Reinforcement	Transverse Reinforcement
Perimeter Beams	900 x 400 mm	4-H24 Top 4-H24 Bottom	4 legs HR10@140 c/c
Cantilever Beams	900 x 400 mm	3-H24 Top 3-H24 Bottom	4 legs HR10@140 c/c
Perimeter Columns At Ground Level	900 x 460 mm	12-H20	5 legs HR12@ 90 c/c 3 legs HR12@ 90 c/c
Perimeter Columns above Level 1	900 x 460 mm	12-H20	5 legs HR10@115 c/c 3 legs HR10@115 c/c
Main Interior Beams	750 x 530 mm	Not specified	Not specified
Interior Columns	650 x 600 mm	Not specified	Not specified

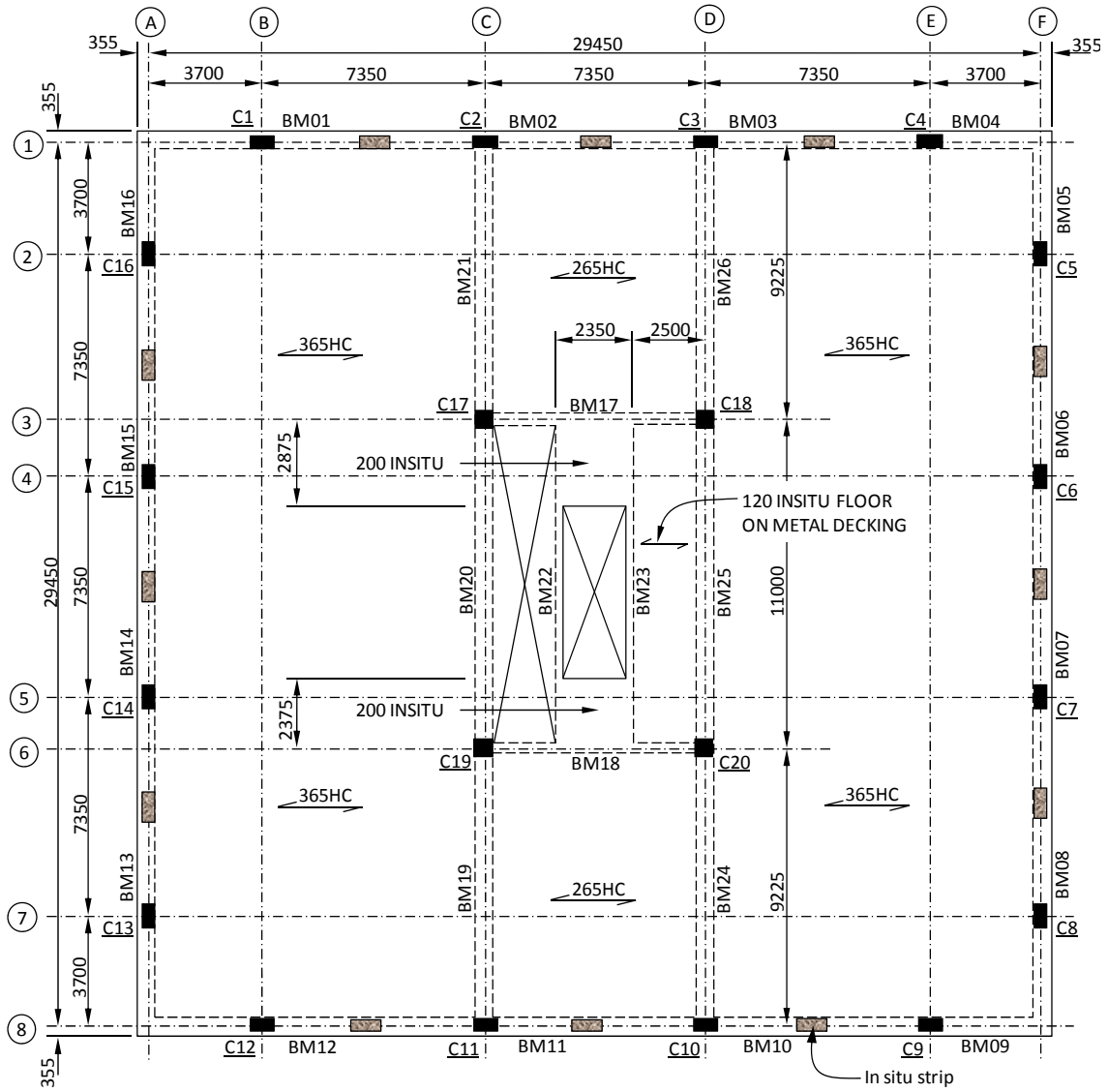


Fig. 6.3: Red Book Building (adapted from CCANZ, 1998) – Typical Floor Plan

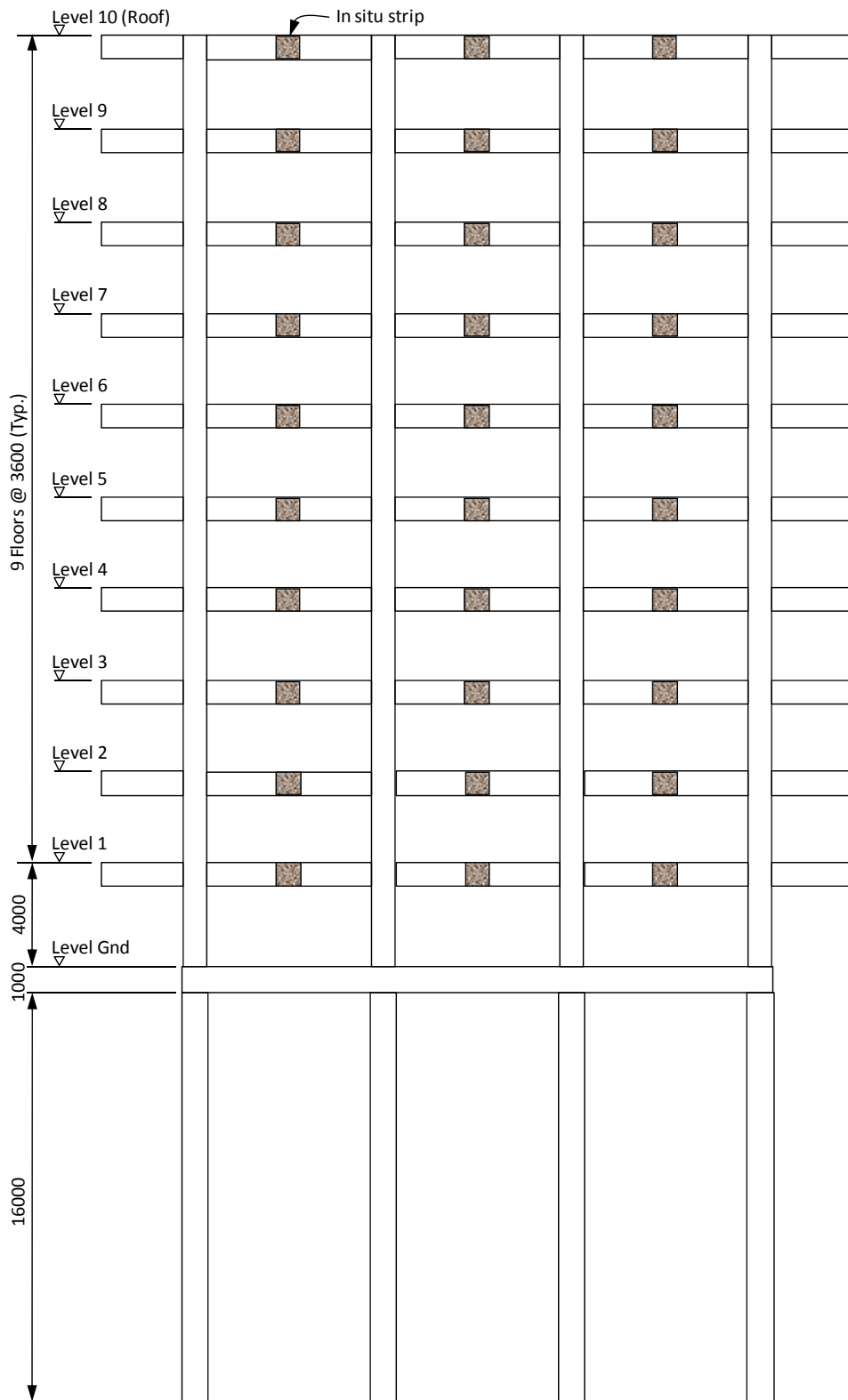


Fig. 6.4: Red Book Building (adapted from CCANZ, 1998) – Grid F Elevation

moment-resisting frame, was modeled. The frames were coupled together at each floor level using high-stiffness pinned struts. Beams and columns were modeled as elastic elements with stiffnesses modified for cracking. Beam-column joints and floor diaphragms were assumed rigid as in the original design (CCANZ, 1998), allowing horizontal degrees of freedom to be slaved at each floor level. A plastic hinge region of half a member depth was placed at the beam- and column-faces for each member. These hinges were modeled using the Takeda hysteresis rule (Takeda et al., 1970) for time-history analyses. Fig. 6.5 shows a schematic of the SAP2000 model. P-delta effects were included in the analyses, and initial stiffness Rayleigh damping of 5% of critical was specified in modes 1 and 9.

Based on the geometry given in Fig. 6.3 for the plan of the Red Book building, floor weights and live loads were assigned to each frame according to tributary areas. The weight of the main structural components was accounted for by using the self-weight option in SAP2000. Additional weight from cladding, glazing, lining, hollow-core floor units, topping and super-imposed dead load (SDL) were applied as uniformly distributed loads (UDLs) on each beam. Gravity loads from adjacent walls were lumped as point loads at the ends of each frame. A basic live load of 2.5 kPa is specified for the Red Book building by NZS 1170.5:2004. This yields an ultimate seismic live load of 0.49 kPa, which was applied to all beams below the roof level as a UDL. To calculate the axial force due to gravity loads in each column under seismic loading, the tributary area was assumed to be roughly the same for each column. Loads are summarized in Table 6.4.

A modal analysis was carried out for the model of the Red Book building. The stiffnesses of beams and columns were modified for cracking by using $EI_{eff} = 0.52EI_g$ for the columns, and $EI_{eff} = 0.25EI_g$ for the beams, where EI_{eff} and EI_g are the effective and gross flexural rigidities, respectively. The loads and damping described above were applied to the structure. The results are compared with those from an analysis presented

in the Red Book (CCANZ, 1998) and with those from a study done by Robertson (2005). The slight difference in results is due to the Red Book assuming a higher EI_{eff} . Table 6.5 shows the results from the first three modes, where available.

Table 6.4: Beam Distributed Gravity Loads and Cumulative Tributary Column Axial Loads for Red Book Building under Ultimate Earthquake Loads

(a) Perimeter Frame

Floor Level	Beam UDL (kN/m)	Beam Point Loads (kN)	Cumulative Tributary Column Axial Loads (kN)	
			Interior ($A_{trib} = 41.4 \text{ m}^2$)	Exterior ($A_{trib} = 40.2 \text{ m}^2$)
Roof	23.8	51.6	265	257
9	26.4	51.6	550	534
8	26.4	51.6	835	811
7	26.4	51.6	1120	1088
6	26.4	51.6	1406	1365
5	26.4	51.6	1691	1642
4	26.4	51.6	1976	1919
3	26.4	51.6	2262	2196
2	26.4	51.6	2547	2473
1	26.4	51.6	2832	2750

(b) Gravity Frame

Floor Level	Beam UDL (kN/m)	Beam Point Loads (kN)	Cumulative Tributary Column Axial Loads (kN)	
			Interior ($A_{trib} = 91.8 \text{ m}^2$)	Exterior ($A_{trib} = 41.5 \text{ m}^2$)
Roof	36.9	85.1	587	266
9	41.2	85.1	1219	551
8	41.2	85.1	1852	837
7	41.2	85.1	2485	1123
6	41.2	85.1	3117	1409
5	41.2	85.1	3750	1695
4	41.2	85.1	4382	1981
3	41.2	85.1	5015	2267
2	41.2	85.1	5647	2553
1	41.2	85.1	6280	2839

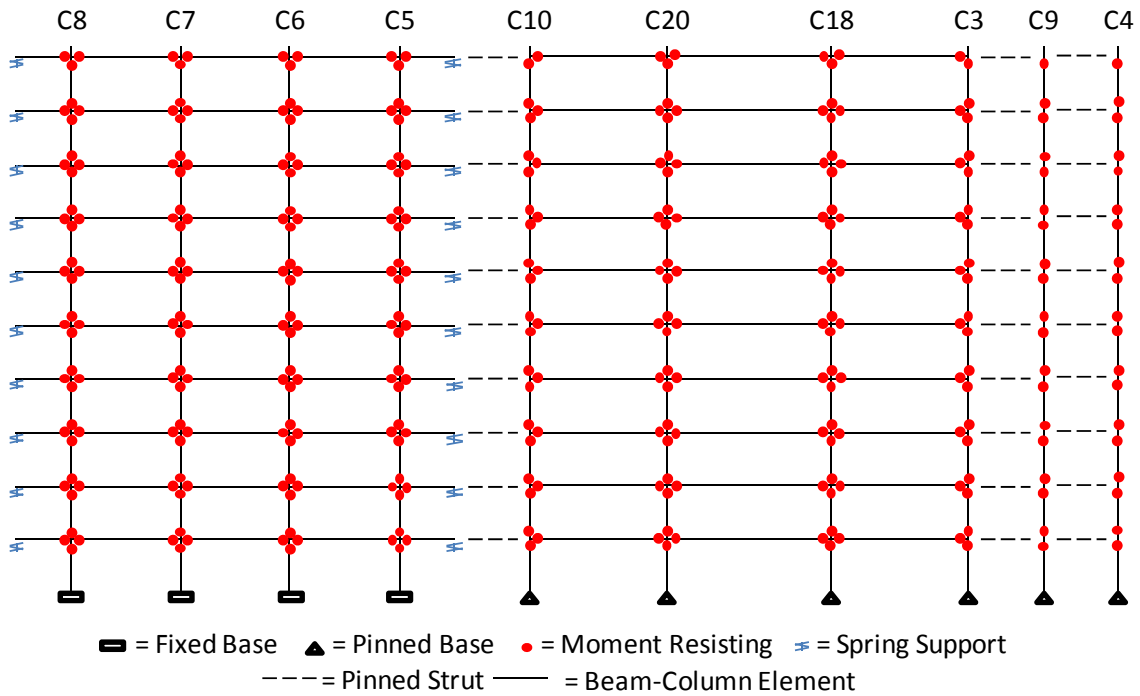


Fig. 6.5: Schematic Diagram of SAP2000 Model of Red Book Building

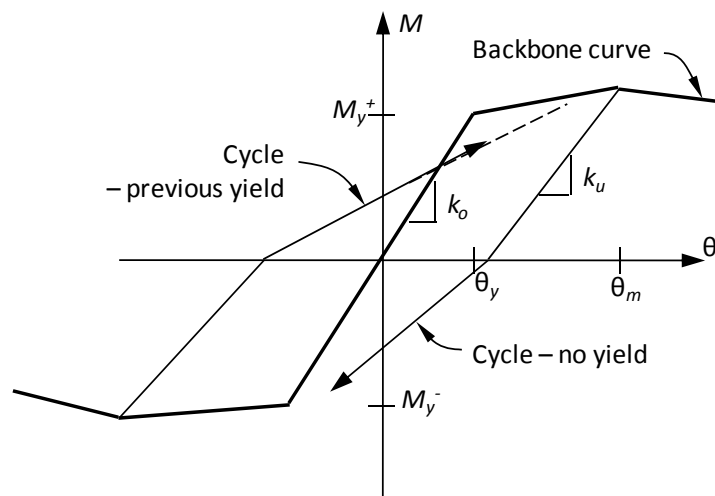
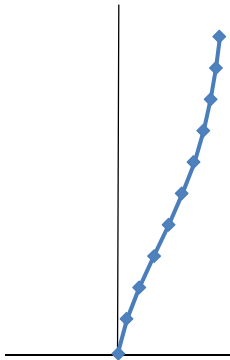
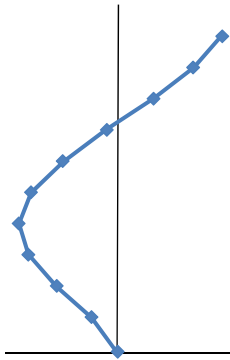
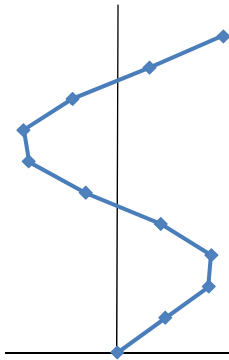


Fig. 6.6: Schematic Diagram of Takeda Hysteretic Model

Table 6.5: Comparison of Modes of Vibration of Red Book Building

Study	Period (s)		
	1 st Mode	2 nd Mode	3 rd Mode
			
CCANZ (1998) ¹	2.04	0.66	-
Robertson (2005)	2.14	0.70	0.41
Present Study	2.15	0.70	0.39

¹ Average of orthogonal directions

Table 6.5 also shows the first three modes of vibration of the Red Book building. The first mode shape is dominated by shear, and all inter-storey drifts are approximately the same. As the mode number increases, inter-storey drifts can become significant, imposing high levels of damage on the structure.

In order to accurately capture the realistic structural demands, it is necessary to include non-linear effects in analyses of the structure. In the model constructed, hinges were placed at beam- and column-faces in all frames with the Takeda model describing hysteretic behavior. The basic Takeda hysteresis is shown in Fig. 6.6. The model consists of three main features – a backbone curve, cycles with no previous yield, and cycles with previous yield. In SAP2000, the backbone curve is user-defined, given as a moment-rotation (M - θ) relationship. The unloading slopes k_u of the cycles are defined in terms of the rotation ductility $\mu_\theta = \theta_m / \theta_y$, where θ_y is the yield rotation and θ_m is the

rotation at initiation of unloading. As μ_θ increases, k_u decreases, indicating higher levels of softening. The points at which the cycles rejoin the backbone curve are defined in terms of the plastic rotation $\theta_p = \theta_m - \theta_y$. Again, as θ_p increases, the slope of the cycle curve gets flatter.

For cases where the reinforcing details were known, the backbone curve was defined from a rigorous moment-curvature analysis of each critical section, allowing for axial load. The analysis technique, presented above, uses stress-strain relationships of reinforcing steel, confined concrete and unconfined concrete to define a full moment-curvature relationship for a reinforced concrete section. Probable strengths of 45MPa for concrete and 450MPa for steel were used. The curvature was multiplied by the plastic hinge length (equal to half the section depth) to obtain the rotation. A simplified check based on rational mechanics was done for each analysis.

The Red Book does not specify the reinforcement details in the gravity frame. Column capacities in the gravity frame were inferred based on the level of axial loads in these columns. For a column under eccentric axial loading, the eccentricity e and compressive stress block height a are defined as

$$a = \frac{P}{0.85f_c'b} \quad (6.1)$$

and

$$e = 0.5(d - a) \quad (6.2)$$

Hence from equilibrium,

$$M = Pe = P \frac{d}{2} \left(1 - \frac{P}{2 \times 0.85f_c'A_g} \right) \quad (6.3)$$

where A_g is the gross area of the cross-section and d is the section depth. Since the second term in the brackets is usually of the order of one third, (6.3) reduces to:

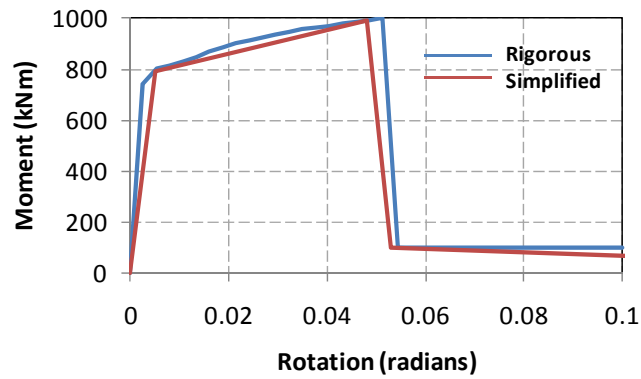
$$M = Pd / 3 \quad (6.4)$$

A similar method was used to obtain the residual moment capacities after failure, where the moment arm is taken as $d - d'$. The beam capacities in the gravity frame were based on the maximum gravity moments, redistributed by 30 percent (as permitted under the provisions of NZS 3101:2006). A post-yield bilinear factor of 0.03 was applied throughout the gravity frame. The moment-rotation relationship was simplified from the original analyses, as shown in Fig. 6.7(a). All hinges used in the analysis are presented in Fig. 6.7(b) to 6.7(e).

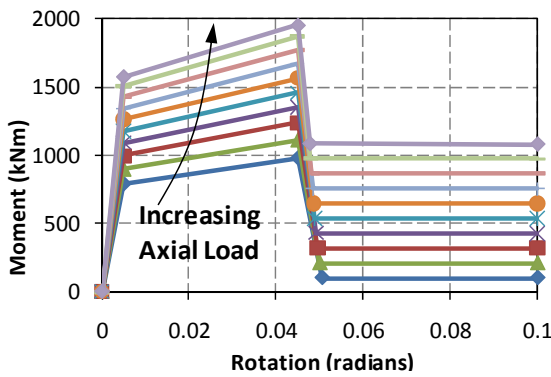
6.4 Pushover Analysis

One option available to determine the ultimate drift capacity of a structure is to conduct a monotonic pushover analysis. Using this method, gravity loads under earthquake conditions are initially applied to the structure. Lateral loads are then applied using, for example, the equivalent static method described in NZS 1170.5:2004. According to CCANZ (1998), for a ductile frame ($\mu = 6$) on intermediate soil with a period of approximately 1.65 seconds, a lateral force coefficient of 0.03 should be used. Hence, the horizontal seismic shear force $V = 1888$ kN. Table 6.6 shows how this is distributed at each level.

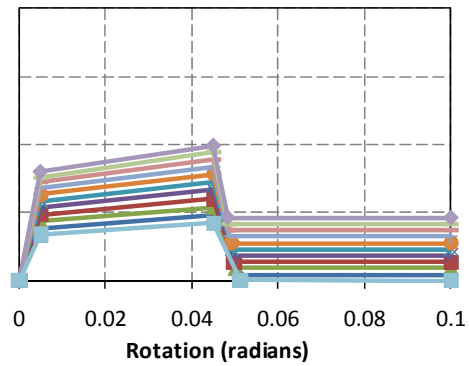
The values shown in Table 6.6 are for an entire storey. Also, these values are for a DBE which has a 10% probability of exceedence in 50 years. To convert these values to those for an MCE with a 10% probability of exceedence in 2500 years, the force at each level was multiplied by 1.8 in accordance with NZS 1170.5:2004. This yields a total base shear of $V = 1700$ kN.



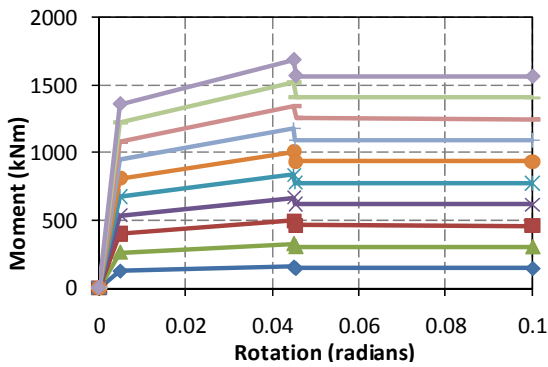
(a) Simplification of Moment-Rotation Relationship (Roof Level, Perimeter Frame)



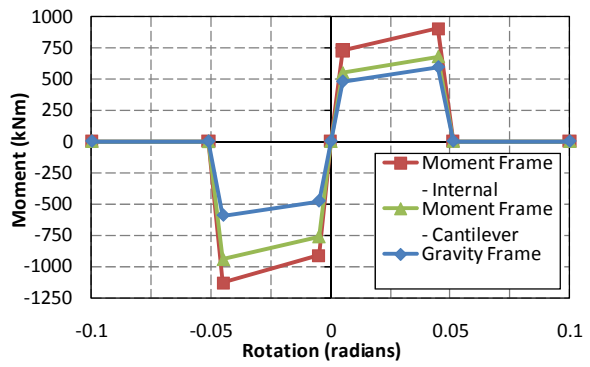
(b) Perimeter Columns – Strong Axis



(c) Perimeter Columns – Weak Axis



(d) Gravity Columns



(e) Beams

Fig. 6.7: Backbone Curves of Hinges Used in SAP2000 Model

Table 6.6: Vertical Distribution of Lateral Forces

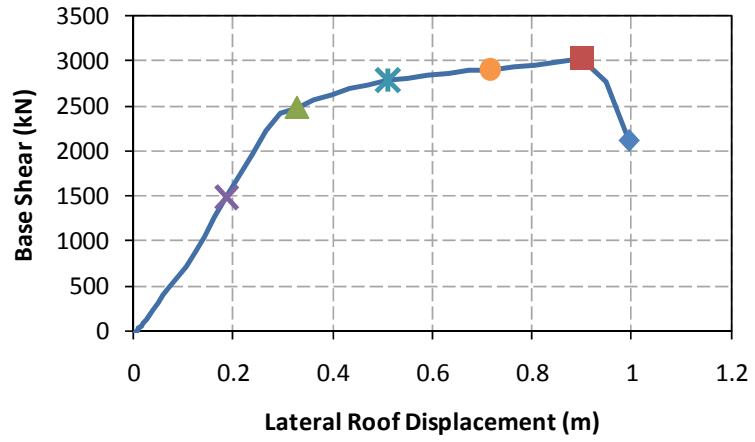
Level	Weight (kN)	h_i (m)	$W_i h_i$ (kNm)	F_i (kN)
Roof	6209	36.4	226008	460
9	6296	32.8	206509	283
8	6296	29.2	183843	252
7	6296	25.6	161178	221
6	6296	22	168512	190
5	6296	18.4	115846	159
4	6296	14.8	93181	128
3	6296	11.2	70515	97
2	6296	7.6	47850	65
1	6372	4.0	25488	35
	$\Sigma = 62949$		$\Sigma = 1268929$	$\Sigma = 1888$

where

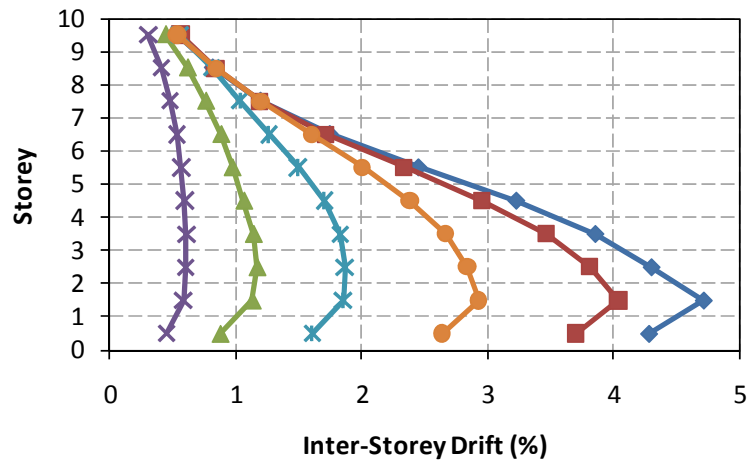
$$F_i = 0.92V \frac{W_i h_i}{\sum (W_i h_i)} \quad (6.5)$$

and an additional $0.08V$ is added to the roof level.

The results of the pushover analysis are shown in Fig. 6.8. The solid line in Fig. 6.8(a) shows the pushover response of the entire frame. The instantaneous vertical drift profiles for each point indicated in Fig. 6.8(a) are shown in Fig. 6.8(b). It is evident from these results that the maximum inter-storey drift takes place in the lower levels of the structure. This highlights the need for appropriate detailing against undesirable modes of failure, since unexpected failure in this area can lead to collapse of the entire structure. The inter-storey drift between levels 1 and 2 at peak lateral load is about 4%. This represents the seismic drift capacity of the structure.



(a) Pushover Force-Displacement Curve



(b) Instantaneous Drift Profiles at Points Indicated in (a)

Fig. 6.8: Results of Pushover Analysis for Red Book Building

6.5 Incremental Dynamic Analysis

An alternative approach in determining the drift capacity of a structure, particularly when dynamic effects are of interest, is to conduct an incremental dynamic analysis (IDA). Although the concept of subjecting a structure to a “dynamic pushover” analysis has been proposed and developed by several researchers, the IDA method developed primarily by Vamvatsikos and Cornell (2002, 2004) is perhaps now the most rigorous and widely used method for IDA. Under this method, a series of time-history analyses are performed on the structure with increasing intensity. The objective is to determine the intensity level leading to collapse, identified by a substantial increase in maximum drift for a relatively small increase in intensity. By carrying out the IDA for a suite of earthquakes, statistical techniques can be applied to the IDA results to determine the intensity leading to various stages of drift, and therefore damage. The IDA method has gained popularity among researchers, particularly in the emerging field of loss estimation (Solberg et al., 2008; Sircar et al., 2009).

The IDA is carried out for the model of the Red Book Building using SAP2000. The analysis consists of subjecting the model to a suite of 20 earthquake ground motion acceleration records. Each record is run repetitively, with incrementally increasing intensity measures (IM). For each run, the maximum absolute drift in the structure is recorded.

Table 6.7 presents details of the 20 earthquake ground motion acceleration records from the PEER Strong Ground Motion Database, used in the Vamvatsikos and Cornell (2004) study. A plot of scaled acceleration response spectra for the suite is given in Fig. 6.9(a). All ground motion records given in the PEER Strong Ground Motion Database are in terms of gravitational acceleration, g . As such, the records should first be converted into the units of the model (in this case mm and N, requiring multiplication by 9180). The records are then normalized with respect to $S_A (T = 1)$; that is, the peak ground acceleration for a building with a period of $T = 1$ s will be g . Finally, the record is multiplied by

the intensity factor, starting with 0.1 and increasing incrementally in steps of 0.1 for each successive run for a given earthquake record. Each individual earthquake record was run as a nonlinear direct integration time history analysis in SAP2000. A step size of 0.005s was used and checked for convergence.

Table 6.7: Details of 20 Ground Motion Records Used in IDA

No.	Event	Station	Φ^* ¹	M^* ²	R^* ³ (km)	PGA (g)
1	Loma Prieta 1989	Agnews State Hospital	90	6.9	28.2	0.159
2	Imperial Valley 1979	Plaster City	135	6.5	31.7	0.057
3	Loma Prieta 1989	Hollister Diff. Array	255	6.9	25.8	0.279
4	Loma Prieta 1989	Anderson Dam	270	6.9	21.4	0.244
5	Loma Prieta 1989	Coyote Lake Dam	285	6.9	22.3	0.179
6	Imperial Valley 1979	Cucapah	85	6.5	23.6	0.309
7	Loma Prieta 1989	Sunnyvale Colton Ave.	270	6.9	28.8	0.207
8	Imperial Valley 1979	El Centro Array #13	140	6.5	21.9	0.117
9	Imperial Valley 1979	Westmoreland Fire Station	90	6.5	15.1	0.074
10	Loma Prieta 1989	Hollister South and Pine	0	6.9	28.8	0.371
11	Loma Prieta 1989	Sunnyvale Colton Ave.	360	6.9	28.8	0.209
12	Superstition Hills 1987	Wildlife Liquefaction Array	90	6.7	24.4	0.181
13	Imperial Valley 1979	Chihuahua	282	6.5	28.7	0.254
14	Imperial Valley 1979	El Centro Array #13	230	6.5	21.9	0.139
15	Imperial Valley 1979	Westmoreland Fire Station	180	6.5	15.1	0.110
16	Loma Prieta 1989	WAHO	0	6.9	16.9	0.370
17	Superstition Hills 1987	Wildlife Liquefaction Array	360	6.7	24.4	0.207
18	Imperial Valley 1979	Plaster City	45	6.5	31.7	0.042
19	Loma Prieta 1989	Hollister Diff. Array	165	6.9	25.8	0.269
20	Loma Prieta 1989	WAHO	90	6.9	16.9	0.638

¹Component

²Moment Magnitude

³Closest Distance to Fault Rupture

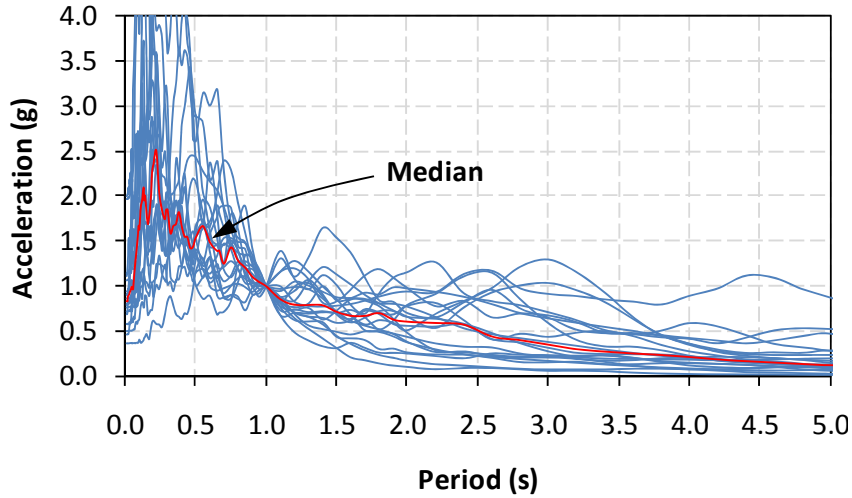
Source: PEER Strong Motion Database, <http://peer.berkeley.edu/smcat>

6.6 IDA Results and Implications

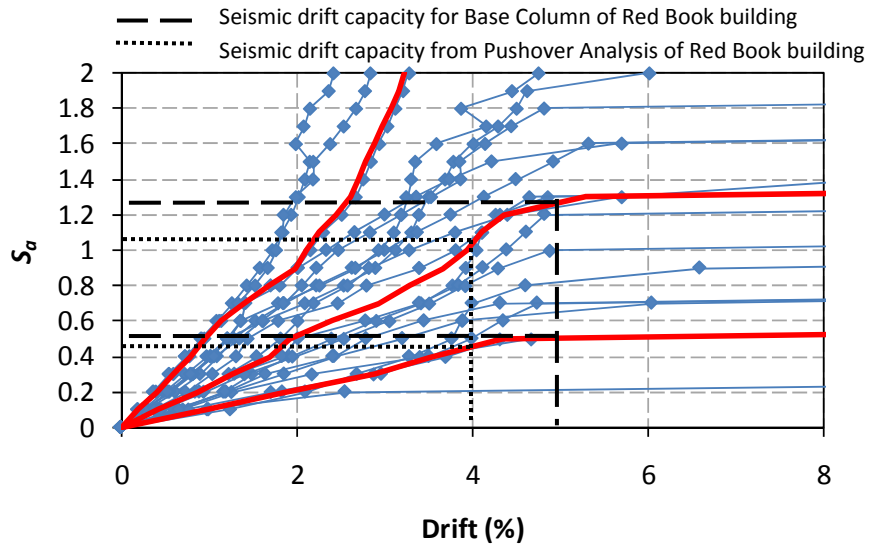
The results of the IDA of the Red Book building are presented in Fig. 6.9(b). These results represent a seismic drift demand for a given spectral acceleration, and to evaluate the performance of a given design, these are compared to the drift capacity for that design. The capacities for two cases are shown on Fig. 6.9(b). Firstly, from a rigorous column pushover analysis for the base columns in the Red Book building, the ultimate drift capacity (governed by global buckling) was determined to be 5.0%. This drift capacity indicates that there is a 90% probability that the building will survive an earthquake with $S_A = 0.52g$ (a moderate sized earthquake), and a 50% probability that it will survive an earthquake with $S_A = 1.27g$ without collapsing. Using the same procedure for the drift capacity given by the pushover analysis of the Red Book building, the respective spectral accelerations are slightly lower, but comparable. For design applications, a similar procedure can be used to determine the required drift capacity for a given earthquake intensity and probability of exceedence.

6.7 Chapter Closure

In preceding chapters, a model has been presented for the prediction of compressive axial force-deformation behavior of reinforcing bars including the effects of buckling. This chapter has completed the picture by demonstrating the use of this model, along with models for other aspects of column behavior, with reference to performance-based analysis and design. This has been done using a static pushover analysis and a more rigorous incremental dynamic analysis.



(a) 5% Damped Acceleration Response Spectra for the Selected Ground Motion Records, Normalized with respect to $S_a(T = 1)$



(b) Results of IDA, Showing Median, 10th and 90th Percentile Responses

Fig. 6.9: Acceleration Response Spectra and IDA Results for Red Book Building

CHAPTER VII

SUMMARY AND CONCLUSIONS

7.1 Summary

The aim of the research presented in this thesis was to develop a robust technique for identifying the critical curvature in reinforced concrete columns based on the four modes of column failure identified by Dutta and Mander (1998). While models exist for identifying failure due to low-cycle fatigue, shear and concrete confinement, no acceptable model was found for predicting the buckling behavior of longitudinal reinforcing steel. As such, a computational algorithm was developed in which the compressive behavior of longitudinal reinforcing steel could be accurately modeled, considering the effects of local and global buckling.

Once the computational algorithm was validated against experimental data, a general set of local buckling data was generated for a range of real steels, and the results interrogated. From computational observations and rational mechanics, an analytical model was developed for the direct prediction of the compressive steel stress-strain behavior based on material and geometric inputs. This analytical model was also validated against experimental results. By incorporating the effects of core concrete expansion and hoop stresses, the computational model was extended for the global buckling case. Using computational observations in a limit analysis, a simplified analysis-and-design equation was developed for global buckling of the longitudinal steel. This, together with a formulation based on hoop fracture, was used to modify the compressive stress-strain relationship to incorporate local and global buckling, and hoop fracture.

The derived buckling models were then incorporated into a moment-curvature analysis, along with models for concrete confinement, shear failure and low-cycle fatigue. Once the moment-curvature routine had been validated against experimental data, a full

pushover analysis was carried out for a ten-storey reinforced concrete frame building to determine the critical drift at collapse. The column moment-curvature routine was used to define the backbone curves for non-linear hinges in critical sections throughout the building. An incremental dynamic analysis of the RC frame building was carried out to demonstrate applications to performance-based analysis and design.

7.2 Design Considerations

In detailing RC columns against local buckling of longitudinal steel, the aim is two-fold. Firstly, a strength of at least f_y should be achieved, since this is what is assumed in design. Secondly, this stress should be sustained over a substantial strain excursion to achieve the levels of ductility required in the section. Current practice is to limit the spacing of hoopsets in these sections to $6d_b$. The computational study carried out in Chapter IV confirmed that this is sufficient to ensure satisfactory behavior from the steel in compression. For some grades of steel, a spacing as high as $10d_b$ is still sufficient to guard against local buckling.

This becomes important when designing against global buckling. It was explained in Chapter V that global buckling is highly undesirable, since other modes of failure such as shear failure, concrete confinement failure and low-cycle fatigue become inevitable. As such, a local buckling failure should be favored over a global buckling failure in design. There exists, however, a dilemma for designers whereby the choice must be made between tightly-spaced, smaller diameter hoops, and larger hoops spaced further apart. While the former is better for confinement of the core concrete, in many cases it will lead to a global buckling failure. The sacrifice of some confinement efficiency is considered necessary, however, to ensure that a global buckling failure does not occur. As such, the designer should favor larger hoops at a higher spacing.

When comparing section geometry, a circular column is a more efficient layout for confinement of the core, but the restraint provided against lateral buckling is much lower

than for a rectangular section. In fact, global buckling is an almost inevitable occurrence in circular columns. Various remedies have been proposed to deal with this, such as having an inner and outer ring of reinforcement, so that the longitudinal steel in the inner ring will not be affected by buckling.

Finally, it was found that current provisions for global buckling (where they exist) that the hoop force at yield be at least one sixteenth of the bar force at yield appear to be woefully inadequate. Computational observations indicate that this will lead to a global buckling failure with a hoop spacing of $6d_b$. In general, hoops that are half the diameter of the longitudinal bars being restrained should be adequate for higher spacing of transverse steel. This is only apparent when the effects of core concrete dilation are considered.

7.3 Recommendations for Future Research

While the work described in this thesis aims to espouse a better understanding of the behavior of RC columns at ultimate limit state, several topics are suggested for further investigation as part of the ongoing research in this field.

7.3.1 Experimental Investigations

The local buckling model derived in this thesis has been validated against a wide range of experimental data. Given the high variability of this data, and given the fact that the model is partly empirically based, it would be beneficial to expand the existing database by carrying out more local buckling experiments, where un-machined steel bars are tested in monotonic compression. The method used should comply with the description given in Chapter II. The current range of parameters in the experimental database is sufficient, but increasing the volume of results will increase the confidence.

As has been pointed out in Chapter V, no studies are known to have been done where global buckling of longitudinal steel is examined in isolation from other aspects of

column behavior. As such, current global buckling models remain speculative until such an experimental investigation is carried out. Although it has been shown that global buckling and other modes of failure are interdependent, these experiments are required in order to better understand the global buckling phenomenon.

An experimental set-up, shown in Fig. 7.1, is proposed whereby a wide range of hoop sizes, hoop spacings and longitudinal bar sizes can be tested. A concrete block is cast with an array of PVC ducts arranged as shown in the diagram. U-shaped hoops are fed through these ducts, and either welded or bolted to a backing plate. This connection to the backing plate should exceed the ultimate tensile strength of the hoops. A longitudinal bar is fed through the hoops, and subjected to a monotonically increasing axial force. The ends of the longitudinal bar are clamped into rigid end blocks to avoid rotation. Axial strains are measured with LVDTs.

7.3.2 Theoretical Investigations

One aspect of concrete material behavior that is in want of attention is the expansion and dilation of confined concrete. In the early stages of loading, Poisson's effect causes a lateral expansion of the core concrete. Under higher axial loads and confining stresses, the volume of the core concrete increases due to dilation effects, as with a sandy soil. While the model derived by Mander et al. (1988a) has been shown to work well for predicting the increase in strength due to confinement, as well as the increase in peak strain, there has been no attempt by researchers to predict the lateral expansion of the core concrete. Currently, only experimental evidence exists for the relationship between axial strains and lateral strains in RC columns (Mander et al., 1983; Mander, 1988b; Sheikh, 1978). A good starting point for deriving such a theoretical model would be a review of existing models for soil dilation, and how these may be adapted to concrete. A better understanding of this phenomenon is invaluable, since it is heavily tied with buckling and hoop fracture.

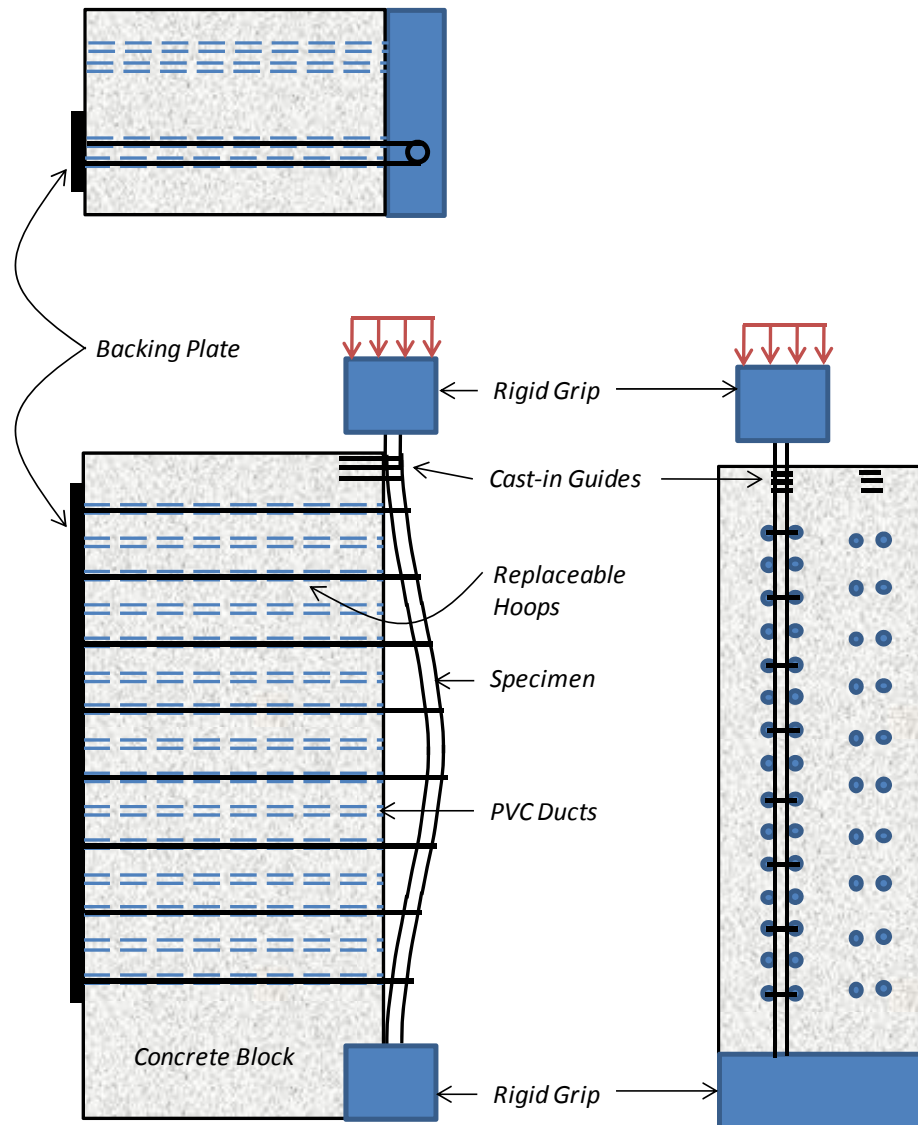


Fig. 7.1: Proposed Experimental Set-up for Global Buckling Experimental Investigation

While an attempt has been made in this research to unify all aspects of column behavior, particularly at the ultimate limit state, there is a considerable amount of research that can be done in this area. Most aspects of column behavior, such as shear, buckling, low-cycle fatigue and hoop fracture, can be well understood and modeled when considered in isolation. However, a unified model incorporating all modes of failure, including the interaction between these, remains an elusive goal. The key to developing such a model relies on accurate prediction of stresses in the transverse steel, since three of these modes of failure are controlled through the use of transverse steel. As a starting point, the instantaneous hoop stresses should be incorporated into the computational moment-curvature analysis of critical column sections.

REFERENCES

- American Concrete Institute (ACI). (2008). "Building code requirements for structural concrete and commentary." *ACI 318-08*, Detroit, MI
- Bae, S., Miseses, A.M. and Bayrak, O. (2005). "Inelastic buckling of reinforcing bars." *Journal of Structural Engineering*, 131, 314 – 321
- Bayrak, O. and Sheikh, S.A. (2001). "Plastic hinge analysis." *Journal of Structural Engineering*, 127(9), 1092 – 1100
- Berry, M.P. and Eberhard, M.O. (2005). "Practical performance model for bar buckling." *Journal of Structural Engineering*, 131(7), 1060 – 1070
- Bresler, B. and Gilbert, P.H. (1961). "Tie requirements for reinforced concrete columns." *ACI Journal*, 58(26), 555 – 570
- Chang, G.A. and Mander, J.B. (1994). "Seismic energy based fatigue damage analysis of bridge columns: Part I – Evaluation of seismic capacity." *NCEER Technical Report No. 94-0006*, Multidisciplinary Center for Earthquake Engineering Research, State University of New York, Buffalo, NY
- Cement and Concrete Association of New Zealand (CCANZ). (1998). *Examples of concrete structural design to NZS 3101:1995 – Red Book*. Cement and Concrete Association of New Zealand, Wellington, New Zealand
- Coffin, L.F., Jr. (1954). "A study of the effect of cyclic thermal stresses on a ductile metal." *Trans ASME*, 76, 931 – 950

- Coffin, L.F., Jr. (1971). "A note on low cycle fatigue laws." *Journal of Materials*, 6, 388 – 402
- Considère, A. (1891). "Resistance des pièces comprimées." *Congrès International des Procédés de Construction*, 3, 371, Paris, France
- Dhakal, R.P. and Maekawa, K. (2002a). "Modeling for postyield buckling of reinforcement." *Journal of Structural Engineering*, 128, 1139 – 1147
- Dhakal, R.P. and Maekawa, K. (2002b). "Path-dependent cyclic stress-strain relationship of reinforcing bar including buckling." *Engineering Structures*, 24, 1383 – 1396
- Dhakal, R.P. and Maekawa, K. (2002c). "Reinforcement stability and fracture of cover concrete in reinforced concrete members." *Journal of Structural Engineering*, 128(10), 1253 – 1262
- Dodd, L.L. and Restrepo-Posada, J.I. (1995). "Model for predicting cyclic behavior of reinforcing steel." *Journal of Structural Engineering*, 121, 433 – 445
- Dutta, A. and Mander, J.B. (1998). "Capacity design and fatigue analysis of confined concrete columns." *NCEER Technical Report No. 98-0007*, Multidisciplinary Center for Earthquake Engineering Research, State University of New York, Buffalo, NY
- Dutta, A. and Mander, J.B. (2001). "Energy based methodology for ductile design of concrete columns." *Journal of Structural Engineering*, 127 (12), 1374 – 1381

- Engesser, F. (1889). “Ueber die Knickfestigkeit gerader Stabe.” *Zeitschrift des Architekten-und Ingenieur – Vereins zu Hannover* 35, 445 and 462
- Engesser, F. (1891). “Die Knickfestigkeit gerader Stabe.” *Zentralblatt der Bauverwaltung*, Berlin (December 5, 1891), 483
- Euler, L. (1744). “De curvis elasticis, additamentum I, methodus inveniendi lineas curvas maximi minimive proprietate gaudentes.” Lausanne and Geneva, 267 – 268
- Euler, L. (1759). “Sur le forces des colonnes.” *Memoires de l’Academie Royale des Sciences et Belles Lettres*, 13, Berlin, Germany
- Falk, W.M. and Govindjee, S. (2000). “Unilateral buckling restrained by initial force supports.” *Journal of Engineering Mechanics*, 126(12), 1301 – 1302
- Gil-Martín, L.M., Hernández-Montes, E., Aschheim, M. and Pantazopoulou, S.J. (2006). “Slenderness effects on the simulated response of longitudinal reinforcement in monotonic compression.” *Structural Engineering and Mechanics*, 23(4), 369 – 386
- Gil-Martín, L.M., Hernández-Montes, E., Aschheim, M. and Pantazopoulou, S.J. (2008). “Approximate expressions for the simulated response of slender longitudinal reinforcement in monotonic compression.” *Magazine of Concrete Research*, 60(6), 391 – 397
- Gomes, A. and Appleton, J. (1997). “Nonlinear cyclic stress-strain relationship of reinforcing bars including buckling.” *Engineering Structures*, 19, 822 – 826

- González, J.J., Setién, J., Álvarez, J.A., Polanco, J.A. and Ferreño, D. (2006). “Failure of reinforcing concrete steel ribbed bars.” *Engineering Failure Analysis*, 13, 1376 – 1387
- Hornbeck, R.W. (1982). *Numerical methods*. Prentice Hall, Upper Saddle River, NJ
- Kim, J.H. and Mander, J.B. (2006). “Influence of transverse reinforcement on elastic shear stiffness of cracked concrete elements.” *Engineering Structures*, 29, 1798 – 1807
- Kunnath, S.K., Heo, Y. and Mohle, J.F. (2009). “Nonlinear uniaxial material model for reinforcing steel bars.” *Journal of Structural Engineering*, 135(4), 335 – 343
- Mander, J.B. (1983). “Seismic design of bridge piers.” PhD Thesis, University of Canterbury Christchurch, New Zealand
- Mander, J.B., Priestley, M.J.N. and Park, R. (1988a). “Theoretical stress-strain model for confined concrete.” *Journal of Structural Engineering*, 114 (8), 1804 – 1826
- Mander, J.B., Priestley, M.J.N. and Park, R. (1988b). “Observed stress-strain behavior of confined concrete.” *Journal of Structural Engineering*, 114(8), 1827 – 1849
- Mander, J.B., Panthaki, F.D. and Kasalanati, A. (1994). “Low-cycle fatigue behavior of reinforcing steel.” *Journal of Materials in Civil Engineering*, 6(4), 453 – 468
- Manson, S.S. (1965). “Fatigue: A complex subject – Some simple approximations.” *Experimental Mechanics*, 5(7), 193 – 226

Massone, L.M. and Moroder, D. (2009). “Buckling modeling of reinforcing bars with imperfections.” *Engineering Structures*, 31, 758 – 767

MATLAB version R2008b (2007). The MathWorks, Inc., Natick, MA

Mau, S.T. and El-Mabsout, M. (1989). “Inelastic buckling of reinforcing bars.” *Journal of Engineering Mechanics*, 115, 1 – 17

Mau, S.T. (1990). “Effect of tie spacing on inelastic buckling of reinforcing bars.” *ACI Structural Journal*, 87, 671 – 677

Menegotto, E. and Pinto, P.E. (1973). “Method of analysis of cyclically loaded RC plane frames including changes in geometry and nonelastic behavior of elements under normal force and bending.” *Structural Engineering International*, IABSE, Zurich, Switzerland, 13, 15 – 22

Monti, G. and Nuti, C. (1992). “Nonlinear cyclic behavior of reinforcing bars including buckling.” *Journal of Structural Engineering*, 118(12), 3268 – 3284

Moyer, M.J. and Kowalsky, M.J. (2003). “Influence of tension strain on buckling of reinforcement in concrete columns.” *ACI Structural Journal*, 100(1), 75 – 85

Pacific Earthquake Engineering Research (PEER). (2000). “PEER strong motion database.” PEER Center, University of California, Berkeley, CA

Pantazopoulou, S.J. (1998). “Detailing for reinforcement stability in RC members.” *Journal of Structural Engineering*, 124(6), 623 – 632

- Papia, M., Russo, G. and Zingone, G. (1988). "Instability of longitudinal bars in RC columns." *Journal of Structural Engineering*, 114(2), 445 – 461
- Papia, M. and Russo, G. (1989). "Compressive concrete strain at buckling of longitudinal reinforcement." *Journal of Structural Engineering*, 115(2), 382 – 397
- Park, R. and Paulay, T. (1975). *Reinforced concrete structures*. John Wiley, New York, NY
- Park, R., Priestley, M.J.N. and Gill, W.D. (1982). "Ductility of square-confined concrete columns." *Proceedings ASCE, Structural Division*, 108(ST4), 929 – 950
- Paulay, T. and Priestley, M.J.N. (1992). *Seismic design of reinforced concrete and masonry buildings*. John Wiley, New York, NY
- Popovics, S. (1973). "A numerical approach to the complete stress-strain curves of concrete." *Cement and Concrete Research*, 3(5), 583 – 599
- Priestley, M.J.N., Park, R. and Potangaroa, R.T. (1981). "Ductility of spirally-confined concrete columns." *Proceedings ASCE, Structural Division*, 107(ST1), 181 – 202
- Priestley, M.J.N. and Calvi, G.M. (1996). *Seismic design and retrofit of bridges*. John Wiley, New York, NY
- Robertson, K.L. (2005). "Probabilistic design and assessment methodologies for the new generation of damage resistant structures." M.E. thesis, University of Canterbury, Christchurch, New Zealand

- Rodriguez, M.E., Botero, J.C. and Villa, J. (1999). "Cyclic stress-strain behavior of reinforcing steel including effect of buckling." *Journal of Structural Engineering*, 125(6), 605 – 612
- Russo, G. (1988). "A buckling model for reinforcing bars." *International Journal of Mechanical Sciences*, 31, 3 – 11
- SAP2000 version 14*. (2009). Computers and Structures, Inc., Berkeley, CA
- Sato, Y. and Ko, H. (2007). "Experimental investigation of conditions of lateral shear reinforcements in RC columns accompanied by buckling of longitudinal bars." *Earthquake Engineering and Structural Dynamics*, 36, 1685 – 1699
- Scribner, C.F. (1986). "Reinforcement buckling in reinforced concrete flexural members." *ACI Journal*, 83(85), 966 – 973
- Shanley, F.R. (1947). "Inelastic column theory." *Journal of Aeronautical Sciences*, 14(5), 261 – 264
- Sheikh, S.A. (1978). "Effectiveness of rectangular ties as confinement steel in reinforced concrete columns." PhD Thesis, University of Toronto, Toronto, Canada
- Sircar, J., Damnjanovic, I., Mander, J.B. and Aslan, Z. (2009). "Catastrophe bonds for transportation assets feasibility analysis for bridges." *Transportation Research Record: Journal of the Transportation Research Board*, 2115, 12 – 19
- Solberg, K.M., Dhakal, R.P., Mander, J.B. and Bradley, B.A. (2008). "Computational and rapid expected annual loss estimation methodologies for structures." *Earthquake Engineering and Structural Dynamics*, 37, 81 – 101

- Standards New Zealand (SNZ). (2004). “Structural design actions – earthquake actions – New Zealand.” *NZS 1170.5:2004*, Wellington, New Zealand
- Standards New Zealand (SNZ). (2006). “Concrete structures standard. Part 1 – The design of concrete structures.” *NZS 3101.1:2006*, Wellington, New Zealand
- Syntzirma, D.V., Pantazopoulou, S.J. and Aschheim, M. (2010). “Load-history effects on deformation capacity of flexural members limited by bar buckling.” *Journal of Structural Engineering*, 136(1), 1 – 11
- Takeda, T., Sozen, M.A. and Nielsen, N.N. (1970). “Reinforced concrete response to simulated earthquakes.” *Journal of Structural Engineering*, 51(5), 2557 – 2573
- Vamvatsikos, D. and Cornell, C.A. (2002). “Incremental dynamic analysis.” *Earthquake Engineering and Structural Dynamics*, 31(3), 491 – 514
- Vamvatsikos, D. and Cornell, C.A. (2004). “Applied incremental dynamic analysis.” *Earthquake Spectra*, 20(2), 523 – 553
- Wight, J.K. and MacGregor, J.G. (2009). *Reinforced concrete mechanics and design*. Pearson Prentice Hall, Upper Saddle River, NJ

APPENDIX A
COMPUTER PROGRAM
FOR BUCKLING ANALYSIS


```

%%% 1. Obtain Input Data:
%%% =====

% AnalysisName, fy (MPa), Es (MPa), eps_sh, Esh (MPa), fsu (MPa), eps_su, s/d:
%%%=====
InputMatrix = { 'Mander84.D16.5.5', 295, 200e3, 0.025, 3500, 433, 0.19, 5.5; ... %1
                'Mander84.D16.6', 295, 200e3, 0.025, 3500, 433, 0.19, 6; ... %2
                'Mander84.D16.6.5', 295, 200e3, 0.025, 3500, 433, 0.19, 6.5; ... %3
                'Mander84.D20.6', 286, 200e3, 0.023, 4000, 446, 0.18, 6; ... %4
                'Mander84.D24.6', 260, 195e3, 0.018, 4500, 429, 0.18, 6; ... %5
                'Mander84.D28.6', 296, 203e3, 0.015, 4700, 484, 0.17, 6; ... %6
                'Mander84.H16.6', 360, 200e3, 0.016, 6000, 567, 0.15, 6; ... %7
                'Mander94.PT.6', 869, 221.3e3, 0.0039, 11030, 1130, 0.063, 6; ... %8
                'Mander94.PT.8', 869, 221.3e3, 0.0039, 11030, 1130, 0.063, 8; ... %9
                'Mander94.PT.9', 869, 221.3e3, 0.0039, 11030, 1130, 0.063, 9; ... %10
                'Mander94.R.6', 331, 215.1e3, 0.0091, 8274, 565, 0.144, 6; ... %11
                'Bayrak01.M20.4', 515, 200e3, 0.0091, 5500, 690, 0.16, 4; ... %12
                'Bayrak01.M20.5', 515, 200e3, 0.0091, 5500, 690, 0.16, 5; ... %13
                'Bayrak01.M20.6', 515, 200e3, 0.0091, 5500, 690, 0.16, 6; ... %14
                'Bayrak01.M20.7', 515, 200e3, 0.0091, 5500, 690, 0.16, 7; ... %15
                'Bae05.No8.5', 437, 198.6e3, 0.0092, 9000, 728, 0.147, 5; ... %16
                'Bae05.No8.6', 437, 198.6e3, 0.0092, 9000, 728, 0.147, 6; ... %17
                'Bae05.No8.7', 437, 198.6e3, 0.0092, 9000, 728, 0.147, 7; ... %18
                'Bae05.No8.8', 437, 198.6e3, 0.0092, 9000, 728, 0.147, 8; ... %19
                'Bae05.No8.9', 437, 198.6e3, 0.0092, 9000, 728, 0.147, 9; ... %20
                'Bae05.No10.4', 444, 202e3, 0.0091, 7000, 638, 0.158, 4; ... %21
                'Bae05.No10.5', 444, 202e3, 0.0091, 7000, 638, 0.158, 5; ... %22
                'Bae05.No10.6', 444, 202e3, 0.0091, 7000, 638, 0.158, 6; ... %23
                'Bae05.No10.7', 444, 202e3, 0.0091, 7000, 638, 0.158, 7; ... %24

for MM = 1 : size (InputMatrix, 1);

Member.BarDiam = 20;
Section.BarDiam = 20;
BarDiam = 20;

% Steel material properties for current steel:
AnalysisName = cell2mat (InputMatrix (MM, 1))
Section.SteelProps.YieldStress = cell2mat (InputMatrix (MM, 2)); %MPa
Section.SteelProps.YoungsMod = cell2mat (InputMatrix (MM, 3)); %MPa
Section.SteelProps.ShStrain = cell2mat (InputMatrix (MM, 4));
Section.SteelProps.ShMod = cell2mat (InputMatrix (MM, 5)); %MPa
Section.SteelProps.UltStress = cell2mat (InputMatrix (MM, 6)); %MPa %%% f_su
Section.SteelProps.UltStrain = cell2mat (InputMatrix (MM, 7));

Section.SteelProps.NYieldStress = -331; %MPa
Section.SteelProps.NShStrain = -0.0091;
Section.SteelProps.NShMod = 8274; %MPa
Section.SteelProps.NUltStress = -565; %MPa
Section.SteelProps.NUltStrain = -0.144;

Section.SteelProps.Spacing = cell2mat (InputMatrix (MM, 8)) * BarDiam;
%mm; NOT INPUT!!!
Section.SteelProps.InitEccent = 0.000001 * (Section.SteelProps.Spacing ^ ...
2) / BarDiam; %mm

Precision.alphaSteel = 20;
Precision.GradFactor = 0.1; % 0.1 is good for monotonic
Precision.DeltaRefStrain = -5e-4; % -5e-4 works for this analysis

```

```

Precision.CurveIncStep = 0.0001; % 0.0001 is good for monotonic
Precision.maxits       = 400000; %
Precision.Tolerance    = 5; % 5 is good
Precision.SectionElements = 24;
Precision.TolEccent    = 0.1 * Section.SteelProps.InitEccent; %
AxialLoad = 0; % N

```

```

% -----
%%% 2. Basic Analysis:
%%% =====

```

```

% USING GAUSS-QUADRATURE FOR CIRCULAR SECTION (24-Point Quadrature)
% -----

```

```

xi_core = [-0.9951872200, ...
-0.9747285560, ...
-0.9382745520, ...
-0.8864155270, ...
-0.8200019860, ...
-0.7401241916, ...
-0.6480936519, ...
-0.5454214714, ...
-0.4337935076, ...
-0.3150426797, ...
-0.1911188675, ...
-0.0640568929, ...
0.0640568929, ...
0.1911188675, ...
0.3150426797, ...
0.4337935076, ...
0.5454214714, ...
0.6480936519, ...
0.7401241916, ...
0.8200019860, ...
0.8864155270, ...
0.9382745520, ...
0.9747285560, ...
0.9951872200];

```

```

w_core = [0.0123412298, ...
0.0285313886, ...
0.0442774388, ...
0.0592985849, ...
0.0733464814, ...
0.0861901615, ...
0.0976186521, ...
0.1074442701, ...
0.1155056681, ...
0.1216704729, ...
0.1258374563, ...
0.1279381953, ...
0.1279381953, ...
0.1258374563, ...
0.1216704729, ...
0.1155056681, ...
0.1074442701, ...
0.0976186521, ...
0.0861901615, ...

```

```

0.0733464814, ...
0.0592985849, ...
0.0442774388, ...
0.0285313886, ...
0.0123412298];

Section.Depth.Steel = xi_core * BarDiam / 2;

% Compute steel areas:
Section.Area.Steel = ((BarDiam ^ 2) * w_core .* sqrt (1 - xi_core ...
.^ 2) / 2);

Member.YieldStrain = Section.SteelProps.YieldStress / ...
    Section.SteelProps.YoungsMod;
PUMoment = (BarDiam ^ 3) * Section.SteelProps.YieldStress / 6; %%% M_pu

% Transpose depth and area vectors:
Section.Depth.Steel      = Section.Depth.Steel';
Section.Area.Steel       = Section.Area.Steel';

% -----
%%% 3. Run Moment-Curvature Analysis:
%%% =====

Marker = 0;
[MomentOut, CurveOut, EccentricityOut, RefStrainOut, ...
    SteelStrainOut, SteelStressOut, YieldMoment, ForceOut] = ...
    MomentCurve08Cyclic (Section, Precision, Marker); %%% M_u, Phi

% Find step corresponding to peak force:
for ww = 1 : length (ForceOut)
    if ForceOut (ww) == min (ForceOut)
        Marker = ww;
    end
end

% Re-run analysis to find required stress and strain profiles:
[MomentOut, CurveOut, EccentricityOut, RefStrainOut, ...
    SteelStrainOut, SteelStressOut, YieldMoment, ForceOut] = ...
    MomentCurve08Cyclic (Section, Precision, Marker); %%% M_u, Phi

ForceMax = - min (ForceOut) / ((pi * Section.BarDiam ^ 2) / 4) * ...
    Section.SteelProps.YieldStress;
CurveMax = CurveOut (Marker) * BarDiam;
MomentMax = MomentOut (Marker) / PUMoment;
EccentricityMax = EccentricityOut (Marker) / BarDiam;
RefStrainMax = RefStrainOut (Marker) - Member.YieldStrain;

% -----
%%% 4. Plot Results:
%%% =====
CurveOut = CurveOut * BarDiam; % Radians to non-dimension

% Moment-curvature plot:
figure (1)
MomentOut = MomentOut / PUMoment; % kNm
plot (CurveOut, MomentOut, 'b-')
xlabel ('Phi * db');
ylabel ('Mu / Mpu');

```

```

title ('Moment-Curvature Relationship for Steel Reinforcing Bar');

v = axis;
xx = linspace (v (1), v (2), 100);
yy = zeros(size (xx)); hold on, plot (xx, yy, 'k')
xx2 = linspace (v (3), v (4), 100);
yy2 = zeros (size (xx)); hold on, plot (yy2, xx2, 'k')
grid on
% Axial load-curvature plot:
figure (2)
StressOut = ForceOut / ((pi * Section.BarDiam ^ 2) / 4); % MPa
StressOut = StressOut / Section.SteelProps.YieldStress;
plot (CurveOut, StressOut, 'k-')
xlabel ('Phi * db');
ylabel ('fcr / fy');
title ('Moment-Curvature Relationship for Steel Reinforcing Bar');
v = axis;
xx = linspace (v (1), v (2), 100);
yy = zeros(size (xx)); hold on, plot (xx, yy, 'k')
xx2 = linspace (v (3), v (4), 100);
yy2 = zeros (size (xx)); hold on, plot (yy2, xx2, 'k')
grid on

% Eccentricity-curvature plot:
figure (3)
plot (CurveOut, EccentricityOut, 'r-')
xlabel ('Phi * db');
ylabel ('del P / del epsilon');
title ('Gradient of Axial Load - Strain Graph for Steel Reinforcing Bar');
v = axis;
xx = linspace (v (1), v (2), 100);
yy = zeros(size (xx)); hold on, plot (xx, yy, 'k')
xx2 = linspace (v (3), v (4), 100);
yy2 = zeros (size (xx)); hold on, plot (yy2, xx2, 'k')
grid on

% -----
%%% 5. Write Main Results to an Output File:
%%% =====

outfile = strcat ('BucklingAnalysisSDB', AnalysisName, '.txt');

dlmwrite (outfile, 'URMSON's Buckling Analysis', 'delimiter', '', 'newline',
'pc');
dlmwrite (outfile, '=====', '-append', 'delimiter', '',
'newline', 'pc');
dlmwrite (outfile, ' ', '-append', 'delimiter', '', 'newline', 'pc'); %blank
line.

line1 = AnalysisName;
line2 = strcat ('S/db = ', num2str (Section.SteelProps.Spacing / BarDiam));
line2a = [' Input: fy, ' ' Es, ' ' eps_sh, ' ' Esh, ' ' fsu, '
eps_su'];
line2b = '-----';
-----';
line2c = [Section.SteelProps.YieldStress Section.SteelProps.YoungsMod
Section.SteelProps.ShStrain ...
Section.SteelProps.ShMod Section.SteelProps.UltStress Sec-
tion.SteelProps.UltStrain];

```

```

line3 = [' Peak: Force,'      ' Moment,'      ' Curvature,'      ' Eccentricity,'      '
Reference Strain'];
line3a = '-----'
-----';
line4 = [ForceMax MomentMax CurveMax EccentricityMax RefStrainMax];
line5 = 'Steel Strains at Curvature =';
line5a = '-----';
line6 = 'Steel Stresses at Curvature =';
line7 = [' History: Force,'      ' Moment,'      ' Curvature,'      ' Eccentricity,'
'Reference Strain'];
line7a = '-----'
-----';

dlmwrite (outfile, line1, '-append', 'delimiter', '', 'newline', 'pc');
dlmwrite (outfile, ' ', '-append', 'delimiter', '', 'newline', 'pc'); %blank
line.
dlmwrite (outfile, line2, '-append', 'delimiter', '', 'newline', 'pc');
dlmwrite (outfile, line2a, '-append', 'delimiter', '', 'newline', 'pc');
dlmwrite (outfile, line2b, '-append', 'delimiter', '', 'newline', 'pc');
dlmwrite (outfile, line2c, '-append', 'delimiter', '\t', 'newline', 'pc');
dlmwrite (outfile, ' ', '-append', 'delimiter', '', 'newline', 'pc'); %blank
line.
dlmwrite (outfile, line3, '-append', 'delimiter', '', 'newline', 'pc');
dlmwrite (outfile, line3a, '-append', 'delimiter', '', 'newline', 'pc');
dlmwrite (outfile, line4, '-append', 'delimiter', '\t', 'newline', 'pc', 'preci-
sion', 6);
dlmwrite (outfile, ' ', '-append', 'delimiter', '', 'newline', 'pc'); %blank
line.
dlmwrite (outfile, line5, '-append', 'delimiter', '', 'newline', 'pc');
dlmwrite (outfile, line5a, '-append', 'delimiter', '', 'newline', 'pc');
for ii = 1 : 6
    TITLE = strcat ('Phi * db = ', num2str ((ii - 1) * CurveMax / 4));
    dlmwrite (outfile, TITLE, '-append', 'delimiter', '', 'newline', 'pc');
end
dlmwrite (outfile, SteelStrainOut, '-append', 'delimiter', '\t', 'newline',
'pc', 'precision', 6);
dlmwrite (outfile, ' ', '-append', 'delimiter', '', 'newline', 'pc'); %blank
line.
dlmwrite (outfile, line6, '-append', 'delimiter', '', 'newline', 'pc');
dlmwrite (outfile, line5a, '-append', 'delimiter', '', 'newline', 'pc');
for ii = 1 : 6
    TITLE = strcat ('Phi * db = ', num2str ((ii - 1) * CurveMax / 4));
    dlmwrite (outfile, TITLE, '-append', 'delimiter', '', 'newline', 'pc');
end
dlmwrite (outfile, SteelStressOut, '-append', 'delimiter', '\t', 'newline',
'pc', 'precision', 6);
dlmwrite (outfile, ' ', '-append', 'delimiter', '', 'newline', 'pc'); %blank
line.
dlmwrite (outfile, line7, '-append', 'delimiter', '', 'newline', 'pc');
dlmwrite (outfile, line7a, '-append', 'delimiter', '', 'newline', 'pc');
for ii = 1 : length (ForceOut)
    ForceOut (ii) = ForceOut (ii) / (((pi * Section.BarDiam ^ 2) / 4) *
Section.SteelProps.YieldStress);
    % Moment and Curvature already normalised
    EccentricityOut (ii) = EccentricityOut (ii) / BarDiam;
    RefStrainOut (ii) = RefStrainOut (ii) - Member.YieldStrain;
    line8etc = [ForceOut(ii), MomentOut(ii), CurveOut(ii), EccentricityOut(ii),
RefStrainOut(ii)];

```

```

    dlmwrite (outfile, line8etc, '-append', 'delimiter', '\t', 'newline', 'pc',
'precision', 6);
end
end
% -----
% END OF FUNCTION

```

A2 Moment-Curvature Analysis Subroutine: MomentCurve08Cyclic.m

```

function [MomentOut, CurveOut, EccentricityOut, RefStrainOut, ...
    SteelStrainOut, SteelStressOut, YieldMoment, ForceOut] = ...
    MomentCurve08Cyclic (Section, Precision, Marker)

% MOMENTCURVE08 runs a numerical algorithm for finding the moment-curvature
% behaviour of a discretised steel reinforcing bar based on section
% properties, applied axial load and specified precision.
% -----
%
% TYPICAL CALL:
% [MomentOut, CurveOut, EccentricityOut, RefStrainOut, ...
% SteelStrainOut, SteelStressOut, YieldMoment, ForceOut] = ...
% MomentCurve08Cyclic (Section, Precision)
%
% DESCRIPTION:
% Function carries out numerical partial differentiation of the
% following equation to determine axial load and curvature:
%

$$\begin{pmatrix} ( & ) \\ ( & ) \\ ( d P & ) \\ ( & ) \\ ( & ) \\ ( d M & ) \\ ( & ) \\ ( & ) \end{pmatrix} = \begin{pmatrix} | & | \\ \text{del P} & \text{del P} \\ \text{-----} & \text{-----} \\ \text{del eps} & \text{del phi} \\ | & | \\ \text{del M} & \text{del M} \\ \text{-----} & \text{-----} \\ \text{del eps} & \text{del phi} \\ | & | \end{pmatrix} \begin{pmatrix} ( & ) \\ ( & ) \\ ( d eps & ) \\ ( & ) \\ ( & ) \\ ( d phi & ) \\ ( & ) \\ ( & ) \end{pmatrix}$$

%
% Successive increments of reference axis strain are applied, and for each
% total strain the curvature is determined to match the required target
% eccentricity as closely as practicable. Then, the bending moment is
% changed to match the target eccentricity to satisfy global equilibrium.
%
% INPUTS:
% Section = Structured array of element depths, areas and
% material properties
% AppliedLoad = Constant axial load applied to the member
% Precision = Structured array of various precision and stability
% parameters
%
% OUTPUTS:
% MomentOut = Output vector of bending moments as curvature varies
% CurveOut = Output vector of curvatures
% LoadOut = Output vector of loads
% YieldMoment = Moment at which steel yields
%
% PROGRAMME HISTORY:

```



```

%      DATE          PROGRAMMER      MODIFICATION
%      ----          -
%      09/29/08     C.R. Urmson      Original Code
%      10/20/08     C.R. Urmson      Added "-" to dP/de, so
%                                     code works properly
%      10/28/08     C.R. Urmson      Yielding Check Enabled
%      02/04/09     C.R. Urmson      Modified for cyclic
%                                     reloading from comp.
%      28/05/09     C.R. Urmson      Modified for Variable M
% -----

% Initialise variables:
% -----
MomentOut = zeros (Precision.maxits, 1);
InitMoment = MomentOut;
CurveOut = MomentOut;
ForceOut = MomentOut;
EccentricityOut = MomentOut;
RefStrainOut = MomentOut;
SteelStressOut = zeros (length (Section.Depth.Steel), 6);
SteelStrainOut = SteelStressOut;
LoadPrev = 0; MomentPrev = 0;
DeltaCurve = 0;
FirstIter = 0;
AppliedLoad = 0;
delLoaddelCurve = 0; delMomentdelStrain = 0;
Stress0 = zeros (length (Section.Depth.Steel), 1);
Strain0 = Stress0;
SteelStrainCompPrev = zeros (length (Section.Depth.Steel), 1);
SteelStressCompPrev = SteelStrainCompPrev;
LoadFlag = Stress0;
kk = 1;
Counter = 1;
CurveIncStep = Precision.GradFactor * Precision.DeltaCurve;
hh = 0;
YieldMoment = 0;
BarLength = Section.SteelProps.Spacing / 4;
Curve = Section.SteelProps.InitEccent * (pi ^ 2) / (4 * BarLength ^ 2);
h = waitbar (0, 'Running moment-curvature analysis. Please wait...');
flag.Correction=0;
% First step with axial rigidity as delLoaddelStrain:
% -----
Stress = AppliedLoad / ((pi * Section.BarDiam ^ 2) / 4);
if Stress > Section.SteelProps.NYieldStress
    EA = (pi * Section.BarDiam ^ 2) * Section.SteelProps.YoungsMod / 4;
    RefStrain = AppliedLoad / EA;
elseif Stress < Section.SteelProps.NYieldStress
    PowerNum = log (abs ((Section.SteelProps.NUltStress - Stress) / ...
        (Section.SteelProps.NUltStress - Section.SteelProps.NYieldStress)));
    PowerDenom = Section.SteelProps.NShMod * ( ...
        Section.SteelProps.NUltStrain - Section.SteelProps.NShStrain) / ...
        (Section.SteelProps.NUltStress - Section.SteelProps.NYieldStress);
    RefStrain = Section.SteelProps.NUltStrain - (( ...
        Section.SteelProps.NUltStrain - Section.SteelProps.NShStrain) * ...
        10 ^ (PowerNum / PowerDenom));
end

[Load1] = MomentLoad08Cyclic (RefStrain, Curve, Section.Depth, Section.Area,
...
```

```

    Section.SteelProps, Precision, Strain0, Stress0, ...
    SteelStrainCompPrev, SteelStressCompPrev, LoadFlag, FirstIter);
DeltaLoad = Load1 - AppliedLoad;

%%% STEP 0: Seed initial eccentricity and find initial Moment:
%%% =====
while InitMoment == 0
    if kk > 1
        RefStrainIncrement = RefStrain + Precision.RefStrainIncStep;
        [LoadIncrement2] = MomentLoad08Cyclic (RefStrainIncrement, Curve, ...
            Section.Depth, Section.Area, Section.SteelProps, Precision, ...
            Strain0, Stress0, SteelStrainCompPrev, SteelStressCompPrev, ...
            LoadFlag, FirstIter);
        delLoaddelStrain = - (LoadIncrement2 - LoadPrev) / ...
            (RefStrainIncrement - RefStrain);

        DeltaRefStrain = (DeltaLoad - (delLoaddelCurve * DeltaCurve)) / ...
            delLoaddelStrain;
        % Sensitivity to Reference strain increment can be controlled here:
        RefStrain = RefStrain + (0.25 * DeltaRefStrain);
    end

    % STEP 3: Determine revised strain profile (in MomentLoad08)
    % STEP 4: Determine section stresses and integrate to find section
    % axial load and bending moment (in MomentLoad08 and functions called
    % from it).
    % -----
    [Load, Moment, flag, SteelStrain1, SteelStress1, Strain0, Stress0, ...
        SteelStrainCompPrev, SteelStressCompPrev, LoadFlag] = ...
        MomentLoad08Cyclic (RefStrain, Curve, Section.Depth, Section.Area, ...
            Section.SteelProps, Precision, Strain0, Stress0, SteelStrainCompPrev,
...
            SteelStressCompPrev, LoadFlag, FirstIter);

    % Hence, calculate the out-of-balance force:
    DeltaLoad = Load - AppliedLoad;

    % STEP 5: Check tolerance of out-of-balance load:
    % -----
    if abs (DeltaLoad) < Precision.Tolerance

        % STEP 6 - check stopping criteria and plot results:
        % -----
        FirstIter = 1;
        [Load, Moment, flag, SteelStrain1, SteelStress1, Strain0, Stress0, ...
            SteelStrainCompPrev, SteelStressCompPrev, LoadFlag] = ...
            MomentLoad08Cyclic (RefStrain, Curve, Section.Depth, Section.Area,
...
                Section.SteelProps, Precision, Strain0, Stress0, SteelStrain-
CompPrev, ...
                SteelStressCompPrev, LoadFlag, FirstIter);
        FirstIter = 0;

        MomentOut (Counter) = Moment;
        CurveOut (Counter) = Curve;
        EccentricityOut (Counter) = Section.SteelProps.InitEccent;
        RefStrainOut (Counter) = RefStrain;
        SteelStressOut (:, 1) = SteelStress1;
    end
end

```

```

SteelStrainOut (:, 1) = SteelStrain1;
ForceOut (Counter) = AppliedLoad;
DeltaCurve = Precision.DeltaCurve;
InitMoment = Moment;

% Store value of yielding moment:
if flag.yield == 1
    hh = hh + 1;
    if hh == 1
        YieldMoment = Moment;
    end
end

% Calculate gradient of plot for next iteration:
CurveIncrement = Curve + CurveIncStep;
[LoadIncrement1] = MomentLoad08Cyclic (RefStrain, CurveIncrement, ...
    Section.Depth, Section.Area, Section.SteelProps, Precision, ...
    Strain0, Stress0, SteelStrainCompPrev, SteelStressCompPrev, ...
    LoadFlag, FirstIter);
delLoaddelCurve = (LoadIncrement1 - Load) / ...
    (CurveIncrement - Curve);

    Counter = Counter + 1;
else
    DeltaCurve = 0; % Go back to Step 1;
end
kk = kk + 1;
LoadPrev = Load;

% wait bar:
if rem (kk, 100) == 0
    waitbar (kk / Precision.maxits)
end
end

Eccentricity = Curve * (4 / (pi ^ 2)) * (BarLength ^ 2); %Total eccentricity
AppliedMoment = InitMoment;
DeltaMoment = 0;

%%% RUN MOMENT-CURVATURE ANALYSIS USING REFERENCE STRAIN:
%%% =====
% THIS CODE WORKS
while (kk < Precision.maxits)

    % STEP 1: Add strain increment to last strain:
    % -----
    RefStrainIncStep = Precision.GradFactor * Precision.DeltaRefStrain;
    RefStrain = RefStrain + DeltaRefStrain;

    % STEP 2: Determine required change in curvature to obtain
    % force-equilibrium of new strain profile:
    % -----
    if kk > 1
        CurveIncrement = Curve + Precision.CurveIncStep;
        FirstIter = 2;
        [LoadIncrement2, MomentIncrement2] = MomentLoad08Cyclic ...
            (RefStrain, CurveIncrement, Section.Depth, Section.Area, ...
            Section.SteelProps, Precision, Strain0, Stress0, ...

```

```

    SteelStrainCompPrev, SteelStressCompPrev, LoadFlag, FirstIter);
    FirstIter = 0;
    delMomentdelCurve = (MomentIncrement2 - MomentPrev) / ...
        (CurveIncrement - Curve);

    DeltaCurve = (DeltaMoment - (delMomentdelStrain * DeltaRefStrain)) /
...
        - delMomentdelCurve;
    % Sensitivity to Reference Strain Increment can be controlled here:
    Curve = Curve + (1 * DeltaCurve);
end
AddStrain = RefStrain - 0.678 * (Eccentricity / BarLength) ^ 2;
Eccentricity = Curve * (0.25 / (pi ^ 2)) * ...
    (Section.SteelProps.Spacing ^ 2) * (1 + AddStrain) ^ 2; %Total eccen-
tricity

% STEP 3: Determine revised strain profile (in MomentLoad08)
% STEP 4: Determine section stresses and integrate to find section
% axial load and bending moment (in MomentLoad08 and functions called
% from it).
% -----
[Load, Moment, flag, SteelStrain1, SteelStress1, Strain0, Stress0, ...
    SteelStrainCompPrev, SteelStressCompPrev, LoadFlag] = ...
    MomentLoad08Cyclic (RefStrain, Curve, Section.Depth, Section.Area, ...
        Section.SteelProps, Precision, Strain0, Stress0, SteelStrainCompPrev,
...
        SteelStressCompPrev, LoadFlag, FirstIter);

% Hence, calculate the out-of-balance moment:
DeltaMoment = (Moment - AppliedMoment);

% STEP 5: Check tolerance of out-of-balance moment:
% -----
if abs (DeltaMoment) < Precision.Tolerance

    % STEP 5a: Check out-of-balance eccentricity:
    % -----
    DeltaEccent = ((AppliedMoment - InitMoment) / Load) + ...
        (Eccentricity);
    if abs (DeltaEccent) < Precision.TolEccent

        % STEP 6 - check stopping criteria and plot results:
        % -----
        FirstIter = 1;
        [Load, Moment, flag, SteelStrain1, SteelStress1, Strain0,
Stress0, ...
            SteelStrainCompPrev, SteelStressCompPrev, LoadFlag] = ...
            MomentLoad08Cyclic (RefStrain, Curve, Section.Depth,
Section.Area, ...
                Section.SteelProps, Precision, Strain0, Stress0, ...
                SteelStrainCompPrev, SteelStressCompPrev, LoadFlag,
FirstIter);

        FirstIter = 0;

        MomentOut (Counter) = Moment;
        CurveOut (Counter) = Curve;
        EccentricityOut (Counter) = Eccentricity;
        RefStrainOut (Counter) = RefStrain;
        if Counter == ceil (Marker / 4)

```

```

        SteelStrainOut (:, 2) = SteelStrain1;
        SteelStressOut (:, 2) = SteelStress1;
    elseif Counter == ceil (Marker / 2);
        SteelStrainOut (:, 3) = SteelStrain1;
        SteelStressOut (:, 3) = SteelStress1;
    elseif Counter == ceil (3 * Marker / 4)
        SteelStrainOut (:, 4) = SteelStrain1;
        SteelStressOut (:, 4) = SteelStress1;
    elseif Counter == Marker
        SteelStrainOut (:, 5) = SteelStrain1;
        SteelStressOut (:, 5) = SteelStress1;
    elseif Counter == ceil (5 * Marker / 4)
        SteelStrainOut (:, 6) = SteelStrain1;
        SteelStressOut (:, 6) = SteelStress1;
    end
    ForceOut (Counter) = Load;
    DeltaRefStrain = Precision.DeltaRefStrain;

    % Store value of yielding moment:
    if flag.yield == 1
        hh = hh + 1;
        if hh == 1
            YieldMoment = Moment;
        end
    end

    % Calculate gradient of plot for next iteration:
    RefStrainIncrement = RefStrain + RefStrainIncStep;
    [LoadIncrement1, MomentIncrement1] = MomentLoad08Cyclic ...
        (RefStrainIncrement, Curve, Section.Depth, ...
        Section.Area, Section.SteelProps, Precision, Strain0, ...
        Stress0, SteelStrainCompPrev, SteelStressCompPrev, ...
        LoadFlag, FirstIter);
    delMomentdelStrain = (MomentIncrement1 - Moment) / ...
        (RefStrainIncrement - RefStrain);
    Counter = Counter + 1;
else % Modify Applied Bending moment to obtain global equilibrium
    AppliedMoment = AppliedMoment * (1 + 0.0001 * (DeltaEccent / ...
        (Eccentricity)));
    DeltaRefStrain = 0;
end

else
    DeltaRefStrain = 0; % Go back to Step 1;
end
kk = kk + 1;
MomentPrev = Moment;

% wait bar:
if rem (kk, 100) == 0
    waitbar (kk / Precision.maxits)
end
end

% Condense Output Matrices:
% -----

STOP = 0;
for JJ = 1 : (Precision.maxits - 1)

```

```

    if (MomentOut (JJ) == 0) && (MomentOut (JJ + 1) == 0) && (STOP == 0);
        OutputLength = JJ - 1;
        STOP = 1;
    end
end

MomentStore = zeros (OutputLength, 1);
ForceStore = MomentStore;
CurveStore = MomentStore;
EccentricityStore = MomentStore;
RefStrainStore = MomentStore;

for LL = 1 : OutputLength
    MomentStore (LL) = MomentOut (LL);
    ForceStore (LL) = ForceOut (LL);
    CurveStore (LL) = CurveOut (LL);
    EccentricityStore (LL) = EccentricityOut (LL);
    RefStrainStore (LL) = RefStrainOut (LL);
end

MomentOut = MomentStore;
ForceOut = ForceStore;
CurveOut = CurveStore;
EccentricityOut = EccentricityStore;
RefStrainOut = RefStrainStore;

close (h);
% END OF FUNCTION

```

A2.1 Modification to MomentCurve08Cyclic.m for Global Buckling

The following is an extract of the additional code used to determine incipient buckling for global buckling analysis.

```

% ++++++
% PROCEDURE FOR FINDING INITIAL ECCENTRICITY
% ++++++
PROCEED = 0;
COUNTERinit = 0;
while PROCEED == 0
    NuPlastic = 2;
    NuInit = 0.3;
    SpallStrain = 0.005;
    Lambda = 1;
    PlastHingeLength = 6 * (Section.SteelProps.Spacing / (NumHoops + 1));

    if COUNTERinit == 100000
        break
    end

    RefStrain = RefStrain + Precision.DeltaRefStrain;
    TransStrain = (NuInit * -RefStrain) + (NuPlastic - NuInit) * max ...
        (0, (-RefStrain - Lambda * SpallStrain));
    Section.SteelProps.InitEccent = 0.5 * (6 * TransStrain * Hoop.Length * ...
        (0.5 * Section.SteelProps.Spacing / PlastHingeLength) ...

```

```

* (1 - (0.5 * Section.SteelProps.Spacing / PlastHingeLength)) - 3 * ...
TransStrain * Hoop.Length * (Section.SteelProps.Spacing / ...
  PlastHingeLength) * (1 - (Section.SteelProps.Spacing / ...
  PlastHingeLength));
Eccentricity = Section.SteelProps.InitEccent;
Bulge = 6 * TransStrain * Hoop.Length * (Section.SteelProps.Spacing / ...
  PlastHingeLength) * (1 - (Section.SteelProps.Spacing / ...      Plas-
tHingeLength));
Curve = 4 * pi ^ 2 * Eccentricity / (Section.SteelProps.Spacing ^ 2);

FirstIter = 1;
[Load, Moment, flag, SteelStrain1, SteelStress1, Strain0, Stress0, ...
  SteelStrainCompPrev, SteelStressCompPrev, LoadFlag] = ...
  MomentLoad08Cyclic (RefStrain, Curve, Section.Depth, Section.Area, ...
  Section.SteelProps, Precision, Strain0, Stress0, SteelStrainCompPrev,
...
  SteelStressCompPrev, LoadFlag, FirstIter);
FirstIter = 0;

% Calculate updated hoopmoment:
[HoopMoment, HoopStress] = MomentHoop (Hoop.YieldStress, Hoop.YoungsMod,
Hoop.ShStrain, ...
  Hoop.ShMod, Hoop.UltStress, Hoop.UltStrain, Hoop.alpha, Hoop.Area,
Hoop.Length, ...
  NumHoops, (Section.SteelProps.Spacing / (NumHoops + 1)), ...
  Eccentricity, Bulge);

ConcForce = (16 / ((NumHoops ^ 2) + 2 * NumHoops + (sin (NumHoops * pi /
2)) ^ 2)) * ...
  ((Moment * (NumHoops + 1) / Section.SteelProps.Spacing) + (HoopMoment *
(NumHoops + 1) / Section.SteelProps.Spacing) ...
  + (Load * Eccentricity * (NumHoops + 1) / Section.SteelProps.Spacing));

Counter = Counter + 1;
MomentOut (Counter) = Moment;
CurveOut (Counter) = Curve;
EccentricityOut (Counter) = Section.SteelProps.InitEccent;
RefStrainOut (Counter) = RefStrain;
SteelStressOut (:, 1) = SteelStress1;
SteelStrainOut (:, 1) = SteelStrain1;
ForceOut (Counter) = Load;
HoopStressOut (Counter) = HoopMoment;
DeltaCurve = Precision.DeltaCurve;
InitMoment = Moment;
COUNTERinit = COUNTERinit + 1;
if ConcForce < 0
  PROCEED = 1;
end
end

```

A3 Section Analysis Subroutine: MomentLoad08Cyclic.m

```

function [Load, Moment, flag, SteelStrain1, SteelStress1, Strain0, Stress0, ...
    SteelStrainCompPrev, SteelStressCompPrev, LoadFlag] = ...
    MomentLoad08Cyclic (RefStrain, Curve, Depth, Area, SteelProps, ...
        Precision, Strain0, Stress0, SteelStrainCompPrev, SteelStressCompPrev, ...
        LoadFlag, FirstIter)

% MOMENTLOAD08a gives the axial load and moment in a discretised steel
% reinforcing bar based on a reference strain and curvature.
% -----
%
% TYPICAL CALL:
%     [Load, Moment] = MomentLoad08a (RefStrain, Curve, Depth, Area, ...
%     ... SteelProps, Precision)
%
% DESCRIPTION:
%     Function uses the Gauss Quadrature to integrate the stresses over a
%     section to give the total section bending moment and section axial
%     load.
%
% INPUTS:
%     RefStrain = Section strain at half of the section depth, epsilon0
%     Curve     = Curvature of the section, Phi
%     Depth     = Structured array of element centroid depths:
%                Depth.Steel = Vector of steel centroid depths
%     Area      = Structured array of element areas:
%                Area.Steel  = Vector of steel element areas
%     SteelProps = Structured array of steel material properties
%     Precision = Precision / Stability parameters for Menegotto-Pinto
%                equation and Popovic's equation
%
% OUTPUTS:
%     Load      = Section axial load, P
%     Moment    = Section bending moment, M
%     flag      = 1 if any element has reached its ultimate strain
%                = 0 if no elements have reached ultimate strain
%
% PROGRAMME HISTORY:
%     DATE          PROGRAMMER          MODIFICATION
%     ----          -
%     09/26/08      C.R. Urmson          Original Code
%     09/29/08      C.R. Urmson          Matrix Algebra Enabled
%     10/19/08      C.R. Urmson          Spalling Enabled
%     10/25/08      C.R. Urmson          Yielding Check Enabled
%     11/22/08      C.R. Urmson          Spalling Modified
%     12/11/08      C.R. Urmson          True Strain Effects Added
%                                     for steel in compression
%     12/22/08      C.R. Urmson          Programme simplified for
%                                     analysis of steel bar
%     02/04/09      C.R. Urmson          Modified for cyclic
%                                     reloading from comp.
% -----

% Calculate the strain profile to obtain the strain for each element:
% -----
SteelStrain = (Curve * Depth.Steel) + RefStrain;

```



```

% Initialise stress vectors:
% -----
flag.ult = 0;
flag.yield = 0;
SteelStress = zeros (length (SteelStrain), 1);
YieldStrain = SteelProps.YieldStress / SteelProps.YoungsMod;

% Calculate the stress in each element:
% -----
% Steel
for ii = 1 : length (SteelStrain)
    % Determine positive or negative stress:
    if SteelStrain (ii) >= 0 %% TENSILE fibre strain
        if LoadFlag (ii) == 0 %% Still on MONOTONIC branch
            StrainO (ii) = 0; StressO (ii) = 0;
            SteelStress (ii) = SteelstressCyclic (SteelProps.YieldStress, ...
                SteelProps.YoungsMod, SteelProps.ShStrain, SteelProps.ShMod, ...
                SteelProps.UltStress, SteelProps.UltStrain, SteelStrain (ii), ...
                Precision.alphaSteel, StrainO (ii), StressO (ii), LoadFlag
(ii));
        else
            %% On RELOADING branch, originally compressive
            SteelStrainComp = - SteelStrain (ii) / (1 + SteelStrain (ii));
            SteelStressComp = SteelstressCyclic (SteelProps.YieldStress, ...
                SteelProps.YoungsMod, SteelProps.ShStrain, SteelProps.ShMod,
...
                SteelProps.UltStress, SteelProps.UltStrain, SteelStrainComp,
...
                Precision.alphaSteel, StrainO (ii), StressO (ii), LoadFlag
(ii));
            SteelStress (ii) = - SteelStressComp * (1 + SteelStrainComp) ^ 2;
        end
    else
        % Convert compressive strain to equivalent tensile strain and
        % calculate equivalent tensile stress. Then convert back:
        SteelStrainComp = - SteelStrain (ii) / (1 + SteelStrain (ii));
        if (SteelStrainCompPrev (ii) > SteelStrainComp) && ...
            (SteelStrainComp > YieldStrain)
            Reload = 1;
        else
            Reload = 0;
        end

        if (Reload == 1) || (LoadFlag (ii) == 1)
            if FirstIter == 1 % Good solution
                LoadFlag (ii) = 1; %% On RELOADING branch
                if (StrainO (ii) == 0) && (StressO (ii) == 0)
                    StrainO (ii) = SteelStrainCompPrev (ii);
                    StressO (ii) = SteelStressCompPrev (ii);
                end
                SteelStressComp = SteelstressCyclic (SteelProps.YieldStress,
...
                    SteelProps.YoungsMod, SteelProps.ShStrain, ...
                    SteelProps.ShMod, SteelProps.UltStress, ...
                    SteelProps.UltStrain, SteelStrainComp, Preci-
sion.alphaSteel, ...
                    StrainO (ii), StressO (ii), LoadFlag (ii));
            else

```

```

        LoadFlagTemp = 1; % Iteration
        if (StrainO (ii) == 0) && (StressO (ii) == 0)
            StrainOTemp = SteelStrainCompPrev (ii);
            StressOTemp = SteelStressCompPrev (ii);
        else
            StrainOTemp = StrainO (ii);
            StressOTemp = StressO (ii);
        end
        SteelStressComp = SteelstressCyclic (SteelProps.YieldStress,
...
            SteelProps.YoungsMod, SteelProps.ShStrain, ...
            SteelProps.ShMod, SteelProps.UltStress, ...
            SteelProps.UltStrain, SteelStrainComp, Preci-
sion.alphaSteel, ...
            StrainOTemp, StressOTemp, LoadFlagTemp);
    end
else
    %% Still MONOTONIC or RELOADED PRE-YIELD
    StrainO (ii) = 0; %% and NOT PREVIOUSLY RELOADED
    StressO (ii) = 0;
    SteelStressComp = SteelstressCyclic (SteelProps.YieldStress, ...
        SteelProps.YoungsMod, SteelProps.ShStrain, ...
        SteelProps.ShMod, SteelProps.UltStress, ...
        SteelProps.UltStrain, SteelStrainComp, Precision.alphaSteel,
...
        StrainO (ii), StressO (ii), LoadFlag (ii));
end

SteelStress (ii) = - SteelStressComp * (1 + SteelStrainComp) ^ 2;
if FirstIter == 1 %% NOT SURE ABOUT THIS YET...
    SteelStrainCompPrev (ii) = SteelStrainComp;
    SteelStressCompPrev (ii) = SteelStressComp;
end
end
% Determine whether ultimate strain has been reached:
if (SteelStrain (ii) > 100 * SteelProps.UltStrain) || ...
    (SteelStrain (ii) < - 100 * SteelProps.UltStrain)
    flag.ult = 1;
end
% Determine whether steel has yielded:
if (SteelStress (ii) > SteelProps.YieldStress) || ...
    (SteelStress (ii) < - SteelProps.YieldStress)
    flag.yield = 1;
end
end

SteelStress1 = SteelStress;
SteelStrain1 = SteelStrain;

% Calculate axial load:
% -----
Load = (SteelStress' * Area.Steel);

% Calculate bending moment:
% -----
Moment = (SteelStress' * (Area.Steel .* Depth.Steel));

% END OF FUNCTION

```

A4 Material Subroutine: SteelStressCyclic.m

```

function [Stress] = SteelstressCyclic (YieldStress, YoungsMod, ShStrain, ...
    ShMod, UltStress, UltStrain, Strain, alpha, Strain0, Stress0, LoadFlag)

% STEELSTRESS gives the stress in a piece of steel for a given strain.
% -----
%
% TYPICAL CALL:
%     Stress = Steelstress (YieldStress, YoungsMod, ShStrain, ShMod, ...
%     ... UltStress, UltStrain, Strain, alpha)
%
% DESCRIPTION:
%     Function determines the stress in a reinforcing steel bar for any
%     given strain value. Uses the Menegotto-Pinto equation (1973) for
%     the strain diagram up to the onset of strain-hardening, and a
%     polynomial approximation of the form  $Y = X^P$  thereafter.
%
% INPUTS:
%     YieldStress = Steel yield stress,  $f_y$ 
%     YoungsMod   = Elastic modulus of steel,  $E_s$ 
%     ShStrain    = Value of strain in the steel at which strain-
%                 hardening commences,  $\epsilon_{sh}$ 
%     ShMod       = "Elastic" modulus of yielded steel in the strain-
%                 hardening portion of the stress-strain curve,  $E_{sh}$ 
%     UltStress   = Ultimate stress of the steel,  $f_u$ 
%     UltStrain   = Ultimate strain of the steel,  $\epsilon_u$ 
%     Strain      = Strain value for which the stress is being
%                 calculated
%     alpha       = Precision / stability parameter, an integer  $\geq 20$ 
%
% OUTPUTS:
%     Stress      = Calculated value of stress,  $f_s$ 
%
% PROGRAMME HISTORY:
%     DATE          PROGRAMMER          MODIFICATION
%     ----          -
%     09/24/08     C.R. Urmson         Original Code
%     02/04/09     C.R. Urmson         Modified for cyclic
%                                     reloading from comp.
% -----

% Calculation of yield strain:
YieldStrain = YieldStress / YoungsMod;

% Calculation of the parameters P, q and R:
P = ShMod * (UltStrain - ShStrain) / (UltStress - YieldStress);
q = 0.935;
R = max (2 - (0.4 * Strain0), 1);

% Calculation of Menegotto-Pinto portion of equation:
MP = YoungsMod * Strain / (1 + (abs (Strain / YieldStrain)) ^ alpha) ^ ...
    (1 / alpha);

% Calculation of denominator in strain-hardening portion:
Denom = (((abs (UltStrain - ShStrain)) ^ (alpha * P)) + ((abs ...
    (UltStrain - Strain)) ^ (alpha * P))) ^ (1 / alpha);

```

```

% Calculation of Strain hardening portion:
SHPor = (UltStress - YieldStress) * (1 - (((abs (UltStrain - Strain)) ...
    ^ P) / Denom));

% Calculation of Stress:
if LoadFlag == 0
    Stress = MP + SHPor;
elseif LoadFlag == 1
    Stress = Stress0 + YoungsMod * (Strain - Strain0) / ((1 + abs ...
        (YoungsMod * (Strain - Strain0) / (-YieldStress - Stress0)) ^ ...
        (q * R)) ^ (1 / R));
end

% END OF FUNCTION

```

A5 Hoop Moment Subroutine: MomentHoop.m

This subroutine is used in the global buckling analysis only.

```

function [TOTHoopMoment, HoopStress] = MomentHoop (HYieldStress, HYoungsMod,
HShStrain, ...
    HShMod, HUltStress, HUltStrain, Halpha, HoopArea, HoopLength, ...
    NumHoops, HoopSpacing, Eccentricity, Bulge)

% MOMENTHOOP finds restraining moment by hoops on a longitudinal bar.
% -----
%
% TYPICAL CALL:
%     [TOTHoopMoment] = MomentHoop (HYieldStress, HYoungsMod, HShStrain, ...
%     HShMod, HUltStress, HUltStrain, Halpha, HoopArea, HoopLength, ...
%     NumHoops, Eccentricity)
%
% DESCRIPTION:
%     Function determines the contribution from each hoop to resisting
%     moment on a globally buckling longitudinal bar. Based on statical
%     derivation by Urmson (2010).
%
% INPUTS:
%     HYieldStress = Hoop steel yield stress, f_y
%     HYoungsMod   = Elastic modulus of hoop steel, E_s
%     HShStrain    = Value of strain in the hoop steel at which strain-
%     hardening commences, epsilon_sh
%     HShMod       = "Elastic" modulus of yielded hoop steel in the strain-
%     hardening portion of the stress-strain curve, E_sh
%     HUltStress   = Ultimate stress of the hoop steel, f_u
%     HUltStrain   = Ultimate strain of the hoop steel, epsilon_u
%     Halpha       = Precision / stability parameter, an integer >= 20
%     HoopArea     = Cross-sectional area of the hoop
%     HoopLength   = Length of the hoop
%     NumHoops     = Number of hoops restraining the longitudinal bar
%     HoopSpacing  = Spacing of transverse reinforcement
%     Eccentricity = Eccentricity of the longitudinal bar
%     Bulge        = Eccentricity due to Poisson's Effect
%
% OUTPUTS:
%     TOTHoopMoment = Calculated Moment provided by all hoops

```

```

%
% PROGRAMME HISTORY:
%      DATE                PROGRAMMER                MODIFICATION
%      ----                -
%      05/16/10           C.R. Urmson                Original Code
%
% -----

% Initialisation of vectors:
HoopStrain = zeros (1, NumHoops);
HoopStress = HoopStrain;
HoopForce = HoopStrain;
HoopMoment = HoopForce;

% Contribution from each individual hoop:
for ii = 1 : NumHoops
    HoopStrain (ii) = (Eccentricity * (1 - cos (2 * pi * ii / ...
        (NumHoops + 1))) / HoopLength) + (Bulge * (NumHoops + 1 - ii) / ...
        ((NumHoops + 1) * HoopLength));
    if HoopStrain (ii) < 0,
        HoopStress (ii) = 0;
    else
        HoopStress (ii) = SteelstressCyclic (HYieldStress, HYoungsMod, ...
            HShStrain, HShMod, HUltStress, HUltStrain, HoopStrain (ii), ...
            Halpha, 0, 0, 0);
    end
    HoopForce (ii) = HoopStress (ii) * HoopArea;
    HoopMoment (ii) = HoopForce (ii) * (0.5 * (NumHoops + 1) - ii);
end

SubtractMoment = 0;

% Add moments to give total contribution from each hoop:
for jj = 1 : ceil (NumHoops / 2)
    SubtractMoment = SubtractMoment + HoopMoment (jj);
end

TOTHoopMoment = (0.25 * (NumHoops + 1) * HoopSpacing * sum (HoopForce) - ...
    SubtractMoment * HoopSpacing) * 0.5;
% END OF FUNCTION

```

A6 Sample Output File: BarBucklingAnalysisSDBMander84.D24.6.txt

This output file was generated for a transverse steel spacing of $6 d_b$ for a Grade 260 steel.

```

URMSON's Buckling Analysis
=====
Mander84.D24.6
S/db =6
Input: fy, Es, eps_sh, Esh, fsu, eps_su
-----
260    1.95e+005    0.018  4500  429    0.18

Peak: Force, Moment, Curvature, Eccentricity, Reference Strain
-----
1.10969    0.733891    0.0751896    0.121893    -0.0276746

Steel Strains at Curvature =
-----
Phi * db =0
Phi * db =0.018797
Phi * db =0.037595
Phi * db =0.056392
Phi * db =0.07519
Phi * db =0.093987
-0.000392884 -0.0178744    -0.0338947    -0.0488093    -0.0628434    -0.0759303
-0.000384807 -0.0176761    -0.0335061    -0.0482304    -0.0620743    -0.0749699
-0.000370416 -0.0173227    -0.0328136    -0.0471989    -0.0607038    -0.0732585
-0.000349943 -0.0168199    -0.0318286    -0.0457316    -0.0587542    -0.070824
-0.000323724 -0.016176    -0.0305671    -0.0438524    -0.0562574    -0.0677062
-0.000292189 -0.0154016    -0.0290498    -0.0415923    -0.0532544    -0.0639564
-0.000255857 -0.0145094    -0.0273017    -0.0389883    -0.0497945    -0.059636
-0.000215324 -0.013514    -0.0253515    -0.0360832    -0.0459346    -0.0548161
-0.000171255 -0.0124318    -0.0232311    -0.0329247    -0.041738    -0.0495758
-0.000124374 -0.0112806    -0.0209755    -0.0295647    -0.0372735    -0.044001
-7.54507e-005 -0.0100792    -0.0186216    -0.0260583    -0.0326147    -0.0381835
-2.52886e-005 -0.00884732    -0.0162081    -0.0224631    -0.0278378    -0.0322186
2.52886e-005 -0.00760529    -0.0137746    -0.0188382    -0.0230214    -0.0262043
7.54507e-005 -0.00637345    -0.011361    -0.015243    -0.0182445    -0.0202394
0.000124374 -0.00517203    -0.00900714    -0.0117366    -0.0135856    -0.0144218
0.000171255 -0.00402077    -0.0067515    -0.00837655    -0.00912121    -0.00884709
0.000215324 -0.00293856    -0.00463115    -0.00521806    -0.00492458    -0.00360674

```

0.000255857	-0.00194318	-0.00268091	-0.00231297	-0.00106464	0.00121318
0.000292189	-0.00105096	-0.000932811	0.000291011	0.00239523	0.00553354
0.000323724	-0.000276563	0.000584451	0.00255114	0.00539822	0.00928338
0.000349943	0.000367302	0.00184596	0.00443029	0.00789502	0.0124012
0.000370416	0.000870064	0.00283101	0.00589763	0.00984465	0.0148357
0.000384807	0.00122348	0.00352345	0.00692909	0.0112151	0.016547
0.000392884	0.00142182	0.00391206	0.00750796	0.0119843	0.0175074

Steel Stresses at Curvature =

Phi * db =0

Phi * db =0.018797

Phi * db =0.037595

Phi * db =0.056392

Phi * db =0.07519

Phi * db =0.093987

-78.743	-543.393	-666.427	-750.732	-808.299	-847.777
-77.1236	-541.64	-663.862	-747.941	-805.601	-845.237
-74.2381	-538.503	-659.243	-742.877	-800.674	-840.59
-70.1338	-534.012	-652.562	-735.471	-793.392	-833.688
-64.8782	-528.213	-643.817	-725.632	-783.576	-824.303
-58.5584	-521.18	-633.012	-713.257	-770.999	-812.119
-51.2785	-513.017	-620.169	-698.243	-755.401	-796.727
-43.1587	-503.893	-605.336	-680.502	-736.51	-777.648
-34.333	-494.095	-588.595	-659.988	-714.073	-754.374
-24.9467	-484.115	-570.071	-636.714	-687.9	-726.425
-15.1544	-474.74	-549.948	-610.774	-657.904	-693.434
-5.1172	-466.912	-528.503	-582.371	-624.153	-655.223
5.11681	-461.207	-506.278	-551.833	-586.904	-611.889
15.151	-457.444	-484.788	-519.732	-546.65	-563.865
24.9374	-454.993	-467.807	-487.985	-504.548	-512.213
34.3154	-453.288	-458.435	-464.493	-468.469	-411.341
43.1309	-451.893	-454.136	-453.651	-393.698	-147.014
51.2392	-389.997	-451.102	-371.974	-142.354	139.461
58.5071	-210.965	-187.187	58.2713	443.843	450.582
64.8153	-55.4272	116.972	447.593	450.461	460.338
70.0602	73.5327	369.002	449.823	454.883	480.48
74.1557	174.11	449.099	450.956	463.271	499.1
77.0346	244.816	449.475	452.513	471.902	512.046
78.6503	284.498	449.603	453.808	477.39	519.129

History: Force, Moment, Curvature, Eccentricity, Reference Strain				

0	0.10379	0.000789568	0.0256	0
-119919	0.10495	0.000889568	0.0288423	-0.00191605
-123682	0.105654	0.000989568	0.0320846	-0.00199519
-125682	0.106369	0.00108957	0.0353268	-0.00204738
-126965	0.107077	0.00118957	0.0385691	-0.00208901
-127862	0.107796	0.00128957	0.0418114	-0.00212516
-128527	0.108508	0.00138957	0.0450537	-0.00215825
-140333	1.17862	0.14229	4.61342	-0.03705
...

A6 References

MATLAB version R2008b. (2007). *The MathWorks, Inc.*, Natick, MA.

APPENDIX B

COMPREHENSIVE RESULTS

OF BUCKLING ANALYSES

B1 Introduction

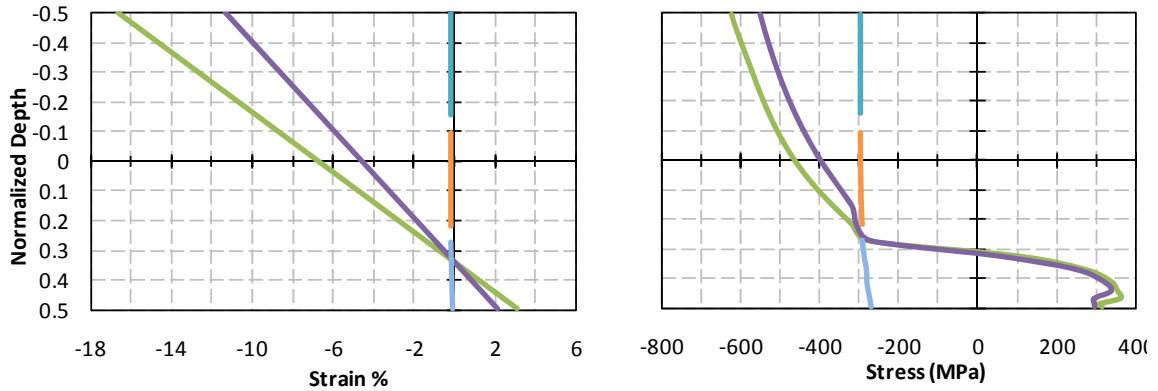
A range of steel types from various experimental studies was examined in the study described in Chapter IV. In addition to a generalized set of results for s / d_b ranging from 4 to 10, computational analyses were run for each s / d_b corresponding to available experimental results. A full set of computational results is presented below, including tensile and compressive stress-strain parameters, computational results and comparisons between analytical, computational and experimental results (where available).

B2 Mander (1983)

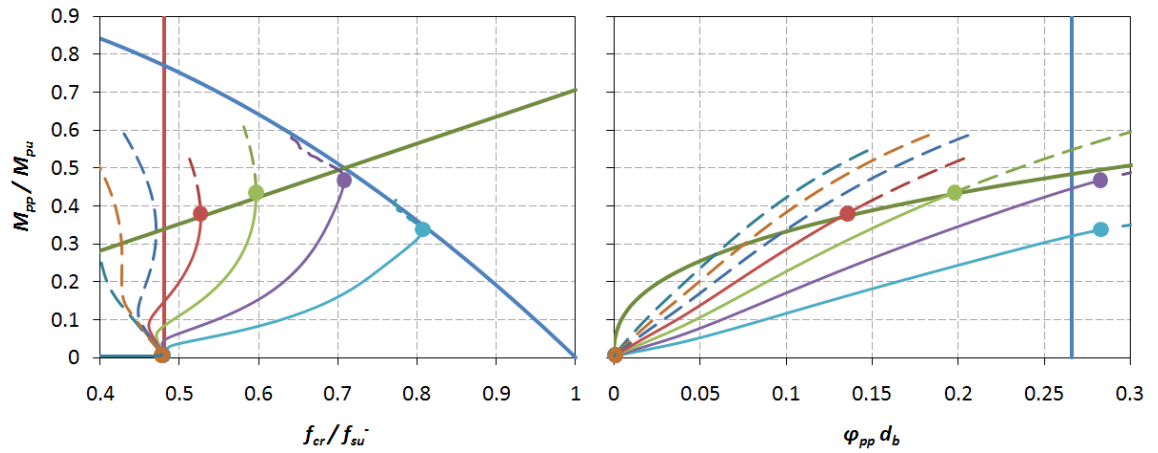
Table B1: Steel Stress-Strain Parameters for Steels from Mander (1983)

Result*	Bar	s / d_b	f_y (MPa)	f_{su} (MPa)	E_s (GPa)	E_{sh} (MPa)	ϵ_{sh}	ϵ_{su}
T	H16	-	360	567	200	6000	0.016	0.150
CE		6	-355	-475	215	8300	-0.011	-0.048
CA		6	-360	-470	200	6000	-0.009	-0.048
T	D16	-	295	433	200	3500	0.025	0.19
CE		5.5	-290	-400	200	4200	-0.016	-0.080
CA		5.5	-295	-371	200	3500	-0.014	-0.067
CE		6	-290	-360	200	3700	-0.015	-0.050
CA		6	-295	-347	200	3500	-0.013	-0.056
CE		6.5	-290	-360	200	3500	-0.016	-0.055
CA		6.5	-295	-326	200	3500	-0.014	-0.048
T	D20	-	286	446	200	4000	0.023	0.180
CE		6	-240	-366	210	6200	-0.011	-0.051
CA		6	-286	-358	200	4000	-0.012	-0.058
T	D24	-	260	429	195	4500	0.018	0.180
CE		6	-234	-385	210	6100	-0.0084	-0.051
CA		6	-260	-343	195	4500	-0.0097	-0.061
T	D28	-	296	484	203	4700	0.015	0.170
CE		6	-280	-450	215	7200	-0.010	-0.050
CA		6	-296	-391	203	4700	-0.008	-0.057

* T = Tension; CE = Compression, Experimental; CA = Compression, Analytical



(a) Cross-Sectional Strain and Stress Profiles at Critical Buckling Load



(b) Moment-Axial Stress Interaction

(c) Moment-Curvature Relationship

Fig. B1: Computational Results for Grade 300 D16 Steel Bars from Mander (1983)

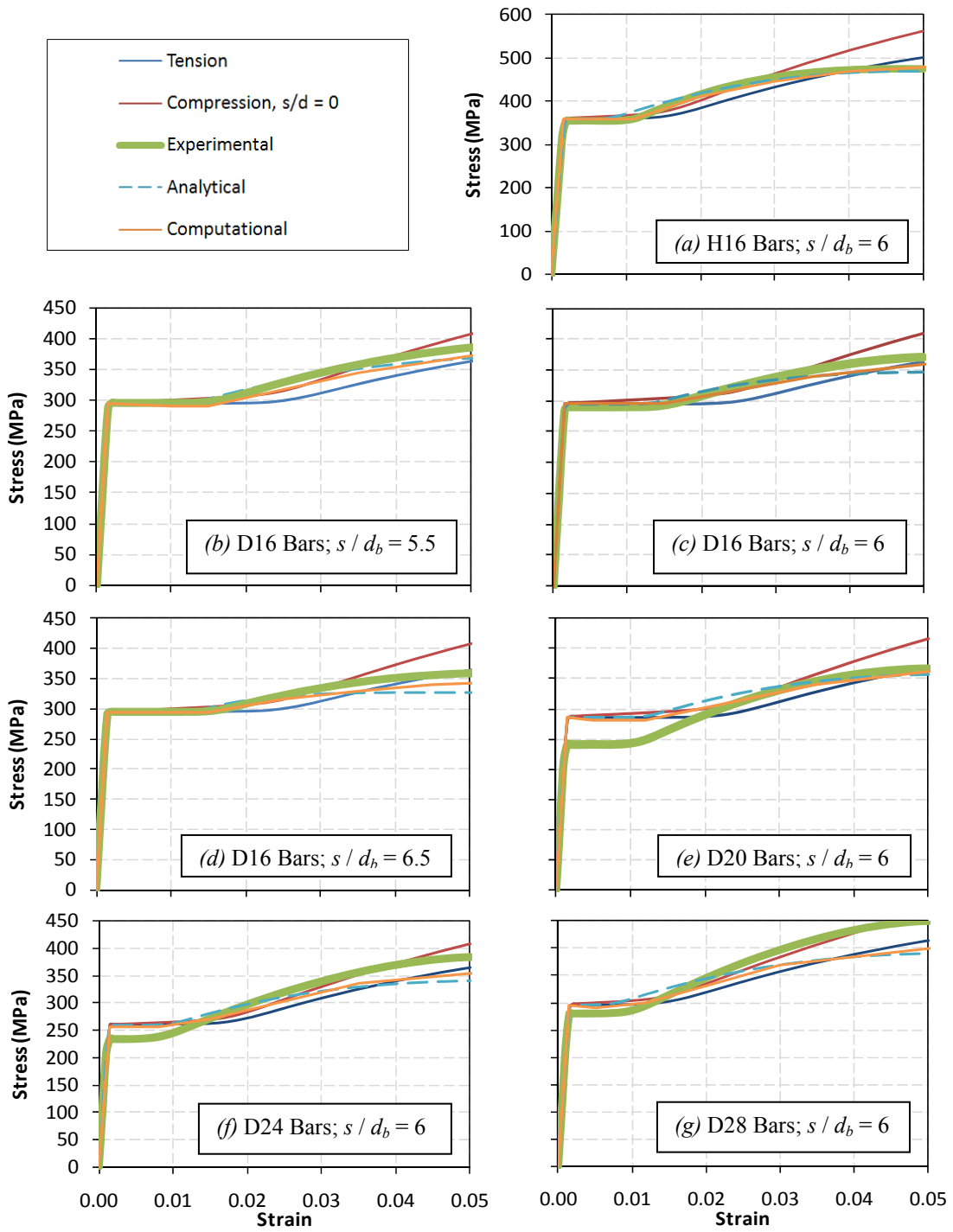


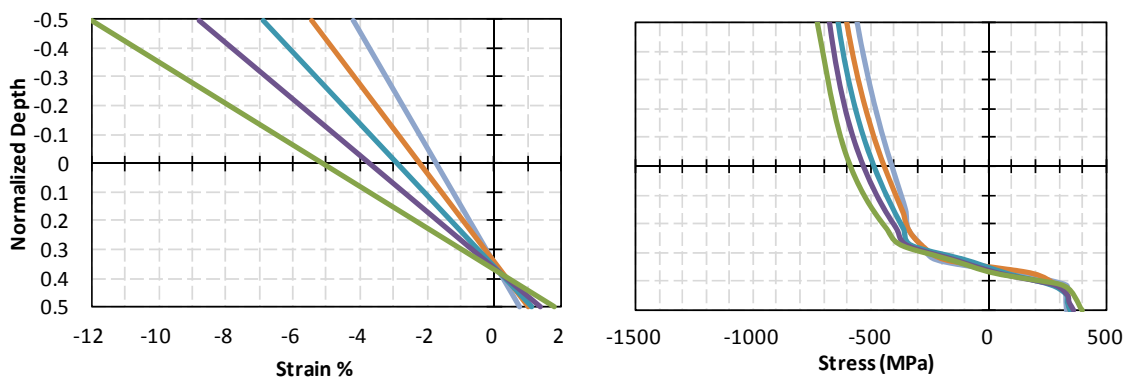
Fig. B2: Comparison of Results from Steels Tested by Mander (1983)

B3 Mander et al. (1994)

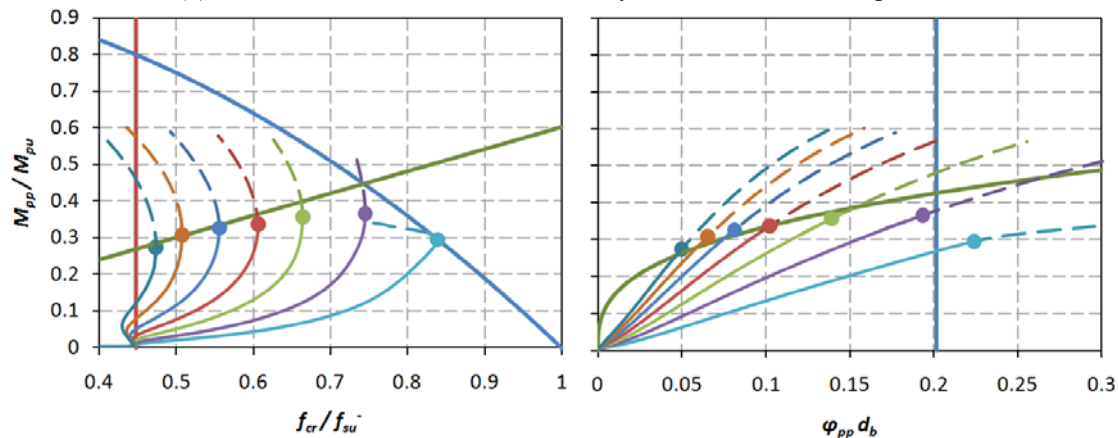
Table B2: Steel Stress-Strain Parameters for Steels from Mander et al. (1994)

Result*	Bar	s / d_b	f_y (MPa)	f_{su} (MPa)	E_s (GPa)	E_{sh} (MPa)	ϵ_{sh}	ϵ_{su}
T	R	-	331	565	215	8274	0.0091	0.144
CE		6	-338	-531	215	8300	-0.0080	-0.045
CA		6	-331	-466	215	8274	-0.005	-0.055
T	P	-	869	1130	221	11030	0.0039	0.063
CE		6	-917	-1076	221	12130	-0.0041	-0.028
CA		6	-869	-1037	221	11030	-0.0040	-0.026
CE		8	-915	-936	219	4380	-0.0042	-0.012
CA		8	-869	-928	221	11030	-0.0040	-0.015
CE		9	-908	-914	234	1170	-0.0039	-0.007
CA		9	-869	-886	221	11030	-0.0040	-0.011

* T = Tension; CE = Compression, Experimental; CA = Compression, Analytical



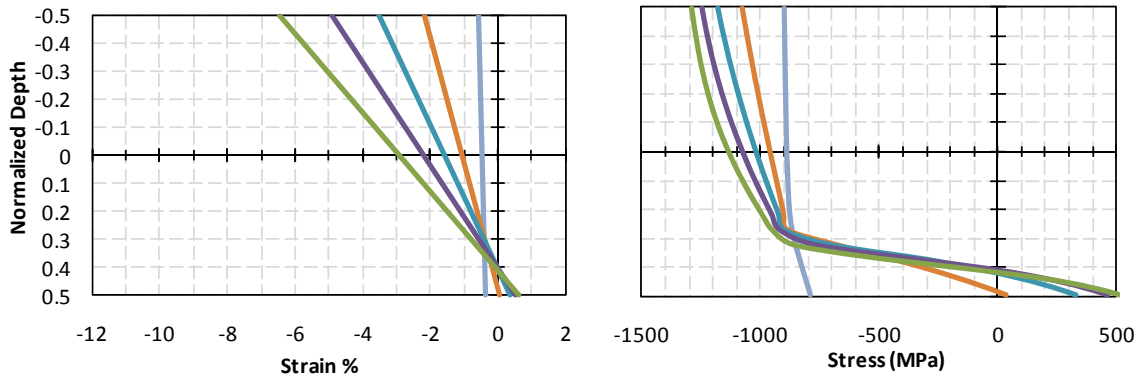
(a) Cross-Sectional Strain and Stress Profiles at Critical Buckling Load



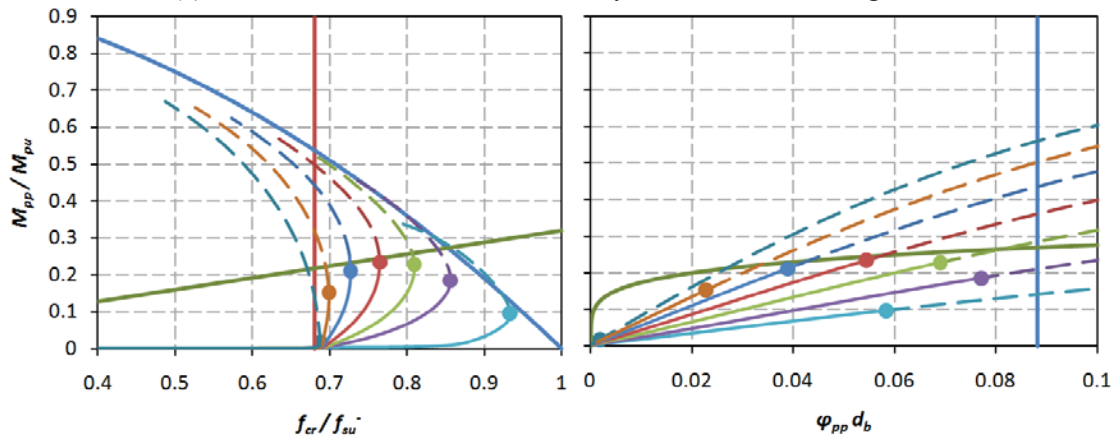
(b) Moment-Axial Stress Interaction

(c) Moment-Curvature Relationship

Fig. B3: Computational Results for Mild Steel Bars from Mander et al. (1994)



(a) Cross-Sectional Strain and Stress Profiles at Critical Buckling Load



(b) Moment-Axial Stress Interaction

(c) Moment-Curvature Relationship

Fig. B4: Computational Results for High-Strength Steel Bars from Mander et al. (1994)

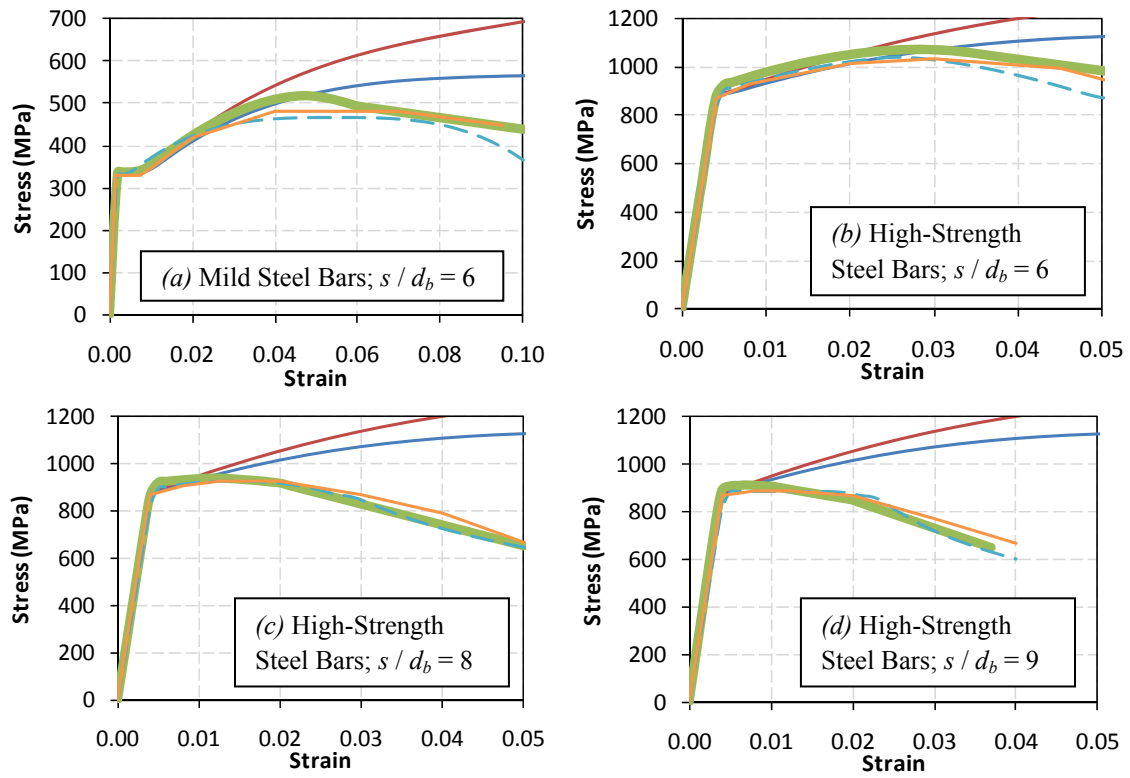
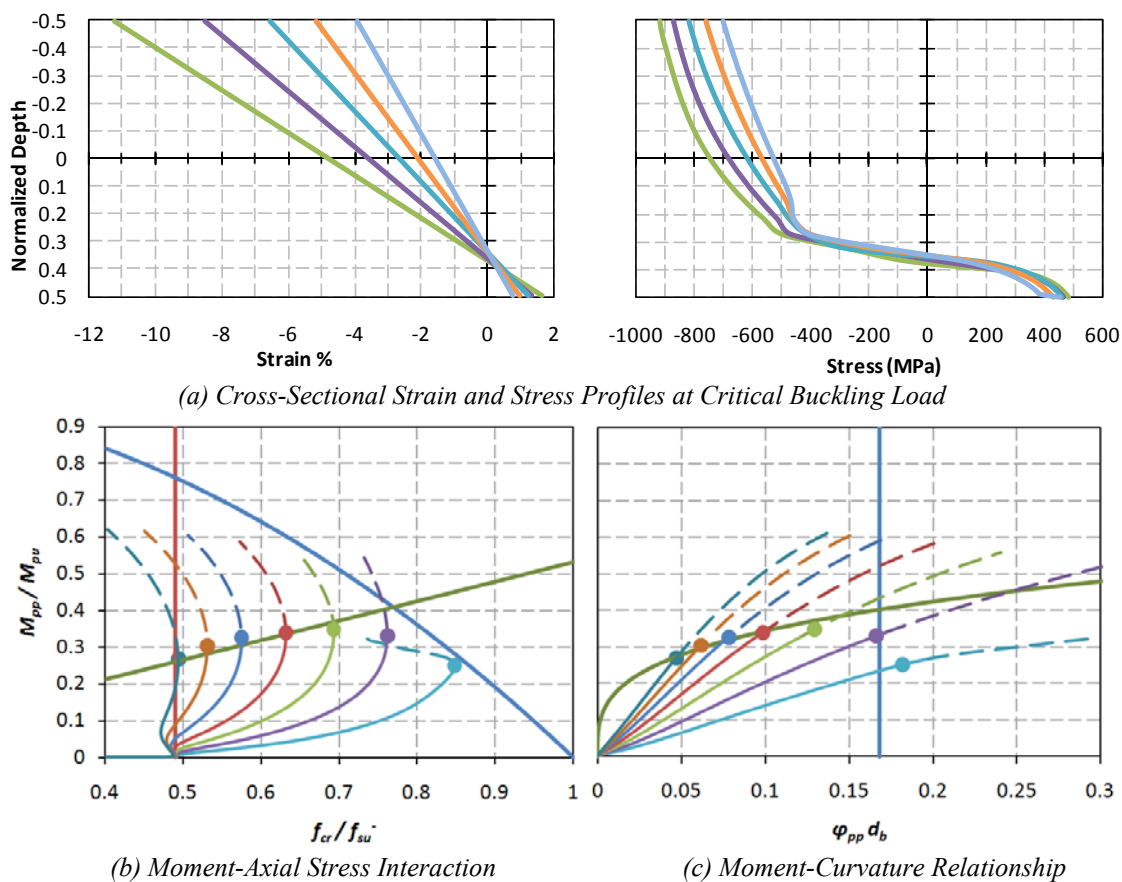


Fig. B5: Comparison of Results from Steels Tested by Mander et al. (1994)

B4 Rodriguez et al. (1999)
Table B3: Steel Stress-Strain Parameters for Steels from Rodriguez et al. (1999)

Result*	Bar	s / d_b	f_y (MPa)	f_{su} (MPa)	E_s (GPa)	E_{sh} (MPa)	ε_{sh}	ε_{su}
T	# 10	-	449	730	200	9000	0.0089	0.12

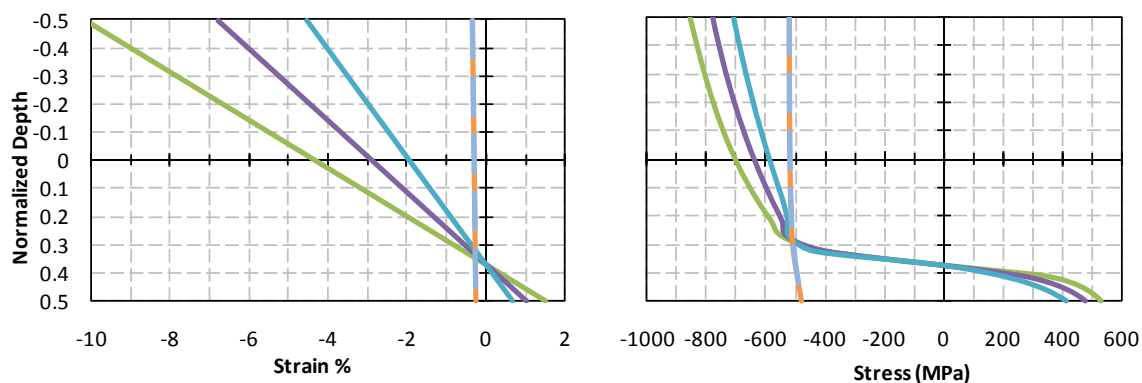
* T = Tension; Compression results not used due to different testing method


Fig. B6: Computational Results for #10 Steel Bars from Rodriguez et al. (1999)

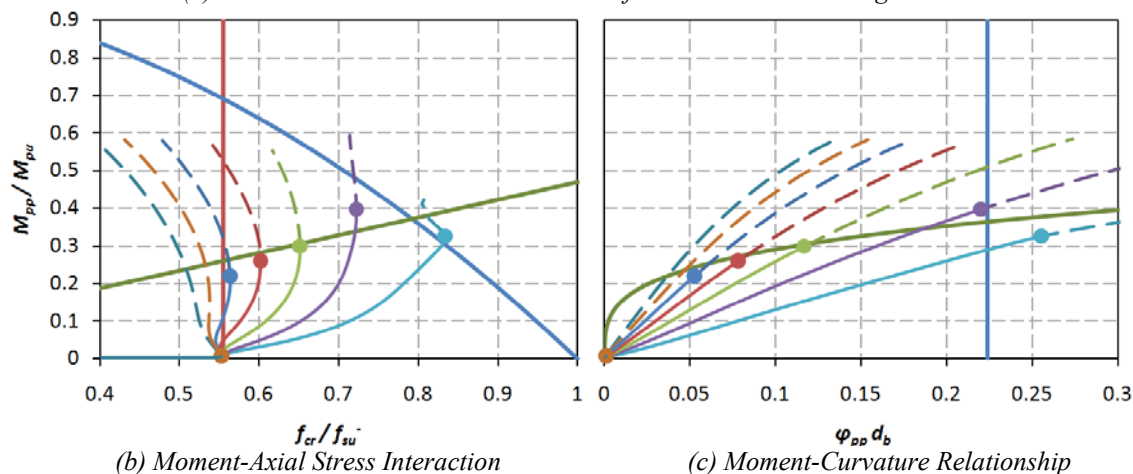
B5 Bayrak and Sheikh (2001)
Table B4: Steel Stress-Strain Parameters for Steels from Bayrak and Sheikh (2001)

Result*	Bar	s / d_b	f_y (MPa)	f_{su} (MPa)	E_s (GPa)	E_{sh} (MPa)	ε_{sh}	ε_{su}
T	M20	-	515	690	200	5500	0.0091	0.160
CE		4	-515	-670	200	6000	-0.010	-0.120
CA		4	-515	-737	200	5500	-0.006	-0.080
CE		5	-515	-600	200	4000	-0.010	-0.070
CA		5	-515	-653	200	5500	-0.006	-0.052
CE		6	-515	-580	200	4000	-0.008	-0.051
CA		6	-515	-592	200	5500	-0.006	-0.036
CE		7	-515	-515	200	7200	-0.007	-0.025
CA		7	-515	-545	200	5500	-0.006	-0.026

* T = Tension; CE = Compression, Experimental; CA = Compression, Analytical



(a) Cross-Sectional Strain and Stress Profiles at Critical Buckling Load



(b) Moment-Axial Stress Interaction

(c) Moment-Curvature Relationship

Fig. B7: Computational Results for M20 Steel Bars from Bayrak and Sheikh (2001)

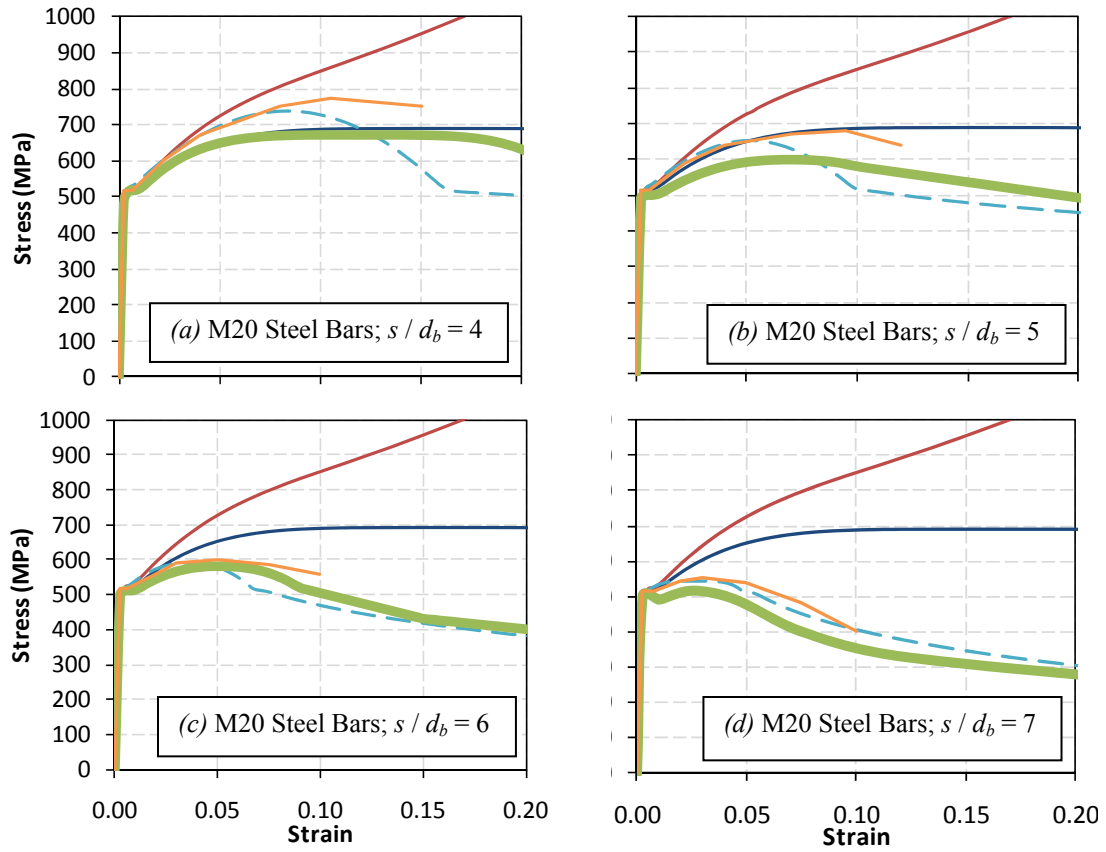


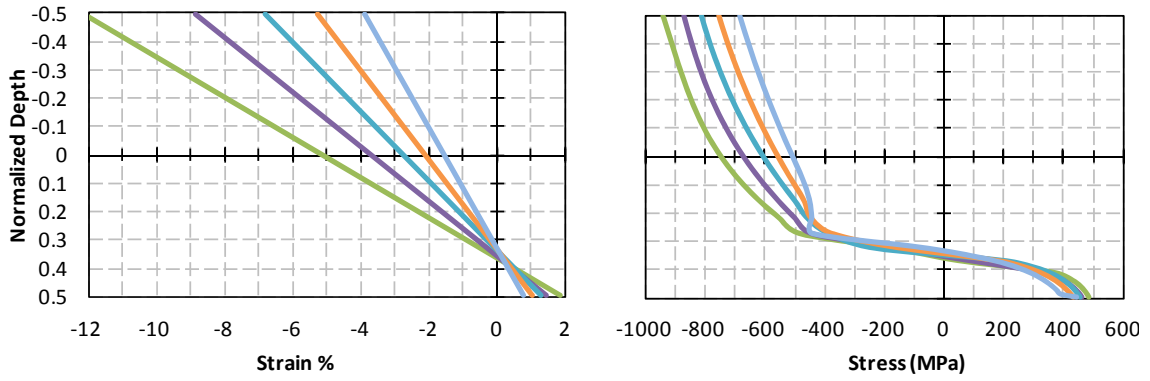
Fig. B8: Comparison of Results from Steels Tested by Bayrak and Sheikh (2001)

B6 Bae et al. (2005)

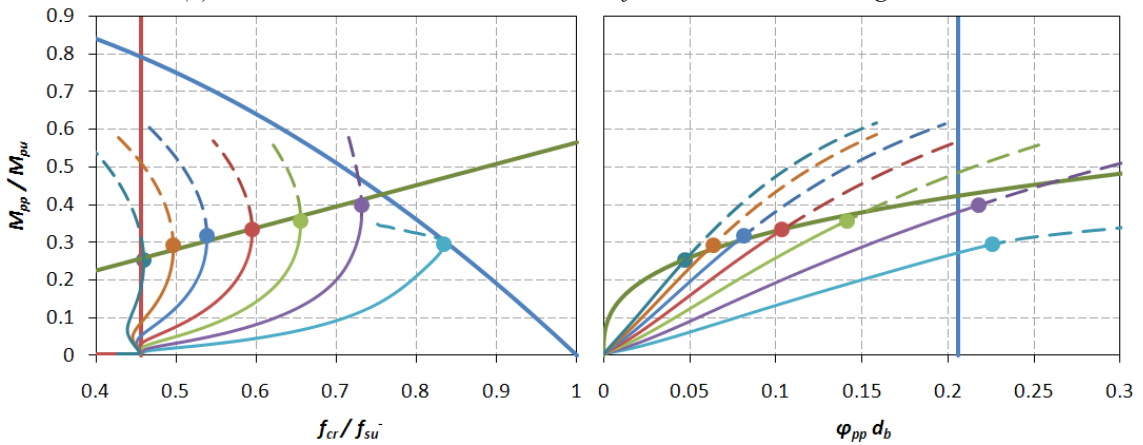
Table B5: Steel Stress-Strain Parameters for Steels from Bae et al. (2005)

Result*	Bar	s / d_b	f_y (MPa)	f_{su} (MPa)	E_s (GPa)	E_{sh} (MPa)	ε_{sh}	ε_{su}
T	#8	-	437	728	198	9000	0.0092	0.147
CE		5	-437	-550	198	5000	-0.005	-0.075
CA		5	-437	-686	198	9000	-0.006	-0.059
CE		6	-437	-500	198	4000	-0.005	-0.050
CA		6	-437	-615	198	9000	-0.006	-0.041
CE		7	-437	-450	198	3000	-0.005	-0.030
CA		7	-437	-560	198	9000	-0.006	-0.030
CE		8	-437	-445	198	3000	-0.004	-0.020
CA		8	-437	-517	198	9000	-0.006	-0.023
CE		9	-437	-437	198	3000	-0.003	-0.002
CA		9	-437	-482	198	9000	-0.006	-0.018
T	#10	-	444	638	202	7000	0.0091	0.158
CE		4	-444	-640	202	7000	-0.005	-0.160
CA		4	-444	-681	202	7000	-0.007	-0.082
CE		5	-444	-550	202	5500	-0.005	-0.065
CA		5	-444	-599	202	7000	-0.007	-0.059
CE		6	-444	-510	202	6100	-0.005	-0.040
CA		6	-444	-537	202	7000	-0.007	-0.041
CE		7	-444	-467	202	7200	-0.005	-0.030
CA		7	-444	-490	202	7000	-0.007	-0.030

* T = Tension; CE = Compression, Experimental; CA = Compression, Analytical



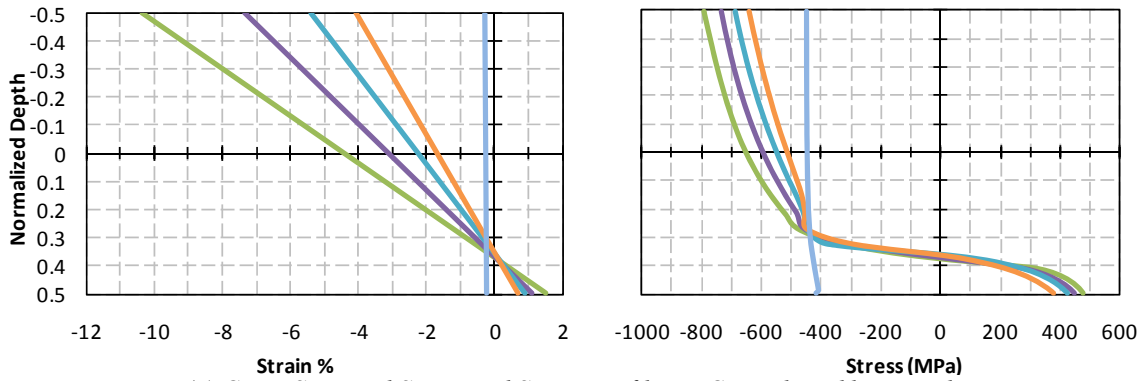
(a) Cross-Sectional Strain and Stress Profiles at Critical Buckling Load



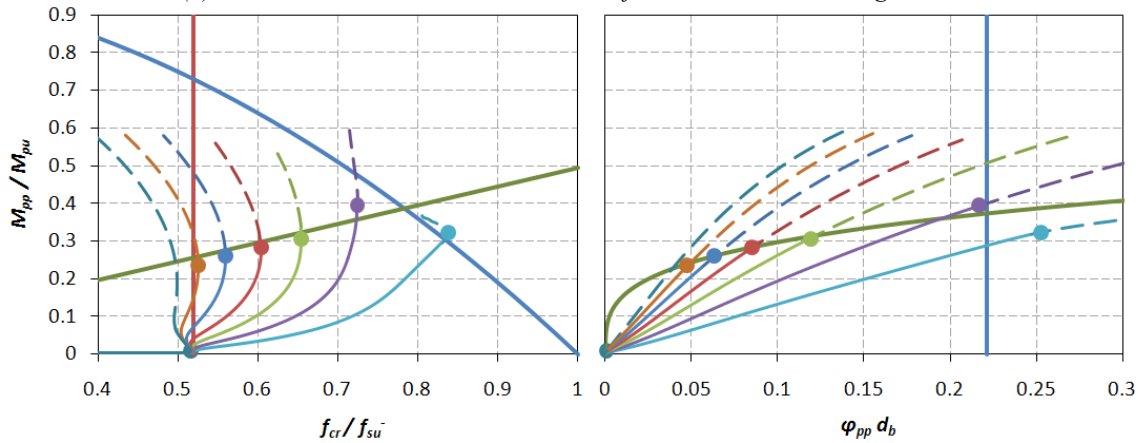
(b) Moment-Axial Stress Interaction

(c) Moment-Curvature Relationship

Fig. B9: Computational Results for #8 Steel Bars from Bae et al. (2005)



(a) Cross-Sectional Strain and Stress Profiles at Critical Buckling Load



(b) Moment-Axial Stress Interaction

(c) Moment-Curvature Relationship

Fig. B10: Computational Results for #10 Steel Bars from Bae et al. (2005)

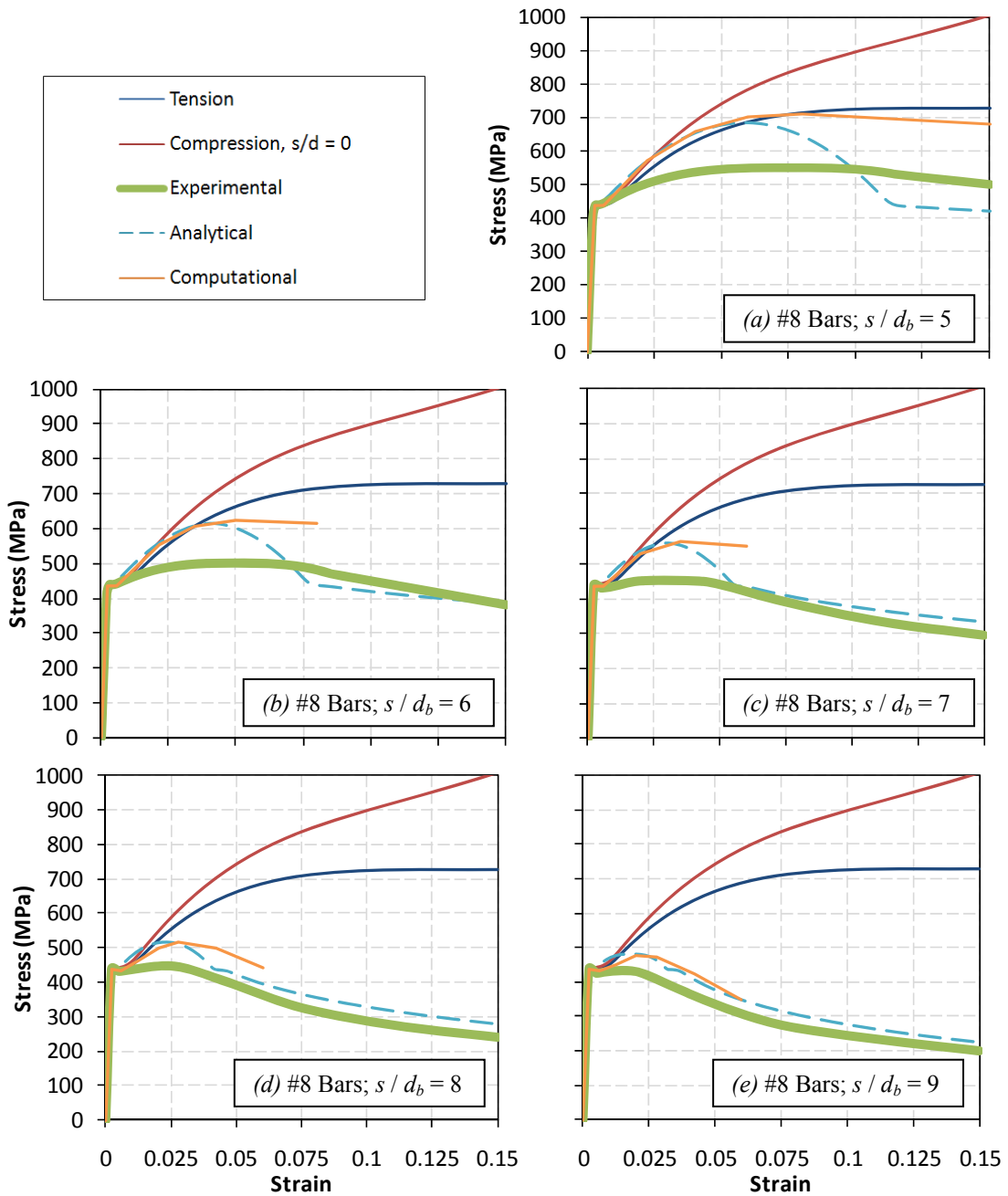


Fig. B11: Comparison of Results from #8 Steel Bars Tested by Bae et al. (2005)

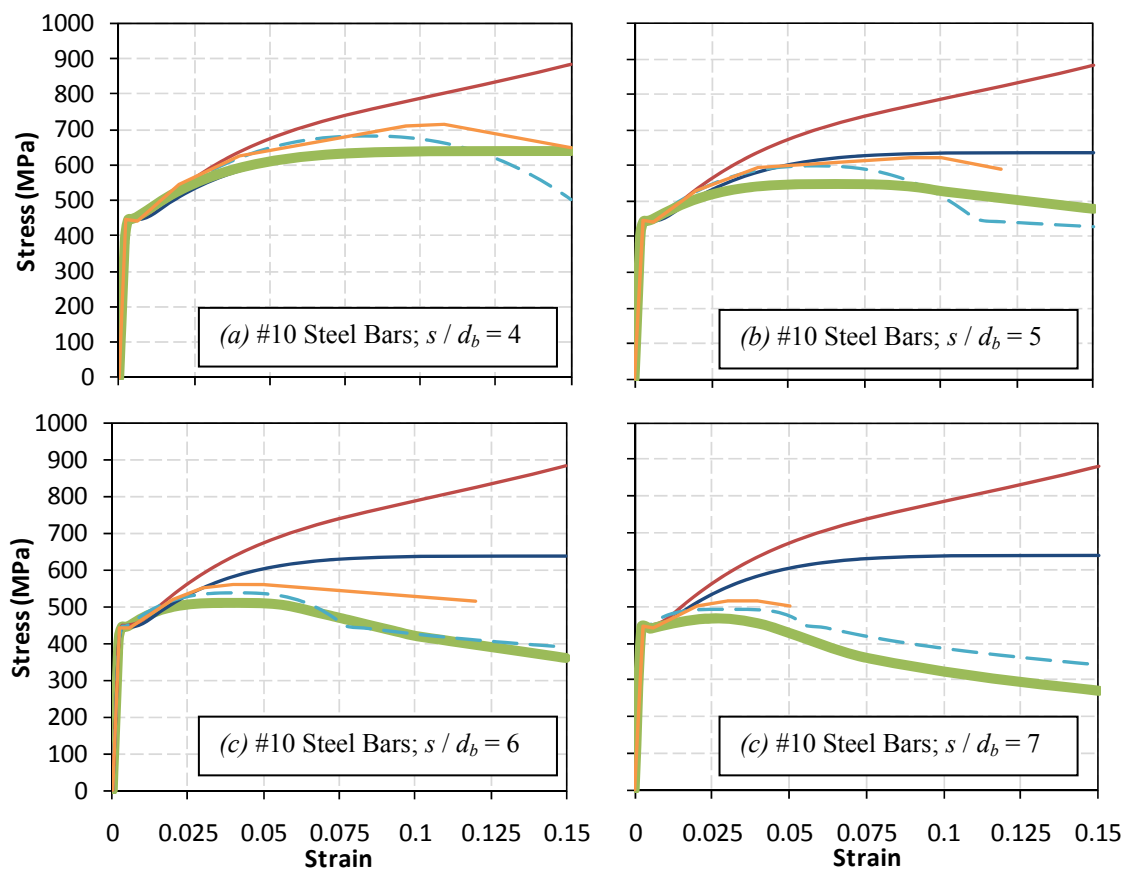


Fig. B12: Comparison of Results from #10 Steel Bars Tested by Bae et al. (2005)

B7 References

- Bae, S., Miseses, A.M. and Bayrak, O. (2005). "Inelastic buckling of reinforcing bars." *Journal of Structural Engineering*, 131, 314 – 321.
- Bayrak, O. and Sheikh, S.A. (2001). "Plastic hinge analysis." *Journal of Structural Engineering*, 127(9), 1092 – 1100.
- Mander, J.B. (1983). "Seismic design of bridge piers." PhD Thesis, University of Canterbury Christchurch, New Zealand.
- Mander, J.B., Panthaki, F.D. and Kasalanati, A. (1994). "Low-cycle fatigue behavior of reinforcing steel." *Journal of Materials in Civil Engineering*, 6(4), 453 – 468.
- Rodriguez, M.E., Botero, J.C. and Villa, J. (1999). "Cyclic stress-strain behavior of reinforcing steel including effect of buckling." *Journal of Structural Engineering*, 125(6), 605 – 612.

VITA

Christopher Richard Urmson received his Bachelor of Engineering with First Class Honours in Civil Engineering from the University of Canterbury, Christchurch, New Zealand in 2007. He entered the Structural Engineering program at Texas A&M University in 2008 as a Graduate Assistant Researcher, where he received his Master of Science degree in 2010. His research interests include analysis and design of reinforced concrete structures; analysis and design of steel structures; analytical and computational modeling techniques; and earthquake engineering and structural dynamics. He has published a paper on the seismic behavior of steel columns, and plans to publish papers on some of the work done in this thesis.

Mr. Urmson has been a teaching assistant for undergraduate surveying laboratories, MATLAB programming, engineering mechanics, fluid mechanics laboratories and reinforced concrete classes. He has professional experience in the design of steel, concrete and timber structures, foundation design and seismic design, as well as construction, surveying, soil investigation and construction monitoring experience.

Mr. Urmson works as a structural engineer for Alan Reay Consultants in Christchurch, New Zealand. He can be reached at Alan Reay Consultants Ltd, 395 Madras Street, Christchurch, New Zealand. His e-mail address is urminator@hotmail.com.